

IPPT Report on Fundamental Technological Research  
7/2013

Krzysztof Dariusz Sekuła

# Real-Time Dynamic Load Identification

PhD Dissertation  
Supervisor: Prof. Jan Holnicki-Szulc

Institute of Fundamental Technological Research  
Polish Academy of Sciences

Warsaw 2013

IPPT Reports on Fundamental Technological Research

ISSN 2299-3657

ISBN 978-83-89687-87-6

Editorial Board/Kolegium Redakcyjne:

Wojciech Nasalski (Editor-in-Chief/Redaktor Naczelny),  
Paweł Dłużewski, Zbigniew Kotulski, Wiera Oliferuk,  
Jerzy Rojek, Zygmunt Szymański, Yuriy Tasinkevych

Reviewer/Recenzent:

prof. dr hab. inż. Zbigniew Kowalewski,  
prof. dr hab. inż. Wiesław Grzesikiewicz

PhD thesis defended in IPPT PAN on the 28th of June 2011  
Received on 29 November 2013

---

Copyright © 2013 by IPPT PAN

Instytut Podstawowych Problemów Techniki Polskiej Akademii Nauk (IPPT PAN)  
(Institute of Fundamental Technological Research Polish Academy of Sciences)  
Pawińskiego 5B, PL 02-106 Warsaw, Poland

---

Printed by/Druk:

EXPOL, P. Rybiński J. Dąbek Sp. J., Brzeska 4, 87-800 Włocławek, Poland

# Contents

- 1. Introduction** **11**
  - 1.1 Motivation . . . . . 12
  - 1.2 Review of the dynamic load identification methods . . . . . 13
  - 1.3 Real-time systems . . . . . 18
  - 1.4 Advantages of the proposed piezo-techniques . . . . . 20
  - 1.5 Thesis objectives . . . . . 23
  - 1.6 Composition of the thesis . . . . . 25
  
- 2. Road Weigh-in-Motion** **27**
  - 2.1 Introduction . . . . . 27
  - 2.2 Review of WIM systems . . . . . 27
    - 2.2.1 Types of sensors used in WIM systems . . . . . 29
    - 2.2.2 Calibration of WIM sensors . . . . . 32
    - 2.2.3 Factors influencing the measurements by the WIM sensors . . . . . 33
  - 2.3 New concept of traffic load identification . . . . . 37
    - 2.3.1 General idea of the beam-shape device . . . . . 37
    - 2.3.2 Laboratory tests of the beam-shape device . . . . . 38
    - 2.3.3 Numerical analysis of the beam-shape device . . . . . 38
    - 2.3.4 Modified load identification algorithm . . . . . 47
    - 2.3.5 Road installation of the beam-shape device . . . . . 50
  - 2.4 Development of the new plate-shape device . . . . . 56
    - 2.4.1 General idea of the plate-shape device . . . . . 57
    - 2.4.2 Numerical analysis of the plate-shape device . . . . . 57
    - 2.4.3 Road installation of the plate-shape device . . . . . 61
  - 2.5 Final remarks . . . . . 67
  
- 3. Weigh-in-Motion system for the railway transport** **69**
  - 3.1 Introduction . . . . . 69
  - 3.2 A review of the existing railways WIM systems . . . . . 69
  - 3.3 The proposed WIM system . . . . . 71
    - 3.3.1 General idea of the WIM system for railways . . . . . 72
    - 3.3.2 Proposed methods of dynamic load identification . . . . . 74
  - 3.4 Pioneer installation of the proposed WIM system *in situ* . . . . . 76

|           |   |            |
|-----------|---|------------|
| 3.4.1     | Experimental tests of the piezo-based WIM system . . . . .                                    | 77         |
| 3.4.2     | Performance comparison of piezo-sensors and strain gauges . . . . .                           | 80         |
| 3.5       | Numerical model vs. experiments . . . . .   | 84         |
| 3.5.1     | A review of railway track models . . . . .  | 84         |
| 3.5.2     | Description of the proposed model . . . . .   | 85         |
| 3.6       | Final remarks . . . . .   | 92         |
| <b>4.</b> | <b>Impact load identification</b>   | <b>93</b>  |
| 4.1       | Introduction . . . . .  | 93         |
| 4.2       | Impact load parameters characteristics . . . . .  | 95         |
| 4.3       | Experimental test stand . . . . .   | 97         |
| 4.4       | Numerical model of the system . . . . .   | 98         |
| 4.5       | Impact scenarios . . . . .  | 102        |
| 4.5.1     | Experimental tests of impact scenarios . . . . .  | 102        |
| 4.5.2     | Numerical simulation of impact scenarios . . . . .  | 108        |
| 4.6       | Impact identification based on “ <i>Peak-to-peak</i> ” approach . . . . .                     | 112        |
| 4.6.1     | The idea . . . . .  | 112        |
| 4.6.2     | Determination of time instants when colliding objects relative<br>velocity vanishes . . . . . | 116        |
| 4.6.3     | Verification of the method . . . . .  | 119        |
| 4.7       | Response map approach . . . . .   | 123        |
| 4.7.1     | The idea . . . . .  | 123        |
| 4.7.2     | Selection of parameters for the response maps . . . . .                                       | 125        |
| 4.7.3     | Verification of response map approach . . . . .   | 128        |
| 4.8       | “Impactometer” device concept . . . . .   | 129        |
| 4.9       | Final remarks . . . . .   | 131        |
| <b>5.</b> | <b>Concluding remarks</b>   | <b>133</b> |
| 5.1       | Thesis summary . . . . .  | 133        |
| 5.2       | Key achievements . . . . .  | 135        |
| <b>A.</b> | <b>Finite element modelling of piezoelectric sensors</b>                                      | <b>137</b> |
| <b>B.</b> | <b>Small testing stand of the beam-shape device</b>   | <b>141</b> |
| <b>C.</b> | <b>Simplified load identification algorithm</b>   | <b>143</b> |
| <b>D.</b> | <b>Full size testing stand of the beam-shape device</b>                                       | <b>147</b> |
| <b>E.</b> | <b>Modal analysis of FE models</b>  | <b>153</b> |
| <b>F.</b> | <b>Real-time impact mass identification methods</b>   | <b>157</b> |
| F.1       | Mass identification based on force and acceleration . . . . .                                 | 157        |
| F.2       | Mass identification based on impulse and momentum change . . . . .                            | 160        |

|   |            |
|---|------------|
| <b>G. The restitution coefficient discussion</b>          | <b>163</b> |
| <b>H. Sensitivity analysis of “Peak-to-peak” approach</b> | <b>165</b> |
| <b>Podsumowanie</b>                                       | <b>168</b> |
| <b>Bibliography</b>                                       | <b>171</b> |



# Acknowledgements

I would like to gratefully acknowledge the financial support through the following projects and funds:

- Project “Health Monitoring and Lifetime Assessment of Structures” – MONIT, No. POIG.01.01.02-00-013/08-00, from the EU Structural Funds in Poland.
- Structural Funds in the Operational Programme – Innovative Economy (IE OP), Project “Modern material technologies in aerospace industry”, No. POIG.01.01.02-00-015/08-00, financed by the European Regional Development Fund.
- Project “Innovative technologies for small aviation safety” – SWING (Safe-Wing), No. POIG.01.04.00-14-100/09, from the EU Structural Funds in Poland.

Moreover, I would like to express my gratitude to the Polish Ministry of Science and Higher Education for financial support through the supervisor (research) grant No. N N509 355734.

I would like to express my sincere thanks to Dr. Jerzy Motylewski, Dr. Przemysław Kołakowski and Mr. Piotr Pawłowski for their assistance in measuring sessions, and to my supervisor prof. Jan Holnicki-Szulc for many valuable advices and his kindness. I would like to thank my colleagues Dr. Łukasz Jankowski, Dr. Tomasz G. Zieliński, Dr. Grzegorz Mikułowski and Mr. Michał Rak for all their help and priceless support. I would like to thank Mr. Cezary Graczykowski for his contribution to the simulation part of the fourth chapter of the thesis.

Finally, I thank my parents, family and friends for providing their love and support.

# Krzysztof Dariusz Sekuła

## Real-Time Dynamic Load Identification

Institute of Fundamental Technological Research  
of the Polish Academy of Sciences

### Abstract

The thesis is devoted to the area of load identification problems. It is rather experimental in matter. However, the experimental research was supplemented with numerical simulations in order to expand the area of investigation.

The thesis contains three main parts of research. In the first one (Chapter 2) the problem of load identification in road transport is considered. The identification task consists of estimation of the tire-pavement contact force as well as the detection of the vehicle mass. The research is devoted to the so-called road Weigh-in-Motion (WIM) techniques utilizing use of piezoelectric strain sensors. The feasibility study of two new types of WIM devices (i.e., a beam-shape one and a plate-shape one) were conducted. Their development was supported by numerical modeling validated experimentally. It allowed to investigate some factors important for the estimation of a moving load by means of proposed devices and moreover the load identification algorithms were proposed for these devices.

In the further part of dissertation (Chapter 3), development and practical implementation of WIM device for the railway transport is discussed. A methodology based on the monitoring of strain development in the rail caused by the running train was proposed. The strain piezoelectric sensors were used and their readings were verified by another measurements techniques, e.g., strain gauges. The experimental research was carried out in-situ and enabled to validate the numerical model of the rail-sleeper-ground system. A numerical and experimental research allowed propose the identification algorithm and to analyze the crucial factors that need to be considered in order to obtain proper values of the dynamic forces exerted by train running on the rail.

The research described in the fourth chapter is fundamental matter. An analysis of the process of a rigid body impact into a pneumatic absorber is considered. Two algorithms for real-time impact load parameters estimation have been defined. The identification of impacting object's mass and initial velocity (i.e., kinetic energy) have been considered. The proposed methods were experimentally and numerically verified.

Krzysztof Dariusz Sekuła

## Identyfikacja obciążeń dynamicznych w czasie rzeczywistym

Instytut Podstawowych Problemów Techniki Polskiej Akademii Nauk

### Streszczenie

Przedmiotem rozprawy jest tematyka związana z identyfikacją obciążeń. Praca ma charakter głównie eksperymentalny, z wykorzystaniem modelowania numerycznego w celu rozszerzenia zbioru testów eksperymentalnych.

Rozprawa zawiera trzy zasadnicze części merytoryczne. W pierwszej z nich (Rozdział 2) jest rozważany problem identyfikacji obciążeń w ruchu drogowym. Zagadnienie to rozumiane jest jako estymacja siły kontaktowej, występującej między kołami pojazdu a nawierzchnią drogi oraz masy pojazdu. Przedmiotem badań są dynamiczne wagi drogowe (ang. Weigh-in-Motion), w których do pomiaru wykorzystano technologię piezoelektrycznych czujników odkształceń. Badania obejmowały symulacje numeryczne oraz testy w rzeczywistych warunkach drogowych dwóch wersji urządzeń zbudowanych na belkowym oraz płytowym przetworniku nacisku. Przeanalizowane zostały czynniki istotne ze względu na dokładność estymacji obciążeń oraz sformułowano algorytmy identyfikacji dedykowane dla dwóch badanych wersji urządzeń.

Kolejna część rozprawy (Rozdział 3) jest ukierunkowana na rozwój i praktyczną realizację dynamicznej wagi kolejowej. Zaproponowano metodę wykorzystującą pomiar odkształceń szyny kolejowej wywołanych przejazdem pociągu. Do pomiaru zastosowano piezoelektryczne czujniki odkształceń, których działanie zweryfikowano stosując tensometry oporowe. Zostały zrealizowane badania w warunkach polowych oraz wykonano model numeryczny układu szynopodkład-podtorze. Testy eksperymentalne i symulacje numeryczne umożliwiły sformułowanie algorytmów identyfikacji oraz analizę parametrów mających wpływ na dokładność wyznaczenia obciążeń.

Rozważania przedstawione w czwartym rozdziale rozprawy mają charakter badań podstawowych. Analizowany był proces uderzenia spadającego obiektu w absorber pneumatyczny. Badania pozwoliły na zaproponowanie dwóch algorytmów detekcji parametrów obciążenia. Rozważano identyfikację masy i prędkości uderzającego obiektu (a więc i jego energii kinetycznej) bez konieczności lokalizacji czujników na uderzającym obiekcie. Zaproponowane metody zweryfikowano numerycznie i eksperymentalnie.



# Introduction

Load identification constitutes an important type of engineering problems. It belongs to the category of inverse problems, since its objective is to determine the reason (load) on the basis of the result (measured response). Therefore, the task is usually not trivial because in many cases inverse identification problems are ill-posed. In case of a static or quasi-static load its determination is usually easy to perform. However, level of difficulty increases drastically in case of dynamic excitation. In dynamic load identification many difficulties tend to appear, especially when impact loads are considered. This is caused by short duration of the phenomenon and might be the result of relatively high load values.

Efficient techniques for load identification are needed in many technical applications (i.e., road and railway transport, aircraft, bridges etc.) and are sometimes important parts of Structural Health Monitoring (SHM) systems. Introduction of such techniques for monitoring of the loads in surface transport (i.e., road and railway) and for impact load identification, used as input measurements for devices in Adaptive Impact Absorption (AIA), are the main objectives of this thesis.

In many cases, important aspects are to keep the operation time in the timing constraints and short computation time of the applied methodology. It is clearly visible, in case of the mentioned AIA systems, when the load parameters must be immediately determined and in predictable time fashion, in order to control the impact process to minimize the structural dynamic response due to random impact loads excitations. So the real-time conditions must be fulfilled. Short response time is also crucial in many safety systems, e.g., when an airbag device is considered, the impact parameters must be immediately obtained for activation. Real-time dynamic load identification techniques can be also used in dynamic scales (i.e., Weigh-In-Motion systems), which should recognize the weights of passing vehicles without delay. Real-time applicability of identification methods is yet another important purpose of the thesis.

There are many applications which use dynamic load identification techniques. Nevertheless, the majority of them are rather expensive which is a reason for their limited applicability. The development of devices which are the subject of the thesis is focused on inexpensive solutions, nevertheless, the precision aspects is not neglected. Therefore, as a measurement methodology the piezo-techniques are chosen. Piezoelectric sensors have excellent dynamic properties and rather acceptable price. Therefore, the aim of the thesis was to obtain devices which are inexpensive yet sufficiently accurate.

## 1.1 Motivation

Great need for the road weigh-in-motion (WIM) devices is related to their usefulness in branches of traffic engineering. There is a vast variety of such devices (see WIM review) mainly developed for estimations of vehicle weights while they travel at high velocities. The measurements detected by these means are useful for statistical and planning purposes. Their importance for overloaded truck detection is indisputable. WIM systems can be also utilized for the fatigue effects prediction and for transport infrastructure (i.e., pavement, bridges, viaducts etc.) lifetime estimation. Nevertheless, all of the currently commercially available systems are very expensive. It is the main barrier precluding popularization of such devices. Another problem is their limited precision. The general motivation of the efforts taken in the second chapter of the thesis is a **demand for inexpensive WIM road technology with metrological parameters, similar to or better than the commercially available systems and much cheaper.**

Since the train operators were separated from the companies owning and maintaining the railroads, the need to monitor and control loading and weight of the rail cars has increased. It is also the result of introduction of railroad pricing and train access charges. The other reason is an increasing interest of the railway industry in implementation of, Structural Health Monitoring (SHM) technologies. According to the idea presented in ref. [1, 2] and the patent pending [3], the identification of train load acting on a bridge is necessary for performing subsequent identification of damage in an analyzed structure. Thus, the motivation of the third chapter of the thesis is a **demand for inexpensive WIM rail technology that enables for monitoring of the railway transport and/or constitutes a part of a larger SHM system.**

The controllable and predictable impact energy dissipation is an important technical problem for several transportation and industry branches. One of the

proposed solutions [4, 5] are the Adaptive Impact Absorption (AIA) devices, dedicated for dissipation of impact energy with simultaneous generation of the minimal deceleration of the protected structure. Nevertheless, identification of the impact parameter is required in order to introduce the mitigation process. Hence, the motivation of the fourth chapter of the thesis is a **demand for real-time impact load identification methodology which enables to predict the impact parameters used to trigger an AIA system.**

## 1.2 Review of the dynamic load identification methods

The load identification in a direct way (i.e., the sensor being located in the point of applied the load) is very often difficult to conduct or even it is impossible; hence, the indirect methods are required. As the consequence, the load identification usually belongs to the class of inverse problems. It can be defined as the finding system inputs, based on the given responses, boundary conditions and system model [6]. Very often the identification leads to optimization problem when the objective function is to minimize the residual error between the measured responses and numerically evaluated ones in the time domain [7]. Another idea is to solve this problem on the basis of the deconvolution technique. It is based on the assumption that the response of a body subjected to excitation is linearly dependent on the applied load [8].

It is worth to point out that the load identification problem is fundamentally an experimental one, requiring good quality data for its successful solution [9]. Several important aspects can be emphasized to make the identification feasible, namely:

- the measurement data should be characterized by high value of the signal-to-noise ratio,
- the number of searching parameters should be lower than the measurements number,
- the sensitivity between the measured data and searching parameters should be high.

The load identification is usually not a trivial problem because most often it is ill-posed and at least one of the following conditions is not fulfilled [6]:

- the solution is unique,
- there exists a globally defined solution for all reasonable data,
- the solution depends continuously on the given data (the stability criterion).

The ill-posed problem is characterized by the fact that the small inaccuracies in experimental measurements can cause very large variances in the identified entities. The general concept for the solution of an ill-posed problem is to transform it into a well-posed problem by using additional information about some expected or typical characteristics of the solution. The techniques, which transform the problem to the form of a well-posed one, are regularization processes. In general, the regularization lead to replace the original problem to the approximate one, the solution of which is considerably less sensitive to errors [10]. Many methods can be listed; nevertheless, the most popular ones are the Truncated Singular Value Decomposition [11] and the Tikhonov method. The second one was introduced in 1963 [12] and was successfully applied by researchers in many kinds of load identification problems [13, 14]. The regularization methods might be generally divided into two groups: the direct and the iterative one [15]. For both of them, a crucial aspect is the proper choice of the regularization parameter. The too small one results in noisy computed solution, while the too high value leads to distorted solution by the regularizing condition. Many techniques for selection of the regularization parameter were proposed but the L-curve method and the generalized cross-validation [14] are most common in use.

Identification problems are notoriously difficult to solve not only because of their ill-conditioning. The second aspect is that many of the proposed solution methods, need to use the system function in analytical form and this means that most of the structural systems analyzed were relatively simple. Both these difficulties are amplified for nonlinear systems [16]. Therefore, the great majority of methods are limited to the linear systems [17] in which assumption of the small displacement and stationary parameters is applied. However, some are devoted to nonlinear [14] or elastoplastic [17] structures. The author of [16] proposed the method, capable of determining multiple isolated force histories as well as multiple forces, in the form of traction distributions for nonlinear structures. The nonlinearities were arising from large deflections and rotations and/or from material behavior in the form of elastic-plastic and hyperelastic responses. The proposed method was based on a sensitivity response approach connected with a general finite element program.

It is worth to mention that non-collocated problems occur if at least one of the loads does not have a distinguishable, immediate influence on any of the sensors. Hence, the important aspect is the optimal distribution of the sensors in the structure such that the resulting measured data are most informative for estimating of the parameters. This problem was analyzed by the researchers in [18–21]. The identification problem in case of a small number of detectors was considered in papers [20, 22].

The big variety of the load identification methods can be found in many papers. References [6, 12, 23, 24] give excellent summary of literature of this problems, as well as an overview of the subject itself. The different criteria of classification of the used ones can be listed. The authors of [23] have classified the methods into two broad groups (i.e., pattern recognition, model-based).

**Pattern recognition** types are the methods, in which the mathematical model of the structure affected by the load is not required. The identification can be performed on the basis of the data base, which is constructed by simulation or by experimental measurements of various load scenarios, affecting on the considered structure, which are to be identified later. This method gives the comparison of the actually measured structure responses to the ones stored in the data base. The point is to retrieve the most similar one. Hence, neither a numerical model of the structure nor a simulation of the actual load scenario are necessary [23]. The pattern matching technique was considered in the thesis [25] for identification of the impact force in a read/write head of hard disc, when a head impacts bump on the disc surface. These methods are also in use for the Structural Health Monitoring problems [26, 27] and are often encoded in the form of the neural networks.

**Model-based** methods required the pre-calibrated numerical model of the structure. The identification is performed on the basis of the interactive modification of the cases of load scenarios affected on the modelled structure. Simulation of the following excitation variants is conducted in order to obtain structural responses and performed for comparison with the experimentally obtained one and to minimize the difference. The model used in order to identify the load parameters might be parametric (finite element, spectral element) or non-parametric (virtual distortion method, neural networks).

One of model-based method has been presented in [8] and was dedicated to identification of the low velocity impact force, acting on laminated plates by use of embedded piezoelectric sensors. The relationship between the impact force and the corresponding strain responses of a plate structure was formulated on the basis of the finite element method and the mode superposition method. The identification of force histories was achieved by defining of an inverse problem, which was solved by the quadratic programming optimization method.

Slightly different classification has been proposed by the authors of [6, 12, 24]. The methods performed for identification of operational loads, based on system response were divided into three main categories: i.e., deterministic, stochastic and based on artificial intelligence.

**Deterministic methods** are based on the system model simulation. Their results depend strongly on the accuracy of the inverse model identification [6].

The model should be validated and this process requires an experiment with input and output measurements. The deterministic method may be classified according to the signal processing methodology applied for experimental data analysis. As a consequence, the frequency-domain methods [25, 28, 29] and time-domain methods [8, 20, 24] are in use. The used domain is a result of load characteristic to be identified. In general, the frequency-domain methods are less time-consuming [12]. It is especially important since the real-time identification problems are considered.

**Stochastic methods** are in use where there is not enough information about the dynamics of the structure, as the consequence, it is impossible to obtain the deterministic relations which are required to calculate the operation loads. The general concept is based on finding statistical relations between the output and the input [6]. To find these relations, measurements of the inputs and outputs during operation of the structure are needed. Sometimes it is difficult to conduct but the numerical simulation of the system behavior might be helpful. In general, the two statistical methods are in use, the multiple regression one and inverse structural filter [12].

Methods based on **artificial intelligence** can be realized using the artificial neural-network (ANN) algorithms [30], the fuzzy algorithms or genetic algorithms [31]. These methods require a learning process in order to find the relation between the input and the outputs. Hence they have a lot in common with the stochastic ones. In general, the considered methods have an advantage over the statistical ones which is caused by its suitability to the highly nonlinear problems [12]. For instance, the authors of the [32] developed an approach for identification of the loads acting on aircraft wings, which uses an artificial neural network to model the load-strain relationship in structural analysis. As the first step of the study, for verification of the concept, the aircraft wing was simplified to a cantilevered beam and distributed loads were approximated by a set of concentrated loads. It was proved that the well-trained Artificial Neural Network reveals an extremely fast convergence and a high degree of accuracy in the load identification. Also in [7] the identification technique of force location and magnitude was proposed, using the strain measurement of an isotropic plate and the Neural Network.

The problem of load identification was understood by the researchers in a different way. Some of them considered the problem as determination of the intensity only with a single point load with location of the source to be known *a priori* [33, 34]. In other cases the identification was focused on the position only [24, 30]. Moreover, there are some more challenging approaches when the load position and its intensity [7, 35] are considered. For instance, the authors

of the [16] developed the methodology enabling to determine multiple isolated force histories as well as multiple forces in the form of traction distributions. Moreover, the different load scenarios were taken into consideration by the researchers. In some papers the impact load identification was analyzed [9, 29, 31], some others considered the moving load [36]. In paper [37], a method of moving force identification is developed using the dynamic programming technique. The forces were identified in the time domain using recursive formula and the responses were reconstructed using the identified forces for comparison. In general, the problem of moving load was mainly devoted to vehicle axle load determination in case of bridge-like structures. Unfortunately, most of the papers are limited to methods verification in the laboratory stage and relatively few have been validated under field measurement conditions with a bridge-vehicle system.

It is worthy to mention that some researchers expand load identification problem. In the paper [17], the authors considered the identification of coexistent load and damage which is referred to the simultaneous reconstruction of an unknown external load and damage (both type and size) of a damaged structure. The patent-pending [3] considered the dynamic load identification as the first stage performed in order to determine the input parameter for structural health monitoring of the bridge structure.

Taking into account the subject of the thesis, an important criteria is operation time of the method (i.e., the time required to identify parameters of the acting load) and predictability of it (i.e., fulfilled deadline constrains). Unfortunately, these parameters are usually not discussed in the literature, hence very often it is complicated to categorize the method to one of the group (i.e., off-line, on-line, real-time method).

The example of the **off-line** identification methods can be found in [17, 20]. The author [20] considers a methodology for *a posteriori* identification of spatial and temporal characteristics of dynamic loads. The proposed methodology was based on the off-line analysis of local structural response (strain, acceleration etc.) and required a dedicated sensors system to be distributed in the structure in order to measure and store the response.

The method dedicated for **on-line** load identification can be found in [5, 17, 38]. The authors [39, 40] applied observer techniques of unknown input estimation and adopted it for on-line estimation of external loads. The two methods for dynamic load identification base on Luenberger observers have been shown in the paper [22]. The first one is based on information about frequency characteristics of loading, while the second one uses only information about deformation of the structure. The authors of the paper [24] give an excellent overview of the topic of on-line load identification topic. The four time-domain methods have

been introduced (i.e., inverse structural filter, partial modal matrix technique, dynamic programming and unknown input observer approach). The paper discusses the advantages and disadvantages of these approaches. A comparison of the technique gives the conclusion that all of them have their own merits, limitations and drawbacks. Therefore, the application is the decisive factor when choosing a particular method.

It should be emphasized that the method of identification should not be very complex to be applicable in **real-time**. Especially in case of phenomena of very short duration (i.e., fast dynamic or impact) and in case when the immediate response is needed. Sophisticated methods usually required long computational time. Nevertheless, because of the increase in the speed of computer analysis, some methods, which were originally used to be applicable off-line, might be applicable in real-time in near future [5]. It can be pointed out that, nowadays, the real-time method should be based on the hardware data processing rather than use of the time-consuming computation. In general, the statistic or pattern recognition techniques are much more suitable for real-time identification because of their relatively low numerical cost, contrary to the deterministic one which usually makes use of a numerical model of the structure and requires long computational time. The deterministic methods defined in the frequency-domain are available for real-time problem because they are usually much less time-consuming than the time-domain ones [12]. In general, there are still limited numbers of methods capable of real-time determination of the dynamic or impact loads acting on an structure. The presented work is dedicated to fill this gap.

In this thesis, the pattern recognition identification techniques were mostly adopted. They were used in the developed WIM devices which are described in the second and third chapter. Moreover, the technique called “response map” described in Chapter four is pattern recognition one, contrary to the method called “peak-to-peak” which is a model-based one.

### 1.3 Real-time systems

The **real-time** expression has been first introduced in the late 1940s [41]. Originally it was associated with the military applications but nowadays it spans a wide range of fields including industrial plants control, automotive, flight control systems, monitoring systems, virtual reality etc. [42]. In fact, this term is applied not only by the scientist and engineers but it is in use in daily life.

In the simplest form, the **real-time systems** can be defined as those systems that respond to the external events in timely fashion [43]. Three main measures that count the merits of real-time systems are: predictable very rapid response to urgent events, high degree of schedulability (i.e., surety of feasible schedule) and stability during transient overload [44, 45]. Another important aspect is that a real-time system should be deterministic. Hence for each possible set of inputs, both a unique set of outputs and the next stage of the system can be determined.

In general, a real-time systems are supposed to satisfy the **deadline** constraints (i.e., maximum time allowed for a computational process to finish its execution [42]) to avoid the failure. Depending on the consequences caused by omitting this condition, a real-time systems can be divided into three categories: hard, soft and the fair ones. A **hard real-time systems** are characterized by the fact that it is absolutely imperative that the responses should occur within the specific deadline because the catastrophe might happen. On the contrary, a **soft real-time systems** might operate properly even if deadlines are occasionally omitted. In these systems, the missing of the deadline leads to the system performance degradation and not to a catastrophe. In general, the hard real-time systems have to handle both hard and soft activities [42]. **Systems** called a **firm real-time** are aimed at bridging the gap between hard and soft ones. In the firm real-time systems, a small fixed number of deadlines can be omitted without the total system failure but missing more may lead to complete and catastrophic system failure.

The real-time expression is always associated with the **reactive** (i.e., system in which scheduling is driven by ongoing interaction with their environment [41]) and the **embedded** (i.e., systems which are found in a system that is not itself a computer [41]) systems. A good example of the system which is supposed to operate in the real-time are car airbags. The airbag should be inflated in the proper time from the very beginning of the car crash (i.e., not too fast and not too late) to protect the driver in the optimal way. This shows that both lower and upper time bounds are important [46].

It should be mentioned that one of the most common misconception is that a real-time system must be “fast”. Indeed, many hard real-time systems deal with deadlines in the tens of microseconds but this is not the rule. Such systems which are supposed to immediately response, are sometimes called **real real-time systems**. The most important property of a real-time system is not a high speed, but predictability [42]. In a predictable system, we should be able to determine in advance whether all computational activities can be completed within their timing constraints.

Taking into account that the subject of this thesis, one of its objectives is to propose systems which fulfill the real-time condition. Thus, the real-time expression should be explained in details. Depending on the chapters of this thesis, slightly different system and conditions were considered. The hard real-time condition is assumed in case of Chapter four (i.e., Impact load identification). There, the potential applications are the AIA devices in which the information about actual loads values allows to design appropriate control strategies for smoothing down the impact process. Taking into account the short duration of this phenomena, the system must be assumed to be real real-time one. In Chapter two (i.e., Road Weight-in-motion), the system can be assumed as the soft real-time one. If we consider that the proposed WIM device will be used as the pre-selection scale, which does not fulfill the real time condition, missing the deadline will lead to the potentially overloaded truck to continue its driving instead to a catastrophe. The Rail Weight-in-motion system considered in Chapter three can be assumed to be a firm real-time one. The load parameters are needed for a bigger structural health monitoring system. So, not satisfying the real-time condition does not have to lead to the catastrophe. The proposed division is rather flexible because it is difficult to strictly classify the systems. Nevertheless, in any case, it is a principal goal of real-time systems engineering to find ways to transform hard deadlines into firm ones, and firm ones into soft ones [42].

## 1.4 Advantages of the proposed piezo-techniques

The presented thesis is rather an experimental than a theoretical one. Most of the experiments were performed using sensors operating on the basis of a piezoelectric effect. Hence, its analysis has been included with considerations focused rather on its sensoric features and mainly from the practical point of view. Its objective was to stress the measurements advantages of the proposed piezo-techniques, nevertheless their drawbacks are not neglected. The presented study was performed on the basis of a literature review, however it is strongly influenced by author's own experience related mainly to the piezoelectric ceramics and strain gauges sensors.

For the piezoelectric transduction elements either single crystal (e.g., quartz) or ceramic (e.g., PZT) materials are most common in use. The quartz is characterized by its better measuring properties. All ceramics inherently have hysteresis while the quartz is almost free from this effect [47]. Poorer insulation resistance in piezoelectric ceramics makes them less suitable for quasi-static

measurements, contrary to quartz sensors which give excellent quasi-static response, too. A slightly poorer linearity and smaller temperature range is also the drawback of piezoelectric ceramic. The operation temperature range for piezoelectric ceramics is limited by the Curie temperature, above which the ceramics loses its polarization and therefore all piezoelectric properties [47]. Its properties are temperature-sensitive (pyroelectric effect) and the operating temperature does not usually exceed  $200^{\circ}\text{C}$ , while quartz is characterized by a high time and temperature stability and the maximum operating temperature of  $500^{\circ}\text{C}$  [48]. Despite the piezoelectric ceramics suffers from some problems inherent to their nature, they are commonly in use as sensors. The reason is that they are characterized by high value of piezoelectric constant and are relatively inexpensive. For example, piezoelectric ceramic strain sensors are comparably priced to strain gauges. Therefore, piezo-techniques are rather inexpensive, contrary to other techniques (e.g., fiber optics). This fact enables to the multiplication of measurements points increasing accuracy of final measurement results.

The important advantage of piezo-techniques is existence of **direct** and **inverse** piezoelectric effects. This enables a vast applicability and makes possible the use of piezoelectric materials as both sensors and actuators. If the activation capabilities are considered, the important aspect is that the piezoelectric ceramics is characterized by the highest energy density [49]. This feature was mentioned in the paper [50] in addition to another actuations materials (i.e., pneumatic, magnetostrictive, shape memory alloy). Nevertheless, the important drawback of piezoelectric actuators is their low stroke. A comprehensive study and recent developments of piezoelectric actuators can be found in [51]. In some devices, both effects (i.e., direct and inverse) are in use. The example of such application are ultrasonic systems where the transducer first transmits a sonic or ultrasonic pulse, and then detects the echoes received from the defect or target [52]. The advantage of the piezo-technique, thanks the both mentioned effects, is the possibility of application of an automatic technique for self-sensing and detecting the potential piezoelectric material failure [53].

The advantage of piezoelectric sensors it is their extremely wide measuring range (span-to-threshold ratio up to 100 million) [48]. It means that, for instance, a force sensor with range MN that can still measure mN, too. From the practical point of view it is an extremely important feature, because the same piezoelectric sensor may be applied for measurements in different applications that require different spans of measurements. Nevertheless, in this case it is recommended not to calibrate over the full range but over a part of it. It is so because, despite its excellent properties, some small hysteresis or nonlinearities are observed in the piezoelectric sensors [47].

The high value of span-to-threshold ratio makes the piezoelectric sensors excellent for strain measurements. Even a small strain can be easily measured. The threshold of such sensors can go below  $0.0001 \mu\epsilon$  [47] – which is far below the threshold of wire strain gauges. The author has observed this feature, where for the same value of the deformation, the signal obtained from the piezoelectric sensor reached the value of volts, contrary to the strain gauges, where millivolts signal level was observed. It lead to a much better signal-to-noise ratio of piezoelectric sensors. Another important practical measurement aspect noticed by the author was that piezoelectric strain sensors did not require as good quality of prepared surface as in case of strain gauges, and the piezoelectric sensors were moreover much less vulnerable to the strain gauges. Nevertheless, one of the drawbacks of piezoelectric surface strain sensors was that they were not suitable for the measurements in case of small, strongly curved surfaces contrary to the strain gauges. This is caused by the fact that piezoelectric ceramic sensors are brittle and they are fabricated as flat-shaped plates. Nevertheless, an alternative might be the piezoelectric foil sensors which slightly overcome this limitation.

The important aspect of piezoelectric sensors is their active operation mode. Contrary to the passive one, no external energy is needed to obtain the output signal. This feature results in smaller installation cost. Only two wires must be lead to a piezoelectric sensors contrary to, for instance, strain gauges in which three wires are needed. With piezoelectric detectors, strong and clear voltage signals are obtained directly from the sensors without the need for intermediate gauge bridges, signal conditioners, and signal amplifiers [52]. The direct sensing piezoelectric materials bring about, moreover, the excellent dynamic properties [49]. The response time form of others sensor's types is rather longer. This is because of the fact that the passive sensors indirectly yield an output, rather they passively change their electric properties (change in resistance, capacitance or inductance) as a function of the measurand [47]. This aspect enables vast application for the piezoelectric sensors especially when the dynamic phenomena are measured.

Piezoelectric sensors suffer from the well known effect of **current leakage** (i.e., undesired change of an output signal in time which is not a function of the measured variable [47, 48]). This feature makes the sensors not useful for static measurements which is a disadvantage. On the other hand, there are claims that this requirement is not so strict and the measurements of quasi-static signals in frequency range below 0.1 Hz, are also possible [48]. As the example, the information introduced in the paper [54] might be mentioned where the signal level of the statically loaded force sensor decreased less than 1% after 30 minutes.

It is worth to mention that, the charge drift effect is systematic and, in general, it superimposes on the measured signal as the linear function of time [48]. Thus this unprofitable effect seems to be predictable and it might be compensated during measurements to make piezoelectric sensors more suitable for quasi-static measurements. A comprehensive electromechanical model for PZT, including drift modelling, was developed and tested experimentally with success in [55].

Piezoelectric sensors inherently have very high natural frequency, which makes them very proper for the dynamic measurements. An important feature is their very wide range of frequency, which makes them suitable for many applications. This allows to measure phenomena ranging from quasi-static to extremely rapid ones.

In general, it might be concluded that the thesis takes into consideration the short duration phenomena, so the choice of the piezo-technology seems to be adequate. Nevertheless, the maximum benefit from piezoelectric measurements can be obtained when a correctly assembled measuring system is applied. Especially important is to obtain a thorough knowledge of limitations of the used methodology. Thus, the choice of a proper sensing system should be strongly related to the considered application. All measurements techniques have some drawbacks and limitations. Therefore, the best way is to compare different methodologies. In the presented thesis, this was done in the case of the weigh-in-motion applications when the research utilized piezoelectric strain sensors and strain gauges. Moreover, few kinds of sensors were used in the fourth Chapter where, for instance, the velocity identifications of the impacted objects were performed on the basis of piezoelectric accelerometers, LVDT displacement sensor and high speed camera movie analysis.

## 1.5 Thesis objectives

The extended literature survey emphasizes the need for popular, inexpensive methodology for monitoring of surface transport (i.e., roads and railways) and maintenance of road and railway infrastructure. As a consequence, the first main objective of this research was:

**To develop a new road WIM system based on strain piezo-sensors, with metrological parameters similar or better to the commercially available WIM devices but less expensive.**

The author's original contributions are:

- development of a new road WIM device in the form of a steel beam

mounted in the road surface and equipped with a system of piezoelectric sensors,

- development of a new road WIM device in the form of a steel plate mounted in the road surface and equipped with a system of piezoelectric sensors,
- numerical modelling of the beam-shaped as well as the plate-shaped WIM device and its experimental verification on the basis on an *in-situ* installation and field demonstration,
- formulation of an algorithm for dynamic load identification dedicated for the beam-shaped as well as the plate-shaped WIM devices,
- formulation of calibration methodology for new WIM devices,
- determination of the factors that are important from the practical point of view for proper dynamic load identification by use of WIM road devices operating on the basis of the piezoelectricity effect.

The potential application for the SHM methodology developed in thesis [56] are railway bridge structures. For its implementation, measurements of the bridge excitations (i.e., load caused by the running trains) are required see [1, 2] and the patent pending [3]. Hence, the second main objective of this research was:

**To develop inexpensive WIM rail technology based on strain piezo-sensors for monitoring of railway transport that constitutes a part of a larger SHM system.**

The author's original contributions are:

- development of the methodology capable of monitoring of the railway transport on the basis of detection of the strain history measured in rail by use of piezoelectric sensors,
- formulation of the measurement algorithm for railway load detection as well as formulation of the procedure of on-line calibration for the rail WIM system,
- numerical modelling of the rail-sleeper-ground interaction and its experimental verification on the basis of chosen measurements techniques,
- determination of the factors that are important from the practical point of view for proper dynamic load identification by use of WIM railway devices operated on the basis of the piezoelectricity effect.

The research performed in the [4, 57] has shown the need for a real-time impact load identification methodology that enables detection of quantities required for optimal control of the impact process. The potential application for

the desired methodologies are the Adaptive Impact Absorption (AIA) devices. Hence, the third main objective of this research was:

**To develop real-time impact load (i.e., mass and initial velocity of the impacting body) identification methodology enabling to predict the impact parameters used to trigger the AIA system.**

The author's original contributions are:

- definition of the two real-time impact load identification procedures capable of detection even if no sensors are fixed to the impacting body,
- development of the stand for dropping tests in order to demonstrate the concept of the real-time dynamic load identification,
- formulation of the concept and patent pending [58] of a new type of device concept (i.e., **impactometer**) that is capable of the real-time impact identification as well as the study of range of its parameters that make the identification feasible.

## 1.6 Composition of the thesis

The contents of individual Chapters of thesis are summarised below.

**Chapter 2** discusses the road Weigh-in-Motion systems. The development of a new device begins with the literature review, which gives an overview of known road WIM devices and emphasizes the problems faced by the researchers. Then, the preliminary concept of the new road WIM device is proposed. The main part of this chapter presents the research performed by the author in order to evaluate the concept. The algorithm for moving load identification is introduced, which can be categorized as a pattern recognition technique capable of identification load intensity and its position (see review of the dynamic load identification methods). The research objective was to analyze the excitation parameters which are important if the load identification is considered by means of the proposed device. The analysis was performed by use of a FE model and a small testing stand for preliminary evaluation of the concept. The research was continued by means of a full scale laboratory testing stand. Later on, the proposed concept of the device was tested *in-situ* in road condition. Because some serious limitation of the idea occurred, a second concept of the device was proposed. The idea was evaluated by use of a FE method. Finally, a prototype has been built according to the second concept and was verified with success in road conditions. The papers [59–61] include the elements of this chapter.

**Chapter 3** is devoted to the Weigh-in-Motion methodology for the railway transport. The literature survey of the known WIM systems used for the railway is discussed similar to the one performed in Chapter two. The main parts of this chapter are focused on the practical implementation of the WIM railway system. The methodology of indirect identification of load based on the analysis of strain histories in the rail is proposed. The measurement sessions, carried out in-situ, enabled to propose the idea of a self-calibration methodology of the WIM device. An experimentally validated numerical model of the rail-sleeper-ground system is preceded by the short literature review of the rail models. The numerical analysis enables to improve the self-calibration methodology. A numerical and experimental research allows to perform analysis of the crucial factors that need to be considered in order to obtain proper values of the identified dynamic forces exerted by train running on the rail. Measurements conducted by the use of few kinds of sensors and different electronics were performed and compared. This proved that the piezo-technique is useful for dynamic load identification. The result presented in this chapter was published in the articles [2, 62].

The research presented in **Chapter 4** is focused on the development of a new type of detector so called (impactometer) as well as the methodology capable for real-time impact load identification on the basis of locally measured response. The fourth Chapter is related to the Adaptive Impact Absorption systems as a potential application for (impactometer) device. Thus, some review of the AIA subject was included. The mass and impact velocity (i.e, kinetic energy) of colliding object are considered to be identified. Two approaches, dedicated to this purpose were numerically and experimentally examined. First approach so called “response map” is based on the measurement of the colliding object contact force. This method utilizes the database of chosen parameters of measured force histories stored for wide variety of impact scenarios. While the second approach makes use of the impact force and acceleration measurements and it is based on the analytical formulation. Finally, the concept of the device (impactometer) is included. The chosen part of the chapter has been published in conference paper [63], in fourth chapter of the book [5] and included in the paper under review [64].

**Chapter 5** underlines the key conclusions of this research and emphasizes the original achievements.

# Road Weigh-in-Motion

## 2.1 Introduction

This chapter is devoted to the so-called *Weigh-in-Motion* (WIM) technologies as an example of application for dynamic load identification techniques. At the beginning, a brief technical review was included. The literature survey was dedicated to an overview of different kinds of WIM systems. The calibration methods as well as the factors influencing the identification precision was taken into account. The main part of the chapter is assigned to the feasibility study of the new WIM devices. Its two types i.e., beam-shape and plate-shape were developed. Both operate on the basis of the monitoring of strain development in deformable bodies by use of piezoelectric strain sensors. The research was aimed at the validation of the proposed algorithms for the inverse problems, which were dedicated to the axle loads identification by means of the proposed devices. The experimental part included laboratory experiments for preliminary evaluation of the ideas. Further, the *Finite Element* (FE) models of the devices were proposed for improvement of these concepts. Finally, a full-scale experimental validation of the WIM algorithms and the proposed devices was performed in field tests.

## 2.2 Review of WIM systems

Weigh-in-Motion (WIM) is the technology that appears to overcome the limitations of static weighing scales. In general, these systems were developed in order to obtain estimations of vehicle weights while they travel with high velocities. Most often the WIM devices are intrusive and the detectors are embedded in a roadway to measure the force exerted by a vehicle acting on the pavement when its axle is passing over the sensors [65].

WIM systems can be classified on the basis of the velocity range, which enables identification of their weights. In general, there are high-speed WIM (for velocities greater than 15 km/h) and low-speed WIM (smaller than 15 km/h) [66].

Another classification can be based on the device montage technology. Detectors can roughly be divided into emplaced and portable. Emplaced detectors, once anchored, are usually not removed and are able to detect the traffic information continuously. Portable detectors are used for short-term data collection and can be moved from place to place [67]. Moreover, WIM systems may be divided into two major groups according to their shape, which is related to their operating rule [68]. The first group are the so-called weight-plate systems, characterized by the fact that the full footprint of a tire is acting onto the sensing elements. On the contrary, the strip shape sensors systems are installed in narrow pavement grooves. The detectors widths, in this case, are smaller than the tire latch so the force signal has to be integrated over the wheel contact length.

WIM devices were developed in order to detect many parameters. The informations achieved by their means are often used for planning purposes, for instance, during traffic design and pavement design phase. The factors like truck-traffic volumes (base year and future growth), truck operating speed, truck lane distribution factors, vehicle class distribution, axle load distribution, axle configurations, tire inflation, and lateral load distribution factors [69] are very often crucial in this case. Especially important for statistical purposes is determination of vehicle class and the total number of vehicles. For instance, the American classification includes 13 classes of vehicles from motorcycles as Class 1 to seven or more axle vehicles with multiple trailers as Class 13 [69].

WIM systems most often contain at least two weight detectors installed exactly parallel and orthogonally to the driving direction. The spacing between the two detectors rows is selected according to the average speed distributions. On highways, typically 4 m with a parallelism of less than 4 mm is ideal to keep velocity errors below other dynamic weight errors [70]. Classical WIM systems are very often equipped with an inductive loops which are emplaced for vehicle detection in weighing area and in order to perform classification of the vehicle [71].

WIM systems have several advantages like:

- possibility of measuring the traffic load without the necessity to stop the vehicles or even to limit their speed,
- capability of performing measurements over a long time periods, which is useful for statistical analysis [72],
- possibility of identification of many parameters.

Nevertheless, few disadvantages can be listed as well. The most important is the limitation of the accuracy of load identification. There is always a difference between the static load of a vehicle and its dynamic load. It is caused by the

dynamic component in the signal. High quality WIM system guarantee 6% accuracy of the actual vehicle weight for 95% of the trucks measured. Therefore, such systems are often used only for preliminary estimation of the weights, while a static scales are necessary for exact measurements, as it is presented in Fig. 2.1.

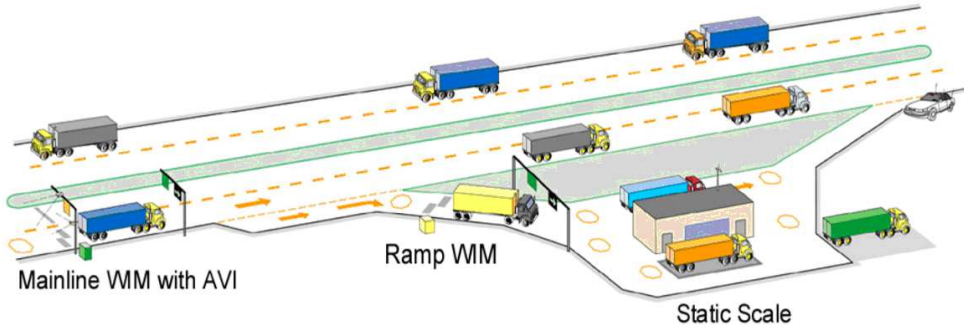


Figure 2.1. Typical configuration of a Weigh-in-motion system [73].

### 2.2.1 Types of sensors used in WIM systems

Many kinds of sensors have been applied in WIM devices. A brief overview of currently used sensors can be find in the papers [65, 66, 69, 72, 74]. The first were used in early 1950's and generally consisted of a number of strain gauges mounted on the underside of bridge girders [75]. Today only few primary WIM technologies are used in number of applications. The most popular of currently used WIM systems operate on the basis of detectors like piezoelectric and quartz sensors (operated in compression mode), bending plates, capacitance sensors, load cells and optic fibers. These sensors utilize different physical principles and are briefly presented bellow.

#### Piezoelectric and quartz sensors

One of the most popular types of WIM detectors are based on piezoelectric and quartz sensors. Detectors of this type are narrow bar-shaped, so that only a small part of the imprint of the passing tire affects the sensor. As a result an integration of the measured signal is necessary. Figure 2.2 presents cross-sections of the detectors.

Detectors of this kind produce voltage signal that is proportional to the stress caused by the passing wheel. The piezoelectric material generates electric

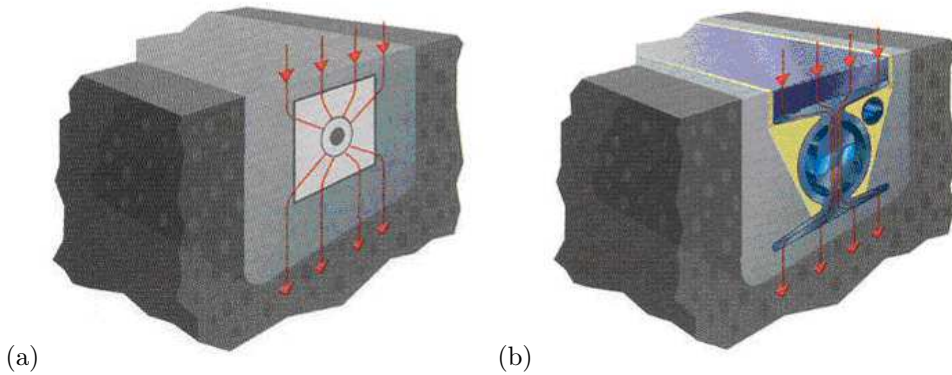


Figure 2.2. Cross section of: (a) piezocable WIM sensor, (b) quartz WIM sensor [72].

current only when the force changes. It means that piezoelectric WIM devices can be applied only in case of dynamic excitation. Therefore, the vehicle must be running during measurements. On the contrary, the quartz WIM devices can be applied in cases of both, quasi-static and dynamic excitations. Because of a high resistance of quartz, these sensors can reliably measure wheel loads down to a very low speed (less than 1 km/h), yet the high rigidity of the quartz elements gives the sensors a wide frequency response, allowing to measure up the vehicle speeds far beyond 100 km/h [70].

Moreover, in contrast to piezocables, quartz crystals do not show pyroelectric effect, thus even fast temperature changes do not cause any drift of the signals. The quartz also has the advantage of an almost negligible temperature coefficient of sensitivity (approx.  $-0.02\%/K$ ), thus no special means for pavement temperature compensation are necessary [68].

Piezoelectric and quartz WIM devices can be installed directly into a slot in the road for permanent applications, or taped down for portable applications [74], which is a significant advantage of narrow strip sensors. It makes the installation of them much easier and takes considerably less time than for wider detectors [76].

### Bending plates

Bending plate technology incorporates a steel plate with strain gauges attached to its underside [66]. The plate is often completely covered with hot vulcanized rubber for durable humidity and corrosion protection [77]. As axles pass over the bending plate, the system measures the strain and calculates the

load required to induce that level of strain [76]. The width of the plate is such that the whole wheel is on the plate. Thus, no integration of the signal is needed, and in principle, only the greatest weight is recorded as the wheel passes over the plate [77]. This provides an accuracy advantage to wider detectors in comparison with the narrow ones.

### Capacitive mats

The capacitance mats consist of two metal sheets separated by a dielectric material. An outer surface layer surrounds the sensor, protects the steel plates, and allows the sensor to be placed on the pavement or in a mounting frame. A voltage is applied across the two metal plates [76]. When a vehicle passes over the mat, the distance between the plates decreases and the capacitance increases [65], what is interpreted as an effect of the vehicle mass.

### Load cells

A load cell type WIM detector comprises one or more fabricated steel or other material beams or plates that are simply supported by a load cell at each corner [66]. Sometimes load cell devices are built in the form of weighing platforms with hydraulic cylinders placed beneath them. The dynamic force of the wheel or axle is measured by analyzing the change in the hydraulic pressure [65].

### Optical fiber sensors

A typical sensor is constructed of two metal plates welded around an optical fiber. An applied force causes change in the properties of the fiber that can be detected in the light passing through it. This change is proportional to the force applied [69, 78]. The optical fiber WIM systems are not fully developed and are not in field-operational use. System accuracy and life have not been established [79].

The main advantage of the sensor is its immunity to corrosion and electromagnetic interference. The disadvantage is a relatively high cost of installation which is the result of the expensive electronics used in this measurement technique.

### Bridge WIM

As an alternative to pavement WIM systems (presented above) the concept of using bridges as scales for vehicle weighing has been proposed [80]. In the

so-called *bridge WIM* system, a bridge is equipped with a set of sensors for detecting the response of the structure caused by traveling vehicles. Weight is determined indirectly by means of strain gauges [80] or fiber optics [81] mounted on the bottom side of the bridge. The best results (approx.  $\pm 10\%$  accuracy) has been obtained in case of sensor installed on a simply supported reinforced concrete slab bridge 5 to 10 meters long [82].

### Multiple sensor systems

If only one detector records the instantaneous load exerted by a tire, a significant error in the determination of the static weight can occur as a consequence of the dynamic load oscillations. In order to improve the accuracy of estimation of the static load on the basis of measurements of dynamic tire forces, multiple WIM sensors system have been introduced. The same axle of a vehicle is measured few times during its transverse movement. The load is identified by means of a simple average of all the sensor readings or sometimes a more sophisticated procedure (e.g., signal reconstruction method, maximum likelihood method etc.) are in use.

#### 2.2.2 Calibration of WIM sensors

The objective of a WIM system is to accurately identify the static value of a load by means of dynamic measurements. Usually, to reduce the uncertainty related to the dynamic effects, the location places of WIM systems are specially prepared, so that the pavement is smooth and flat. Another crucial aspect is related to the calibration procedure of the device.

In general, the calibration is a test during which known values of the measurand are applied to the sensor and the corresponding output readings are recorded under specific condition [47]. The objective of the calibration is to experimentally obtain the calibration coefficient, which is a multiplication coefficient applied to the actually observed value to minimize the uncertainty [83]. Scale calibration factors are adjusted to minimize the mean error obtained when comparing static and dynamic weights [76]. The calibration coefficient can depend on many factors like: car velocity, outdoor temperature, etc. That is why the calibration process should enable determination of the calibration coefficient as a function of the mentioned factors [84].

Few calibration techniques have been proposed by the researchers in the past. A brief overview of calibration techniques can be find in [66, 76, 77, 84]. A review of static methods has been presented in [85]; these techniques are

limited to static sensors like strain gauges, fiber optic or capacitive sensors. Another disadvantage is that they do not take into account the effects of dynamic loading, neither does the specific tire impact. In general, the static methods are used as the first step of the calibration process.

A dynamic procedure of calibration has been proposed e.g., in [86]. Few techniques of this kind can be listed. Some of them require special excitation devices used for the generation of the dynamic excitation such as the *Falling Weight Deflectometer*. Others make use of vehicles with known weight. First, their axle loads are measured statically, and then vehicles pass several times through the WIM system which is being calibrated. Their payload and speed should be varied. The number of the calibrating vehicles is usually limited to two or three of different types that are representative for the vehicles to be weighted [77].

The calibration can be also applied using especially equipped vehicles. A set of sensors installed in suspension and in tires allows the dynamic load of each of the vehicle axles to be measured in a continuous way. Dynamic loads are matched to the places of the WIM sensors. Because there is no exact method of calibrating the instrumented vehicle, the real accuracy of the measurements has not been exactly established [77].

An interesting technique of self-calibration has been proposed in [83, 87]. The method is based on the statistical assumption that the average axle load of the first axle of a lorry with a three axle trailer varies relatively low. Its mean load is equal to 61 677 N with the standard deviation of 7.3% [83]. The calibration factor is obtained by comparing the statistical mean weight and the measured weight.

### 2.2.3 Factors influencing the measurements by the WIM sensors

This section is devoted to the factors that may affect the measurement results of WIM system. In general, some of the factors are related to the vehicle and its driving condition, some to the road, and others to the WIM sensing system [77].

The challenge for the researchers and engineers developing WIM systems is to identify the value of the static load (which directly corresponds to the weight of the vehicle) on the basis of the measured dynamic interaction between vehicles and the road surface. The dynamic behavior of a vehicle is influenced by vehicle speed, its air resistance, non-linear suspension characteristics, non-linear tire behavior and tire pressure. The wheel loads are not constant what is a result of the vehicle dynamic interaction with the road [88]. The main movements of a vehicle body bounce (between 1.2 and 3 Hz) and the axle hop

(around 10 Hz). An example of the measured relative changes of the vehicle axle load are presented in Fig. 2.3. This unprofitable effect is one of the main factor leading to lower precision of WIM systems in comparison to the static scales.

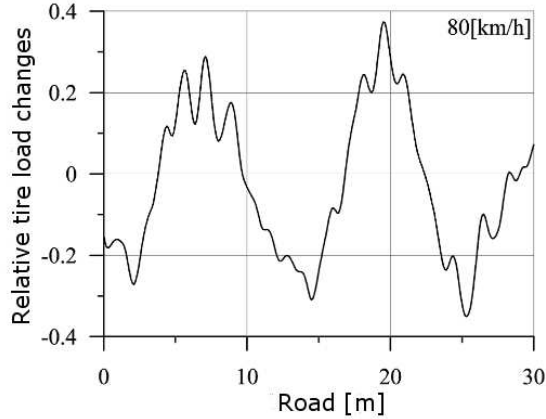


Figure 2.3. Relative changes of vehicle axle load at the velocity of 80 km/h [89].

### Tire footprint area and pressure distribution

One of the factors that may influence the estimation of vehicle weight is the results of tire footprint shape and size variation. In general, the tire footprint (latch) length varies typically from 100 mm to 300 mm [70]. The width of the footprint can vary considerably, especially if both single and double tire wheels are considered.

Recent studies have demonstrated that the tire-pavement contact stress is far from being uniformly distributed. The distribution of the contact stress depends on: tire pressure, tire load and tire type. Measurements of tire imprints at various loading conditions showed that the contact area is more rectangular at a low tire pressure and more circular at a high tire pressure [90]. A most apparent effect of the increased tire pressure would be a reduction in the tire-pavement contact area, which may in turn result in an increase of the tire-pavement contact stress and consequently, more damaging effects to the pavement. Lowering the tire pressure leads to a larger contact area, reducing pavement's stresses and strains [90]. The example of the mentioned effect is presented in Fig. 2.4 [70].

The most current research [88] was performed by means of a commercially available strip-type piezo-electric WIM sensor. The measurements were repeated for three different tire pressure configurations: 70% of the rated pressure, the

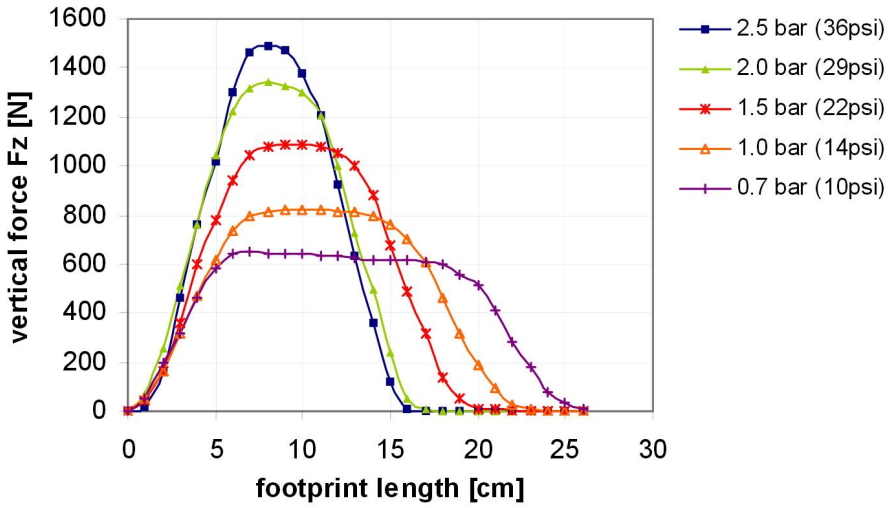


Figure 2.4. Examples of signal shapes for varying tire pressures [70].

rated pressure and 130% of the rated pressure. According to the results, the tire pressure is not found to be the most significant factor affecting the dynamic loads. A similar conclusion can be drawn (for the rigid pavement) on the basis of [91].

Another factor which has an influence on the footprint shape is the value of the driving torque applied via the tire to the road. The literature studies [84, 92] confirm that the distribution of the tire pressure differs considerably between the driving and not driving axles, as presented in Fig. 2.5.

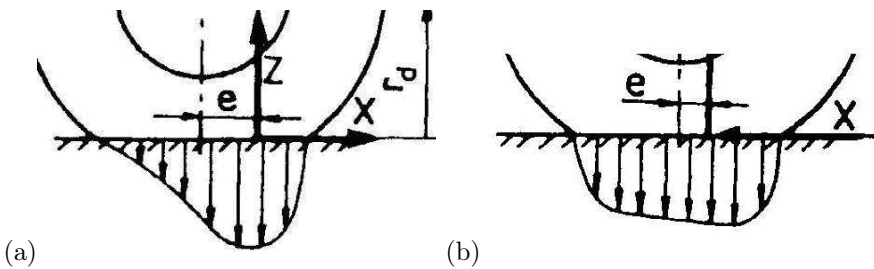


Figure 2.5. Experimental measurements of tire-pavement contact stress distribution: (a) driving wheel, (b) not driving wheel [92].

## Climate conditions

WIM systems are typically outdoor devices so that the climate conditions like temperature and humidity should be considered by the designers. In general, temperature has a significantly more important influence on its operation than humidity [89]. In the Polish climatic conditions, the temperature can vary in the range from  $-30$  to  $+40^{\circ}\text{C}$  [71]. This factor might considerably effect the sensor sensitivity. It is prominent, for instance, in case of piezoelectric sensors, because their signal for a given axle force changes with the temperature. In case of piezoelectric material, mostly a direct proportion between the temperature and the sensitivity was observed [47, 89, 93]. The temperature dependence was noticed also for the bending plate WIM system produced by PAT company. A temperature compensation was needed during the cold period [77].

To compensate the temperature influences, WIM system can be equipped with additional temperature sensors. The temperature measurements can be taken into account in identification algorithms by means of the additional correction coefficient [89]. The two method of compensation of the climate effects were considered in [83].

## Velocity effect

Monitoring of the velocity is important; first of all from the preventive and statistical points of view. Moreover, the velocity might have a significant influence on the weight identification, which is due to the sensors behavior. For instance, piezoelectric sensors can generate different voltage signals as a function of the vehicle velocity [85]. Especially, for relative low velocities (20–30 km/h), they can give the underestimated values [94]. As a consequence, the velocity effects have to be compensated in the load identifications algorithms.

## Other factors

Many other factors which may have influence on the accuracy of WIM system can be listed. One of them is improper mounting of the device and bad pavement condition. For proper measurements, the road pavement conditions before the WIM sensor system must be possibly well prepared in order to minimize the dynamical effects. It should be noted that even if the road is very smooth and the suspensions are good, there is always some dynamic component of the loading, so that in practice the axle load varies at least  $\pm 10\%$  [77].

Other effects can be caused deliberately by vehicle drivers. If, for instance, braking or rapid acceleration occurs, the obtained measurement results are corrupted by additional dynamic effect and can be inaccurate.

some unprofitable effects can be minimised by proper algorithms and extended calibration procedures. For instance, in case of nonlinear sensors the load value should be taken into account in the identification algorithm. As a results, the calibration factors may depend on the load values.

An important part of this Chapter was dedicated to the research of the factors important from the point of view of load identification precision. The objective was to consider them in proposed algorithms and in device design phase.

## 2.3 New concept of traffic load identification

In this section, a new methodology of identification of dynamic loads acting on road surface is presented. The concept has been invented and developed in Smart-Tech Centre at Institute of Fundamental Technological Research since 2003. The practical implementation of the device was introduced in cooperation with the company “Contec”. This section is focused on the study of so called beam-shape WIM device. The research was performed in order to validate the proposed technique and algorithm based on the inverse problem solution. The objective was to make the identification of unknown parameters such as location of the axle load, its intensity and vehicle velocity feasible by means of the proposed device.

### 2.3.1 General idea of the beam-shape device

The proposed approach is based on the concept of monitoring of strain development in a deformable body affected by a moving load. According to the general idea, the beam-shape WIM device is a symmetrically supported steel pipe mounted in the road pavement and equipped with a system of piezoelectric sensors, see the scheme in Fig. 2.6. When car wheel passes over the beam, its deformation is observed and the piezoelectric sensors produce signals. The longitudinal dimensions (2 m length) and its road locations were assumed that only one wheel in each vehicle axles is loading the beam-shape device. The axle load identification is performed on the basis of the measured beam response and using an algorithm which operates on the basis of solving the corresponding inverse problem.

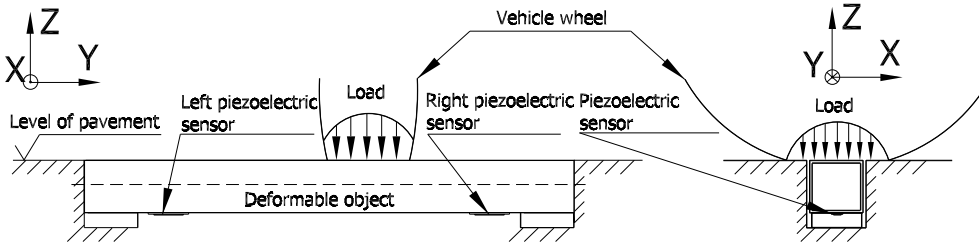


Figure 2.6. General concept of the proposed beam-shape WIM device.

### 2.3.2 Laboratory tests of the beam-shape device

Laboratory tests were performed for a feasibility study of the idea of beam-shape WIM device. The thorough explanation and preliminary laboratory tests can be found in Appendix B. This research enables to develop the algorithm of the load identification which is explained in Appendix C.

In the next stage of laboratory experiments a full-size beam-shape WIM device was tested see, Appendix D. This research was done for preliminary calibration of the device prepared for road tests and moreover was dedicated to obtain the reliable results needed for finite element model validation.

### 2.3.3 Numerical analysis of the beam-shape device

The finite element (FE) model of the proposed beam-shape device was prepared. Commercially available software “ADINA” was used. The model dimensions as well as the boundary conditions i.e., support conditions were analogical like in case of beam used in laboratory test (see Appendix D) and in roads experiments. In order to the boundary conditions be the most similar to “real” ones in the numerical model for the nodes localized on the supports and bolts edges, the degrees corresponding to Z-axis were fixed. The general view of the model is shown in Fig. 2.7.

Since small deformations in steel were assumed, the elastic-isotropic material model of the structure was used. Taking into consideration the WIM device shape and its dimensions i.e., thin wall structure, the model utilized the shell type of finite elements. A more sophisticated model which utilizes a 3D FE mesh was not required and not recommended due to the numerical costs. The model utilized a four-node type of finite element which was based on the Reissner/Mindlin plate theory [95]. The density of the mesh discretization was determined by the sensors dimensions (5×25 mm) and its location (see Fig. 2.8).

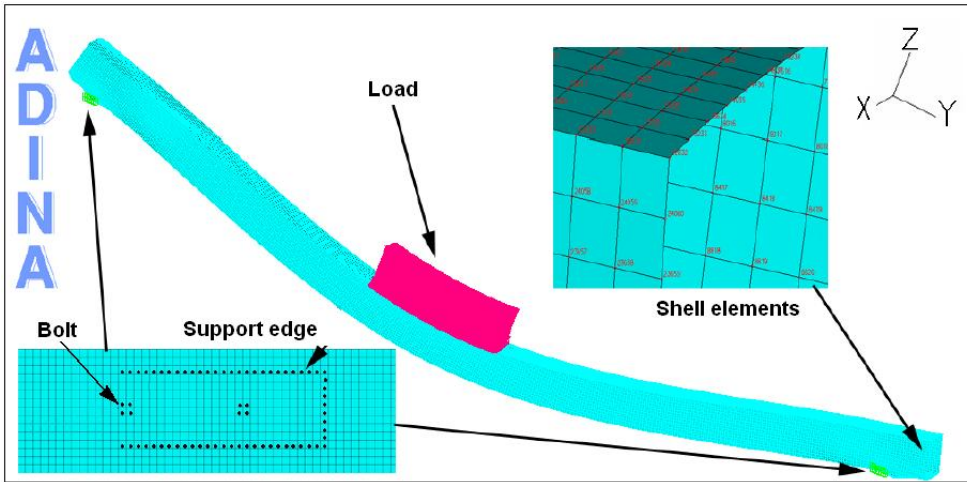


Figure 2.7. Numerical model of the beam under interaction of moving wheel.

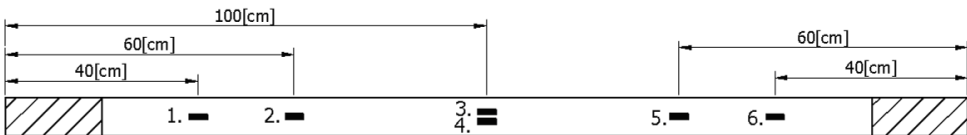


Figure 2.8. Piezoelectric strain sensors distribution in the beam-shape WIM device (bottom side).

Thus, the  $5 \times 5$  mm square-shape finite element was used. Total number of the nodes applied in the model was approximately 24 000.

Sensors were modelled by use of the simplified procedure presented e.g., [96]. It is generally based on the analysis of the linear and rotation displacement in nodes overlapped with the edge of “real” sensor. The procedure takes into consideration the thickness of modelled sensor and piezoelectric constants. More thorough explanation can be found in Appendix A.

The general objective of numerical simulation was to analyze the factors associated with the vehicle wheel interaction that may influence the load identification. The parameters like: load position, tire-pavement contact stress distribution, width of the tire imprint and velocity of the travelling load (vehicle velocity) have been considered.

## Numerical model validation

The numerical model of the beam-shape device has been validated on the basis of the laboratory experimental results (see Appendix D). Force histories (see Fig. D.2 in Appendix D) and load positions were analogical to the laboratory tests. The comparison of the experimentally and numerically obtained results are presented in Fig. 2.9. The graph illustrates the signal amplitude with respect to the load position obtained from six “real”/modelled sensors. Sensor numbers presented in this figure correspond to Fig. 2.8. The similarity of the values is satisfactory, what proves the correctness of assumptions made in the prepared numerical model.

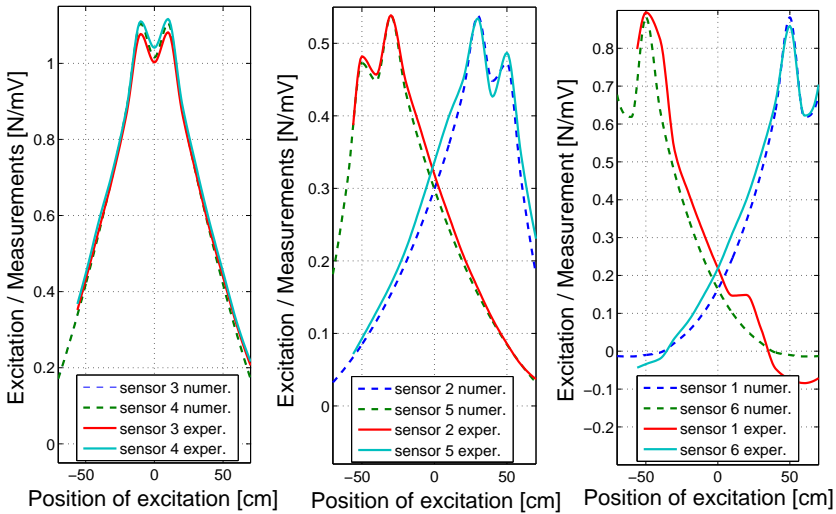


Figure 2.9. Comparison of the experimental and numerical results (horizontal axis corresponds to the load position).

The validated in Appendix E *FE* model of beam-shape device enable to perform the analysis of the tire-structure interaction. The objective was to analyze the factors associated with the vehicle wheel interaction that may influence the device response and load identification. The parameters like: tire-pavement contact stress distribution, width of the tire imprint and velocity of the travelling load (vehicle velocity) have been considered and are briefly presented bellow.

Contact stress distribution effect

The objective of the research presented in this section was dedicated to the beam structural sensitivity for the tire contact stress distribution. It was modelled by means of force vectors affecting the structure (see Fig. 2.7) which were moved in each simulation step. The horizontal velocity of moving load was equal to 10 m/s (36 km/h).

Two stress-shape distributions were introduced in to the numerical analysis as the interaction of the tire. The first corresponded to the driving tire while second to the not driving one (see Fig. 2.5). In both cases the same total load (5 kN) as well as tire foot print area (300 × 300 mm) were applied as the excitation for the modeled structures. The lateral load distribution was modelled as uniform as shown in Fig. 2.10. The tire pavement tangent forces was neglected in numerical analysis as the consequence of the assumption of the vehicle constant velocity.

The obtained results of signals' amplitudes as functions of positions of load excitations are presented in Fig. 2.11(a), while the signals shape examples for two analyzed excitations scenarios are shown in Fig. 2.11(b). The analysis is rather qualitative and as the consequence the arbitrary units are use. The numbers of modelled sensors corresponds to the graph in Fig. 2.8.

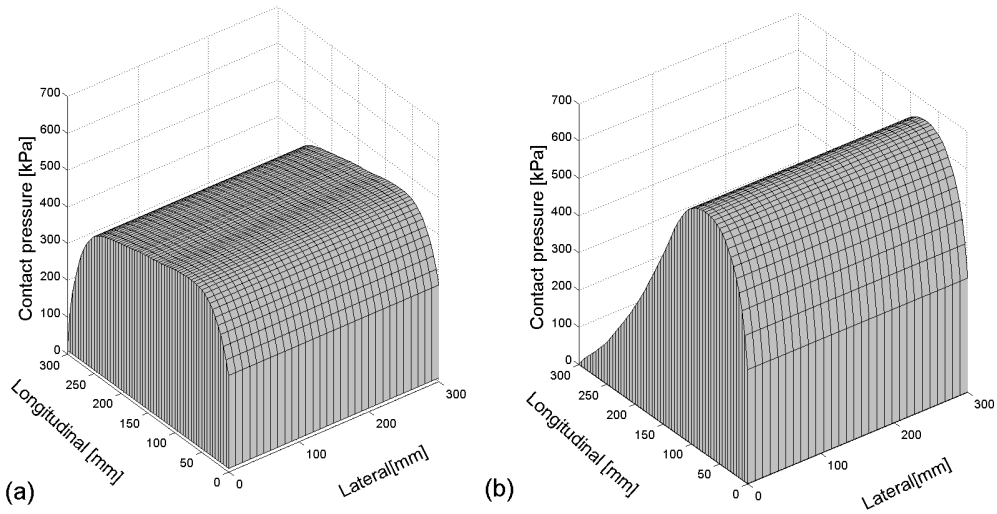


Figure 2.10. Distribution of the load vectors used in FE model: (a) not driving tire, (b) driving tire.

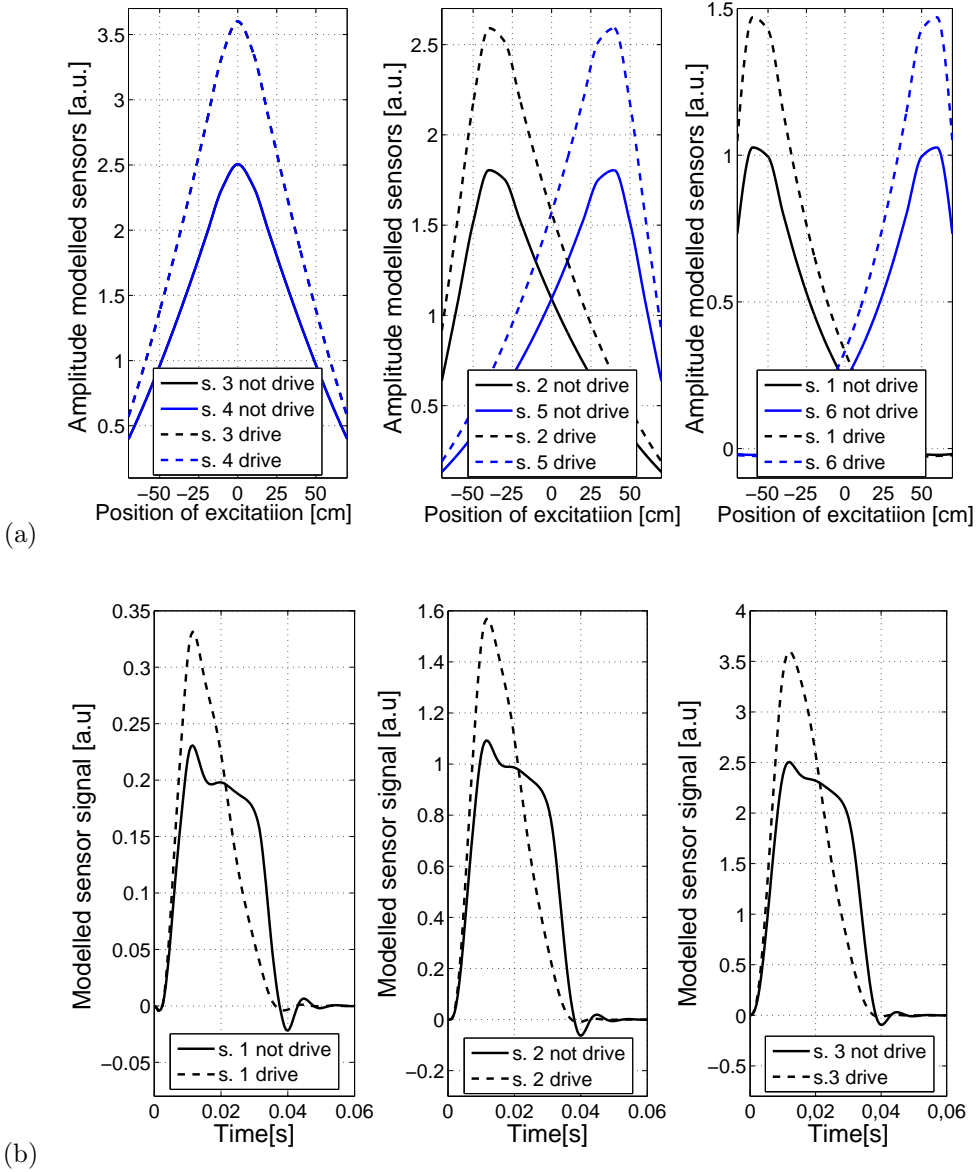


Figure 2.11. Simulation results for two shapes of load distribution: (a) amplitude of the signal in function of the excitation position, (b) example of sensors response.

Contact stress distribution shape was found to be an important factor affecting the structural response. For driving tire the signal amplitude was much higher. It was the result of the higher maximum value of the contact stress in comparison to the not driving tire. Therefore, in order to neglect this “shape effect”, instead identification of the peaks values of the signals, the area under the detected axle signals was taken into consideration (see results presented in Fig. 2.12). The data were available in a digitalized form, so the calculations were performed using the following formula

$$SA = \sum_{i=1}^n \left[ S(t_{i+1}) + S(t_i) \right] \frac{t_{i+1} - t_i}{2}, \quad (2.1)$$

where  $n$  – the number of the samples,  $S$  – the value of the sample,  $SA$  – the area under the curve,  $t$  – time.

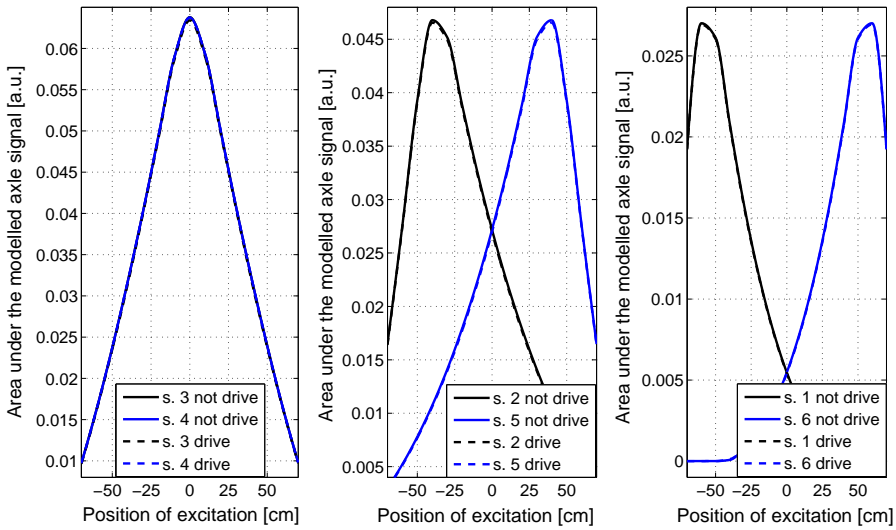


Figure 2.12. Area under the axle signal as a function of the excitation position in case of two shapes of the contact load.

The analysis proved that the shape of the contact stress distribution has no crucial influence on the obtained results since the area under the curve of the axle load is considered instead of signal amplitude.

It might be concluded that the peak value of the signal can not be an accurate representation of the weight of the vehicle, since its tire footprint is considerably

larger than the width of the WIM detector. In the analysed case, the structure width is 80 mm, while the footprint is usually more than 100 mm [70]. Consequently, the peak of the signal does not represent the whole wheel load but rather a portion of the total load [97]. Moreover, it should be noticed that the weight estimation method based on the computation of the area under the axle load signal was originally recommended by Kistler company and has been used in their commercial products [98], i.e., striped shape quartz WIM sensors.

### Tire width effect

An analysis presented in this section was performed in order to test the tire width effect on considered structure response. The WIM devices were developed for axle load identification especially in case of trucks. The widths of tires vary a lot especially, in case of a heavy vehicle where single or double tires can be used. Moreover, the imprint of tire-pavement area is a function of the inflation pressure and the load on the tire.

Four variants of tire-pavement interaction width (150, 300, 450 and 600 mm) were considered in FE simulations. The total load value, longitude of modelled imprint and the vertical load velocity were assumed to be constant in all analysis presented in this section. The contact stress distribution was assumed to be the one of the not driving wheel, see Fig. 2.10(b). The obtained results are presented in Fig. 2.13.

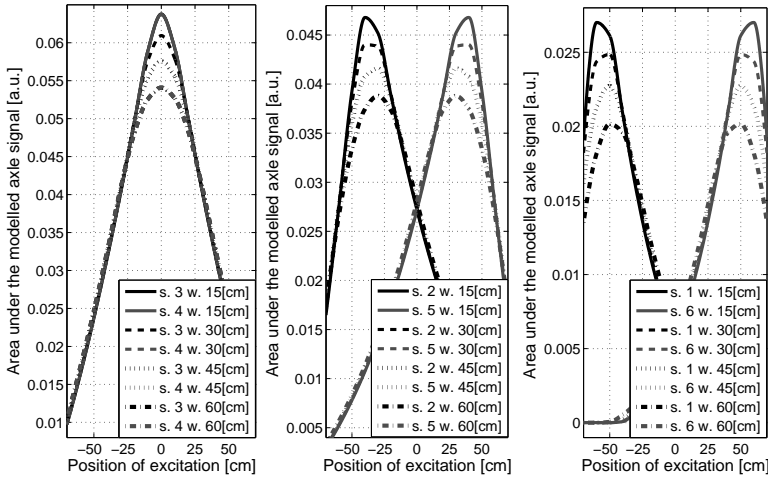


Figure 2.13. Area under the axle signal as a function of the excitation position in case of few widths of contact load distribution.

The significant effect of the load width was noticed. In general, the more narrow load distribution, the higher the signal value. The load of the width of 15 cm caused 20% to 30% higher signal value than the load of the width of 60 cm. Therefore, in order to the load estimation be possibly accurate, the width effect must be considered in the identification algorithm. This could be obtained by means of adding compensation factors. The main problem is to detect “which tire is single or double”. The development and implementation of the vehicle class identification algorithm might be helpful. The assumption that vehicles belonging to the same class have rather constant tire width distribution can be applied.

### Load velocity effect

The analysis presented in this section were used to forecast the sensitivity of the beam-shape WIM device on the travelling load velocity. The modal analysis of the structures has been presented in Appendix E. It shows relatively low value of resonance frequency of the beam-shape device. Thus, this structure is claimed to be sensitive to velocity effect of vehicle travelling over the detector.

The research considered five different load velocities (10, 20, ..., 50 m/s) traveling over the modeled structure. The load distribution area, total load value and location were constant. In case of the lowest velocity the load structure interaction time was 40 ms while for 50 m/s was equal 8 ms. The examples of the sensor signals for different velocities are shown in Fig. 2.14.

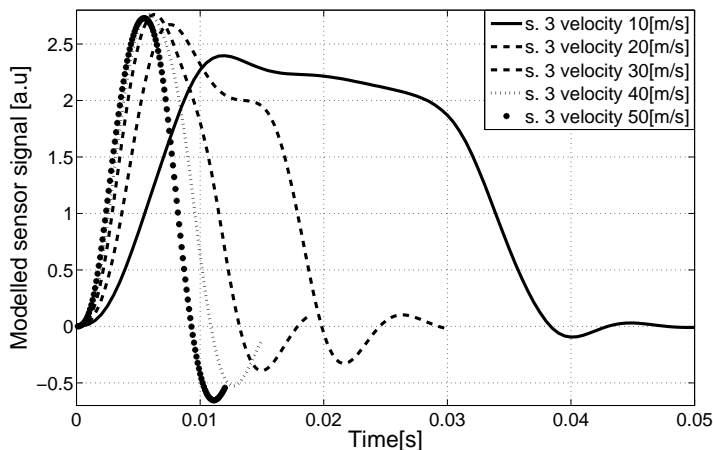


Figure 2.14. Responses from sensor 3 for different load velocities.

The increase of the signal response amplitude due to the increase of the load travelling velocity was observed. For the velocities higher than 30 m/s, the peak values of the axle load were rather constant. Thus, if the amplitude of the signal would be used as the load equivalent, the velocity identification is not crucial. On the contrary, to the case when the area under the signal is considered as a load equivalent. It should be noticed that the area under the axle signal is approximately inversely proportional to the speed [98]. This is the result of different tire-structure time contacts. Hence, in order to obtain proper load estimation on the basis of the area under the axle signal the velocity must be considered in algorithm. As the consequence the velocity must be accurately detected.

The results of the velocity effects on the area under the axle signals as a function of the load position are illustrated in Fig. 2.15. In this case, the area under the axle signal was consequently multiplied by the corresponding velocities in each of the modelled cases.

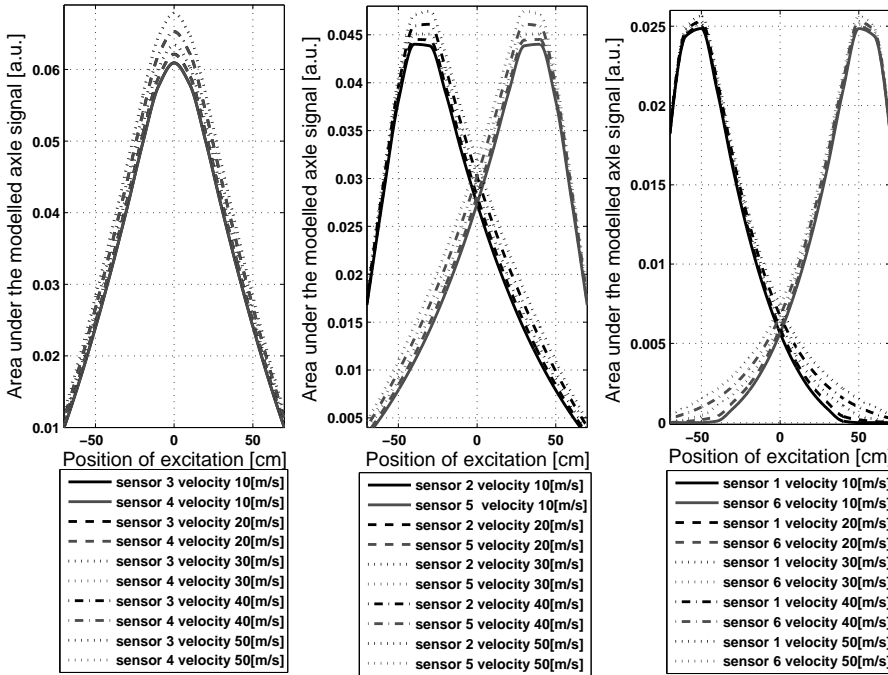


Figure 2.15. Area under the axle signal as a function of the excitation position for different traveling velocities of the excitation.

### 2.3.4 Modified load identification algorithm

The research conducted in laboratory using the full-size beam-shape see (Appendix D) and the FE simulation enable to develop the axle load identification algorithm which simplified form was presented in Appendix C. The methodology was modified in order to be applicable in case of higher number of used sensors and for taking into account the investigated factors influencing the measurements.

The velocity of the travelling vehicle was found to be an important factor influencing the beam-shape device response. The most convenient way for velocity identification is to use two parallel WIM sensors with known spacing. The time delay between the peak signals generated by means of the same vehicle axle detected by different WIM detectors can be used for velocity estimation [97]. To this end, the following formula can be used which assumes a constant vehicle speed while passing the sensors:

$$v = \frac{D_S}{S_R \cdot \Delta_P}, \quad (2.2)$$

where  $v$  – the vehicle velocity,  $D_S$  – the distance between upstream and downstream WIM detectors,  $S_R$  – the sampling rate,  $\Delta_P$  – the number of the samples between the matching upstream and downstream peaks.

The proposed device is assumed to be used for statistical purposes. Therefore, the algorithm must be able to determine the vehicle class. It can be performed on the basis of the factors like: number of axles, wheelbase and individual axle weight.

The axle distance may be computed using the calculated vehicle velocity and the travel time between the consecutive axles [97], namely:

$$D_{\text{axle}} = \frac{v}{\Delta_{\text{axle-axle}} \cdot S_R}, \quad (2.3)$$

where  $D_{\text{axle}}$  – the axle-to-axle spacing,  $\Delta_{\text{axle-axle}}$  – the number of samples.

Taking into account the limited number of vehicle classes, the classification quantities like axle loads do not need to be determined very accurately. Thus, the preliminary axle weight  $AW_P$  can be estimated as follows

$$AW_P = \gamma \cdot \sum_{i=1}^n SA_i, \quad (2.4)$$

where  $\gamma$  – the sensor sensitivity,  $SA_i$  – the area under the axle signal produced by the  $i$ -th sensor, see Eq. (2.1).

Determination of the parameters presented above enables to estimate the vehicle class, which is important, first of all, for statistical purposes. Moreover, the information about the vehicle class will be used in the further steps of the algorithm for the tire width estimation. The assumption about the constant tire width distribution for one vehicle class will be used.

Taking into consideration the beam-shape device response sensitivity to excitation position, the excitation position has to be determined precisely. It can be achieved on the basis of prepared “solution maps”, i.e., stored sensors responses for different excitation scenarios. Since a larger number of piezoelectric sensors are in use in comparison to the beam used in experiment (see Appendix B), the formula (C.1) from Appendix C takes the following form

$$F(x, v, w) = \sum_{i=1}^n \frac{L_i - R_i}{L_i + R_i}, \quad (2.5)$$

where  $L_i$  – the area under the axle signal produced by the sensor located on the left-hand side and  $i$  cm from the middle of the beam,  $R_i$  – the area under the axle signal produced by the sensor located on the right-hand side and  $i$  cm from the middle of the beam,  $w$  – the tire width,  $x$  – the load position.

The results prepared by means of this formula are shown in Fig. 2.16 as a function of the velocity and the position, see Fig. 2.16(a), and moreover, as a function of the tire width and the position, see Fig. 2.16(b). The excitation position is related with respect to the very center of the structure. The analysis considered the signals produced respectively by the sensors 1, 6 and 2, 5.

If the variables  $v$  and  $w$  are known Eq. (2.5) can be rewritten in the following form:

$$F_{v,w}(x) = F(x, v, w). \quad (2.6)$$

On the basis of numerical experiments, a single-valued function  $F_{v,w}(x)$ , was observed for  $x \in (-70, \dots, +70)$  cm, that is, the load positions with respect to the very centre of the beam. Hence, the load position determination is feasible by interpolating the values of the signals produced by the sensor pairs using the curves presented in Fig. 2.16. Finally, the excitation position is determined as

$$x = F_{v,w}^{-1} \sum_{i=1}^n \frac{L_i - R_i}{L_i + R_i}. \quad (2.7)$$

In order to perform axle load identification, the empirical parameter  $K$  (“calibration factor of the beam-shape device”) must be determined. This parameter

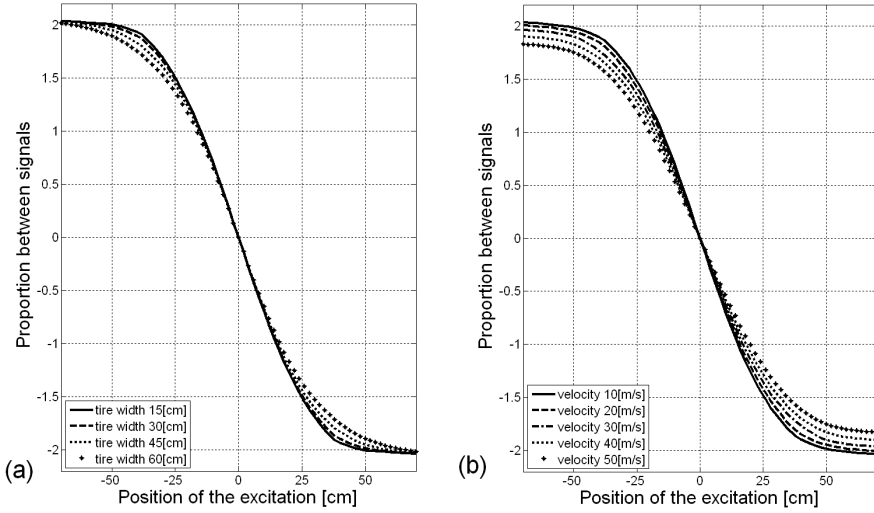


Figure 2.16. Proportion of the axle load signals between symmetrically located sensors: (a) as a function of the excitation position and the tire width, assuming the constant velocity of 10 m/s, (b) as a function of the excitation position and the velocity, for the tire width of 30 cm.

generally depends on the electromechanical properties of the device and describes the relationship between the load value and area under the axle signal produced by the piezoelectric sensors located in the middle of the device as a function of velocity, tire width and excitation position. It might be described as follows:

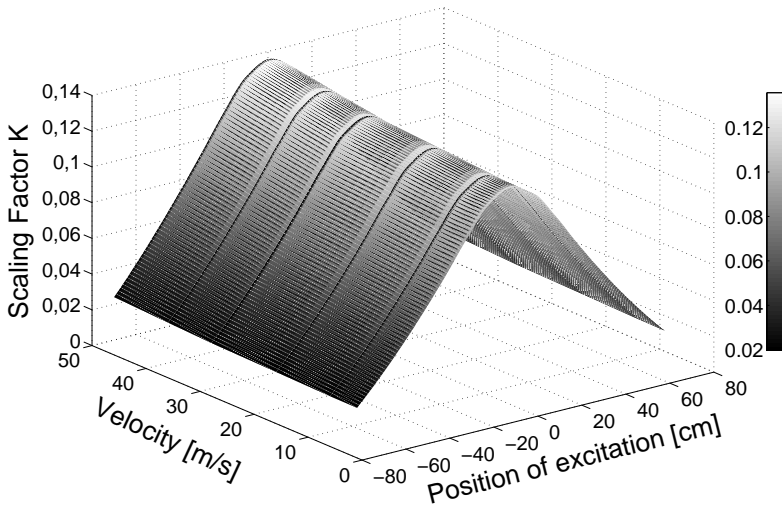
$$K(v, w, x, \gamma) = \sum_{i=1}^n \frac{AL}{M_i}, \quad (2.8)$$

where  $AL$  – the axle load value,  $M_i$  – the area under the signal produced by the centrally located  $i$ -th sensor,  $\gamma$  – the sensor constant.

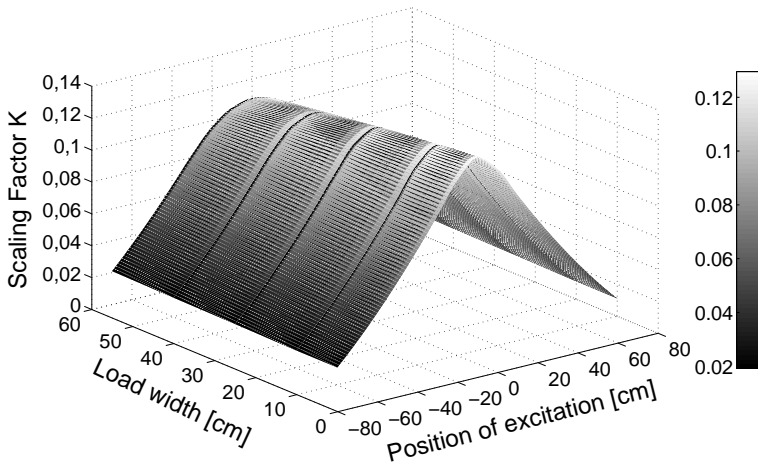
The calibration factor  $K$  obtained by means of the numerical analysis as a function of the excitation position, velocity and tire width is illustrated in Fig. 2.17. The results were obtained by means of two modelled sensors, located in the very center of the tested structure.

Finally, when the load position, car velocity and tire width are all known (obtained in the previous steps of the algorithm), it is possible to obtain the value of the parameter  $K$  using the interpolation. Finally, the value of the axle load affecting the device can be determined using the following formula:

$$AL = \sum_{i=1}^n M_i \cdot K(v, w, x, \gamma). \quad (2.9)$$



(a)



(b)

Figure 2.17. Calibration factor  $K$  as a function of: (a) the excitation position and the velocity (for the constant tire width of 30 cm), (b) the excitation position and the tire width (for the constant velocity of 10 m/s).

### 2.3.5 Road installation of the beam-shape device

In order to perform a practical verification of the proposed device concept and the load identification algorithm, field test were carried out. The beam

used in the laboratory test (see Appendix D) was applied in the experiment as a detecting element. The beam was located in the prepared support, see Fig. 2.18(a). The structure was laid in the road and fixed to the concrete. The top surface of the beam was on the level of the road pavement, see Fig. 2.18(b).

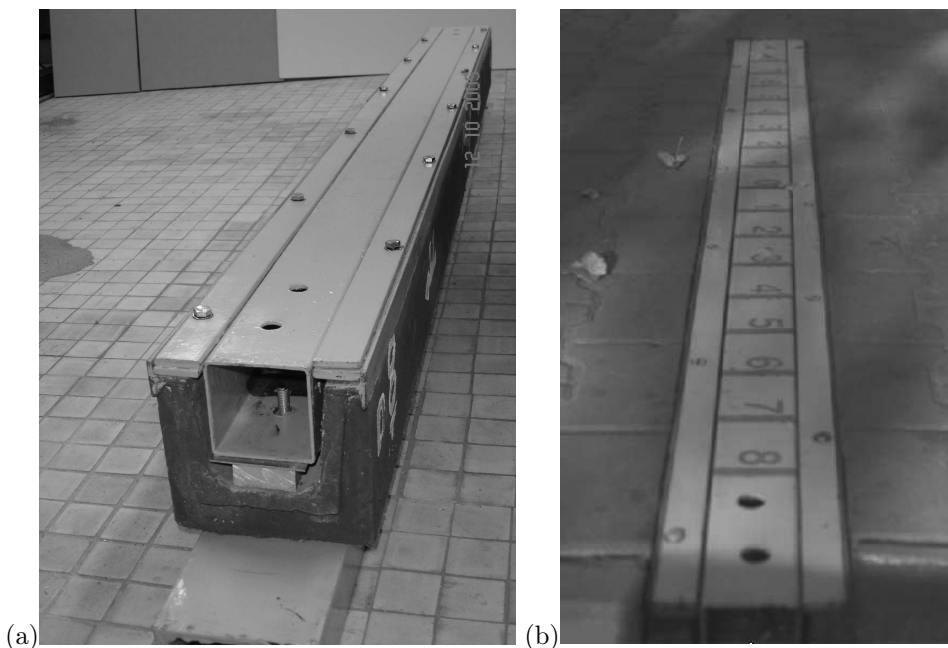


Figure 2.18. Installation of the beam-shape WIM device: (a) prepared support, (b) structure located in the road.

### Field tests

The field tests were performed. During the research several crossings over the installed beam were conducted. A bicycle, motorbike and a small passenger car were used as testing vehicles.

The most of the trials were performed by means of the motorcycle Honda CM 125. It is characterized by the static mass distribution (with the driver): front axle 82 kg, rear axle 125 kg and the wheelbase 1350 mm. An example of the axles load signals are presented in Fig. 2.19. The results correspond to the motorbike crossing over the tested structure with the velocity of 20 km/h and 20 cm from the center of the structure. The front wheel and the back wheel peak signals are visible.

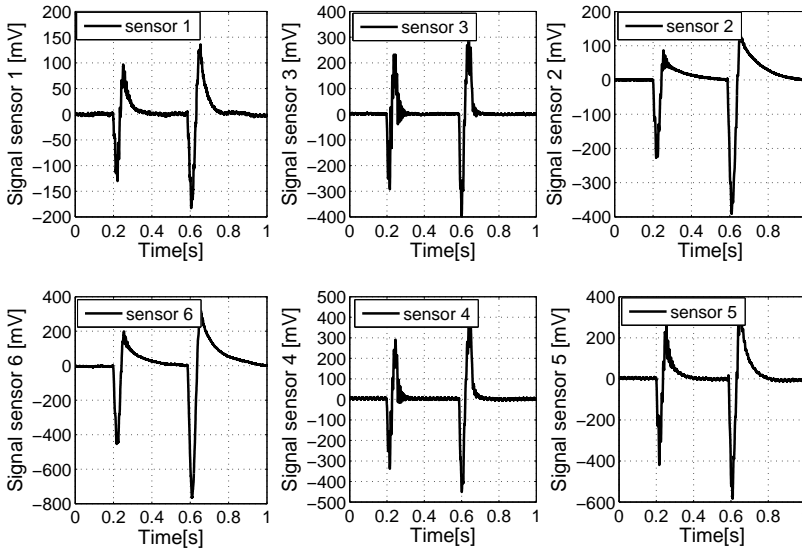


Figure 2.19. Examples of signals produced by the sensors during the field tests.

The main part of the research considered the analysis of the influence of the excitation position on the value of the signal produced by means of the six piezoelectric sensors. Each test was made with the same load value; similarly, the velocity was also relatively the same (approx. 15 km/h). The signal intensity distributions in case of different load location are presented in Fig. 2.20. The value presented on the ordinate axis represent the normalized response described by means of the ratio between the static axle load [N] and the area under the curve [mV·s]. Results for both axles are presented. The analysis enables to determine the calibration coefficient.

The obtained results are not fully symmetric. This could be caused by the fact that the position of the excitation was not measured so the trials were not fully repeatable. The position was set manually (limited precision) based on the lines painted on the top surface of the beam. In further steps of research it is planned to apply a fast camera in order to improve the accuracy of identification of load location. The first trials were already made, see Fig. 2.21.

The algorithm of the load identification presented in Section 2.3.4 was used. The procedure was performed on the basis of the numerically obtained “response maps”. Moreover, the calibration coefficients were applied. The obtained results are shown in Fig. 2.22. The graph presents the percentage accuracy of the identified dynamic axle loads for several trials with respect to the accurate (statically

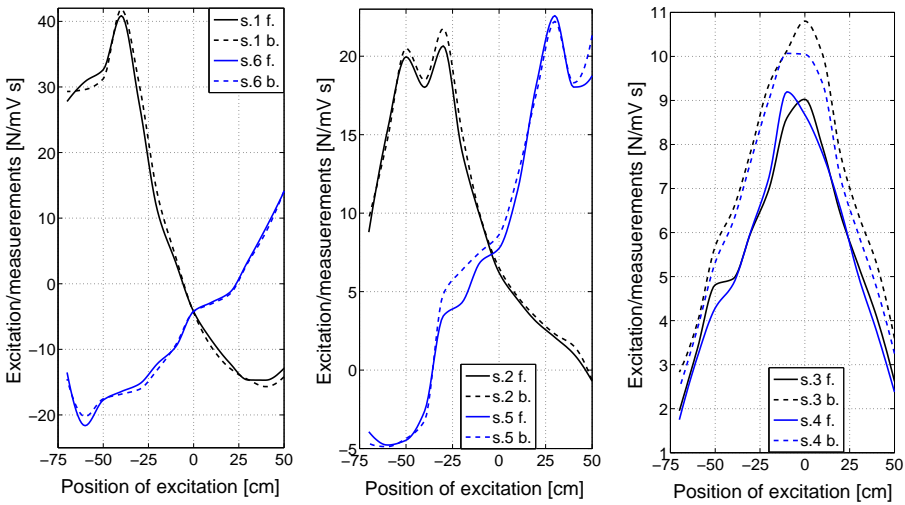


Figure 2.20. Axle signals values with respect to the excitation position.

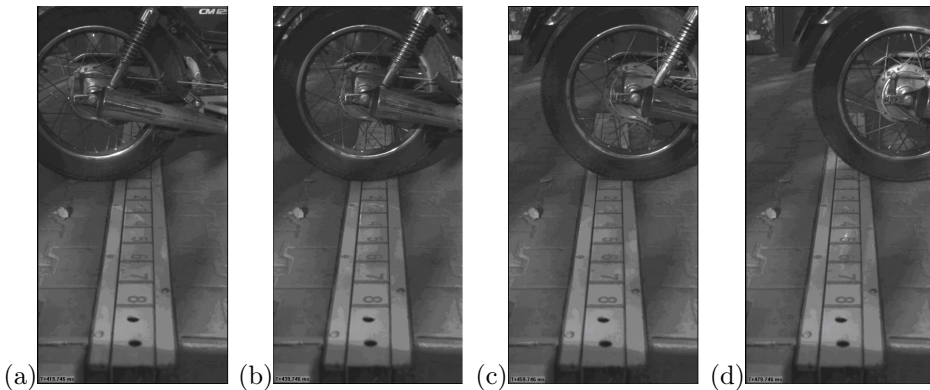


Figure 2.21. High-speed snapshots of the motorbike cross-over the beam: (a) 0 ms, (b) 20 ms, (c) 40 ms, (d) 60 ms.

measured) axle load as the function of the position of the excitation. The accuracy of identified load values was  $\pm 20\%$  while its the standard deviation was equal 0.126.

The location of the beam (small and closed area) made it impossible for test involving higher velocities. Moreover, the number of vehicle types was limited. As a consequence more experimental work was needed.

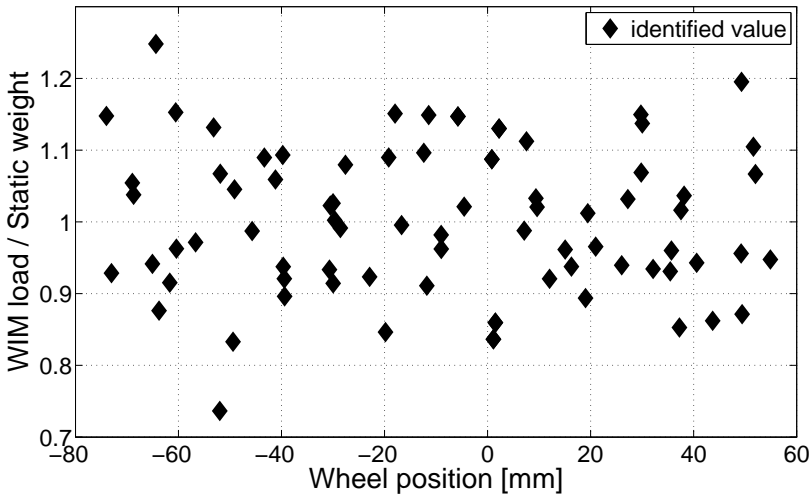


Figure 2.22. Accuracy of the axle load identification.

### Comparison of used sensors

In order to perform the research of comparison of measurements by means of different electronics, the new beam-shape device presented in Fig. 2.23 was installed. The strain gauges sensors in the half-bridge configuration as well as the



Figure 2.23. Second version of the beam-shape WIM device mounted on public road.

piezoelectric sensors were installed in the beam surface. Two kind of amplifiers (voltage and charge) were used in the piezoelectric measurement. The mentioned sensors were placed very close to each other. Thus, the assumption that the sensors were measured very similar physical quantity can be applied.

The comparison of the detected signals by means of different electronic setups is shown in Fig. 2.24. The presented results correspond to very slow (quasi-static) traveling of the wheel of the truck over the beam. The signals detected by use of the strain gauges and the piezoelectric sensors and the charge amplifier are very similar from the quantitative point of view. Very different is the signal obtained with the use of the voltage amplifier. The last example does not correspond to the real deformation of the beam. The general conclusion might be drawn, that it is much more suitable to apply the charge amplifiers in case of the piezoelectric measurements by the WIM devices. This is especially observable in the quasi-static measurements, where the voltage amplifier results in signal distortion.

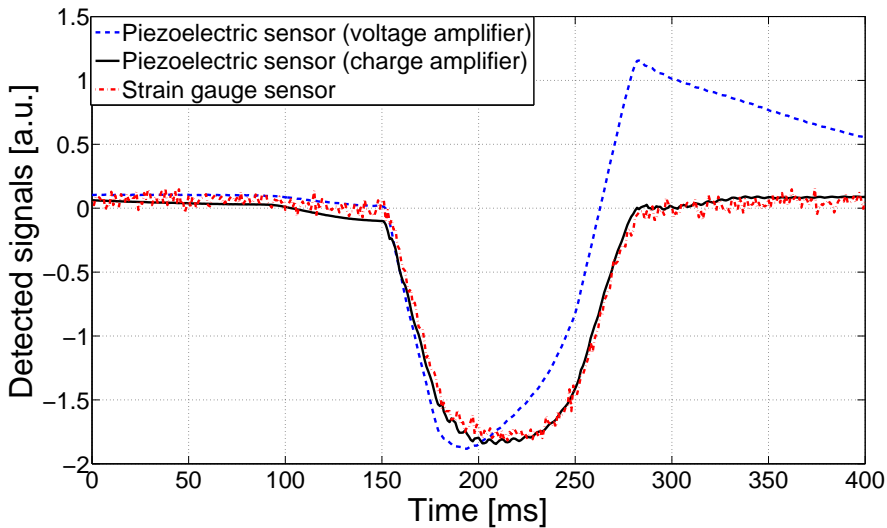


Figure 2.24. Comparison of results obtained with different measuring electronics.

The similar results to presented in Fig. 2.24 can be found in the [72] where the researches compared the signals generated by the piezoelectric and quartz WIM sensors. The differences were not commented in this paper. In the opinion of the author of this thesis this could be the result not only of used detectors kind but moreover of applied electronics i.e., voltage/charge amplifiers.

### Velocity effect

The research presented in this section was focused on the beam-shape device velocity tests. The same vehicle was passing over the structure with different velocities while the tire position was similar for all of this trials. Figure 2.25 presents the obtained voltage signals generated by sensor number four under different speeds. The velocity effect was found to be significant for the measurements. The velocity increase results in increase of the unprofitable vibration of the beam-shape device. Generally, velocity increase leads to the poorer accuracy of the device and difficulty in axle load identification caused by unprofitable vibrations effects. It might be summarize that the proposed beam-shape device can be used when the velocity of the vehicles to be identified is lower than 50 km/h.

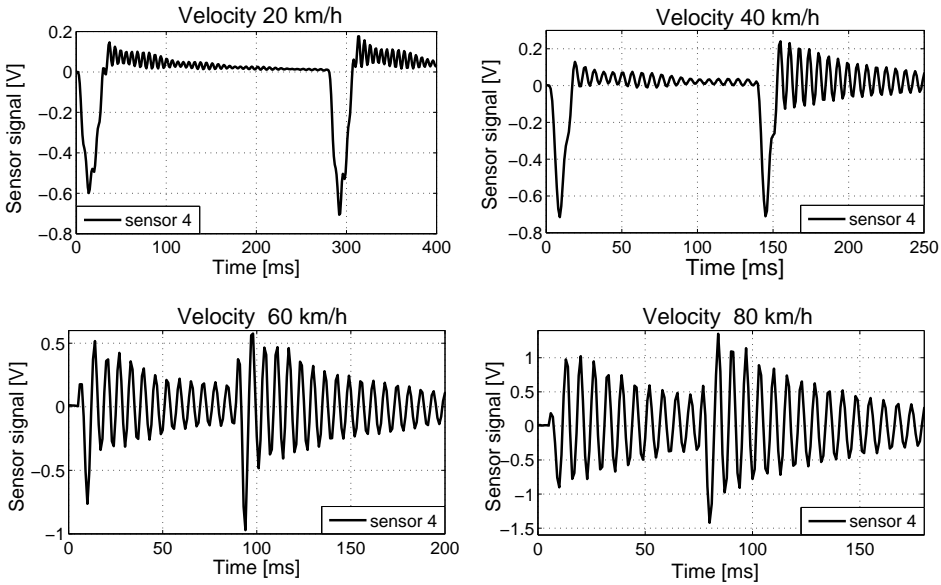


Figure 2.25. Velocity effect.

## 2.4 Development of the new plate-shape device

The beam-shape WIM device was found to have serious drawbacks i.e., relatively poor identification precision and available estimation in limited velocity range. As a consequence another concept of the WIM device was proposed.

### 2.4.1 General idea of the plate-shape device

The new devices utilize steel plate with detectors bonded to the underside. Contrary to the “classical” bending plate devices, instead of, strain gauges, piezoelectric strain sensors are in use as it is shown in the scheme see Fig. 2.26. The sensors distribution is assumed to be regular. The plate is supported along its longer edges and it is fixed by use of bolts into a steel frame placed in the pavement.

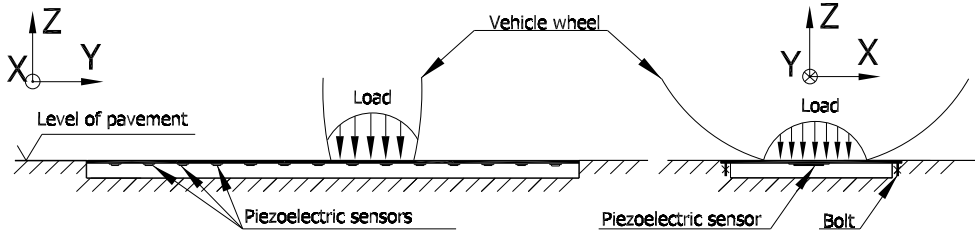


Figure 2.26. General concept of the proposed plate-shape device.

As axles pass over the bending plate, the piezoelectric-sensors generate signal proportional to the deflection of the plate under a vehicle axle. The measurement system, then, records the voltage and calculates the dynamic load. The static load is estimated using dynamic load and calibration parameters.

### 2.4.2 Numerical analysis of the plate-shape device

The numerical analysis of the plate-shape device has been performed. This research was focused on two main factors to be analyzed. First one was devoted to density distribution of the sensors while the second one was focused on the analysis of the width-effect of the plate device.

#### Sensors density distribution effect

The FE model of the device was prepared (see Fig. 2.27). The modelled plate was 2000 mm long, 280 mm wide while its thickness was 8 mm. The dimensions as well as the boundary conditions i.e., support conditions were analogical like in “real” device. The modelled sensors were placed in the middle of the plate with regards to its shorter edge, because the biggest strain of the plate was expected to be there. The localization of the modelled sensors was regular. The sensors were modelled on the basis of the methodology considered in the Appendix A. Tire-bending plate interaction, was modelled similar to the case of

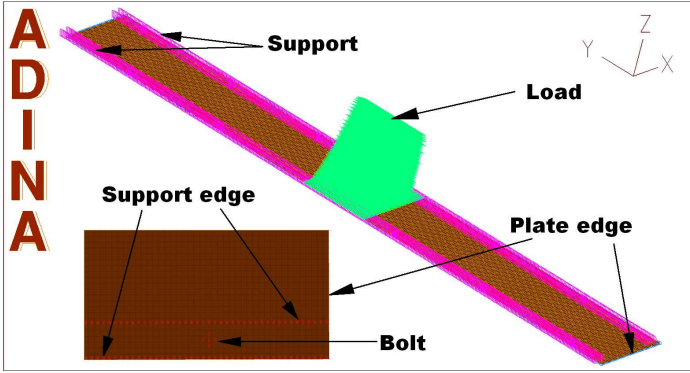


Figure 2.27. FE model of the proposed plate-shape device.

the beam-shape device (see Section 2.3.3). The contact stress distribution, i.e., the tire vs. bending plate interaction, corresponded to the not-driving wheel, see Fig. 2.10(b). The constant and the same, in all of the modelled cases, horizontal tire interaction velocity as well as the constant summarize load value were applied.

The research were perform for sensitivity analysis of the sensors density distribution on its summarize response. The three parameters were use as a variable for analysis:

- load positions were modelled in fifty locations where the middle of the contact stress distributions area was in the range (50, 51, ..., 100 cm) from the plate edge,
- stress distributions width was modelled in six variants (8, 15, 22, 30, 45 and 60 cm) as a consequence of different width of car tires,
- sensors distributions density was modelled in six variants (5, 10, 15, 20, 25 and 30 cm).

The examples of the sensors responses are shown in Fig. 2.28. The presented results correspond to sensors distribution with 10 cm density while width of the stress distribution area was 30 cm, located in the very center of modelled plate.

The load identification algorithm was assumed to be based on the sensor signals peak values. The sum of the signal responses should be constant i.e., insensitive to load location since the infinite number of the sensor will be considered, which is unobtainable in practice. Hence, the analysis has been performed. General objective was to determine, the minimum number of the sensors required to make the sum of its responses insensitive to load location in the accepted range, i.e., the average change below 1%.

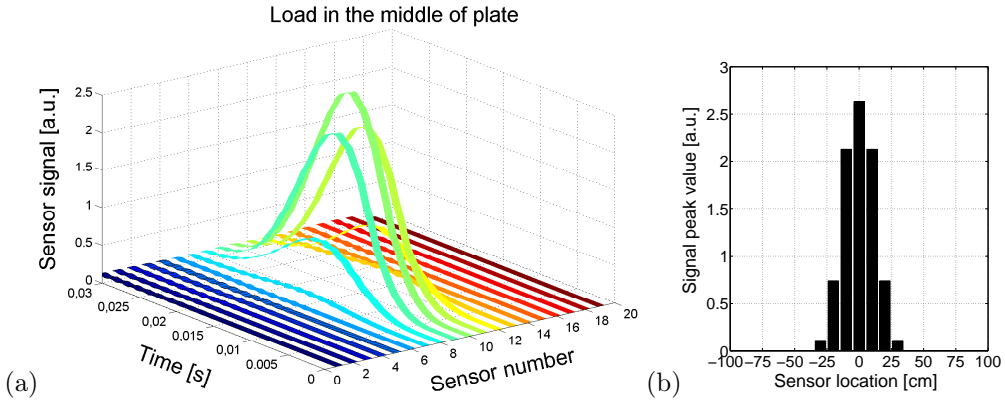


Figure 2.28. Example of numerical results: (a) sensor signals in time domain, (b) sensor signals pick values.

The results of the sensitivity analysis are shown in Fig. 2.29. Figure 2.29(a) represents the percentage change of sum of the sensor signals pick values for the different sensor distribution density and the width of an contact area. Figure 2.29(b) shows the average percentage change of the sum of the sensors signals obtained for different variants of the load width.

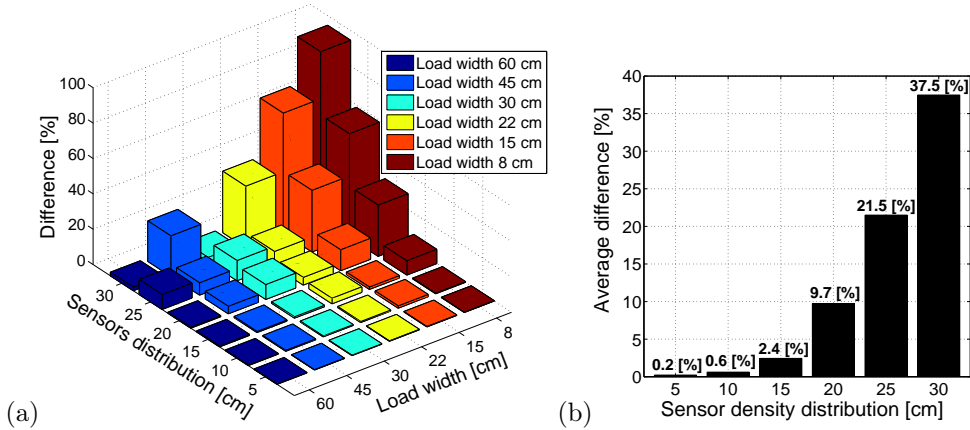


Figure 2.29. Sum of the sensors responses: (a) percentage difference as a function of sensor signal distribution density and the width of load area, (b) average percentage difference as a function of sensor signal distribution density.

Analysis enable to draw the conclusion. It was found that the sum of the sensor signals peak values were not constant with regard to the load position. The strong influence on this parameter change have the sensors density distribution as well as it depends on width of the applied load area. Its smaller fluctuations

were observed in case of the higher sensors density distribution as well as wider load area. It can be summarized that the accepted results were obtained for sensors distribution density of 10 cm. Hence this distribution density will be used in the constructed device.

### Plate width effect

It is known that the larger width of the WIM detector results in the longer period during which the force is measured i.e, longer tire-detector contact. This generally provides the accuracy advantage for wider detector in comparison to the narrow sensor. Nevertheless, a significant advantage of narrow strip detectors is that installation is much easier and it takes considerably less time than for wider sensors [76] which lead to lower price for such systems.

The numerical tests presented in this section were devoted to the sensitivity analysis of the plate width. The load identification algorithm was assumed to be based on the axle signal peak values. Hence, the test were performed for analysis of plate width effect on the observed sensor signals.

In order to decrease the numerical costs for analysis, the FE beam models were used. Their length simulated the width of the plate-shape device. The sixteen models characterized by the various length (in the range from 5 to 75 cm) were prepared. Each of them was loaded by two variants of axle load contact stress distributions which were consequently corresponding to the not-driving wheel and driving wheel, see Fig. 2.10. These variants were characterized by the analogical contact stress length, i.e., 20 cm and the same total loads values. Nevertheless, different amplitude, i.e., the maximal value of load in those two variants were used. Namely, the proportion between the amplitudes was equal to 1.4.

The obtained simulation results are shown in the Fig. 2.30. The results correspond to the signals peak values proportion i.e., the signal amplitude for the driving wheel to the signal amplitude for the not-driving wheel with regard to the detector dimensions i.e., representing the bending plate width. The analysis enables to conclude that the wider detector i.e., bending plate, the smaller effect of the shape contact stress distribution on the sensor response is observed. The general conclusion can be drawn that the peak value of the signal can be useful for axle load estimation only when the detector is wide i.e., considerably wider than the tire pavement contact area i.e., latch footprint length. The author of this thesis believes that since the detector is wider than the 40 cm, the load estimation might be performed on the basis of signal peaks values, while the more narrow detectors require estimation on the basis of signal area integration.

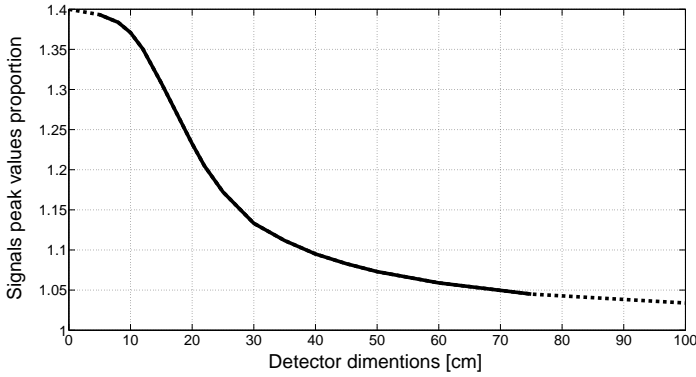


Figure 2.30. Contact stress distribution effect with regards to the detector dimensions.

### 2.4.3 Road installation of the plate-shape device

The concept of the plate-shape WIM device was tested in practice in the road test research. A rectangular shape plate, with 8 mm thickness, was equipped with the set of fifteen piezoelectric sensors, see Fig. 2.31(a). The same type like in the beam-shape WIM device sensors one was used. Its distribution was regular with 100 mm spacing. Total number of piezoelectric strain sensors was fifteen and additionally two strain gauges were used. The plate dimensions, i.e.,  $280 \times 2000$  mm were limited by the dimensions of commercially available steel-concrete flume drainage which was used as the plate’s support. The plate was fixed by means of bolts to stale frame and supported along its longer edges. The top surface of the plate was equal to the pavement level, see Fig. 2.31(b).

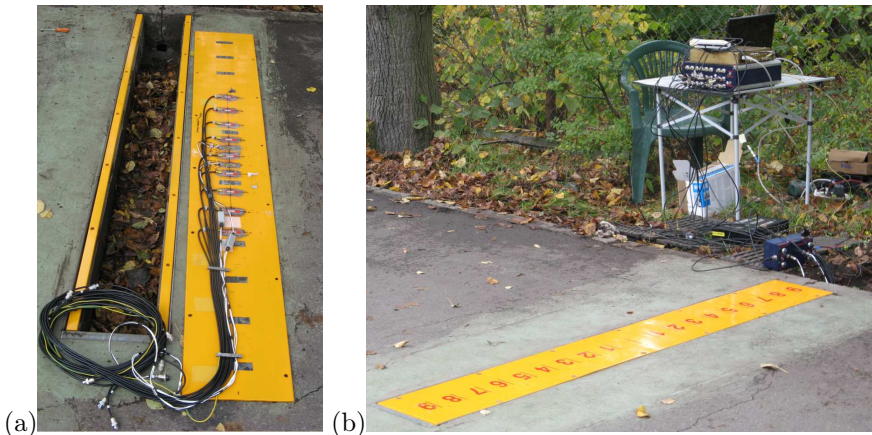


Figure 2.31. View of the plate-shape device: (a) before assembly, (b) after assembly in the road.

### Calibration process

The first step of the road experiment was done for the calibration of the device. All of the piezoelectric sensors fixed to the bottom side of the plate were the same type. Nevertheless, they might have characterized slightly different sensitivities as well as the amplifying factor in the used charge amplifier might not have been the same in all of the channels. Hence, this research were devoted to obtain the proportional calibration factors for all of the piezoelectric sensors. The other aspect was to find the mass-voltage calibration relation for the device.

The numerical test enables to conclude that, if the same vehicle, i.e., same axle load passes few times over the plate-shape device with different lateral position, the sum of the signals generated by the sensors should be close to constant ( $>1\%$  differences), i.e., sensors global response is almost insensitive to position since all of the used sensors will characterized by the same sensitivity. Thus, the objective was to find the multiplying factor for each of the sensor which would enable to unify the sensors sensitivity.

The calibration procedures consisted of repeatedly passing test of pre-weighed vehicle over the bending plate. One vehicle passed several times. The constant velocity and the same weight were used. All of the passes were perpendicular and completed with minimal speed in order to obtain maximal repeatability of passes and to minimize the dynamical effects. The lateral position of the vehicle was changed with 10 cm spacing. The example of the axles-signals measured by the set of the sensors is shown in Fig 2.32.

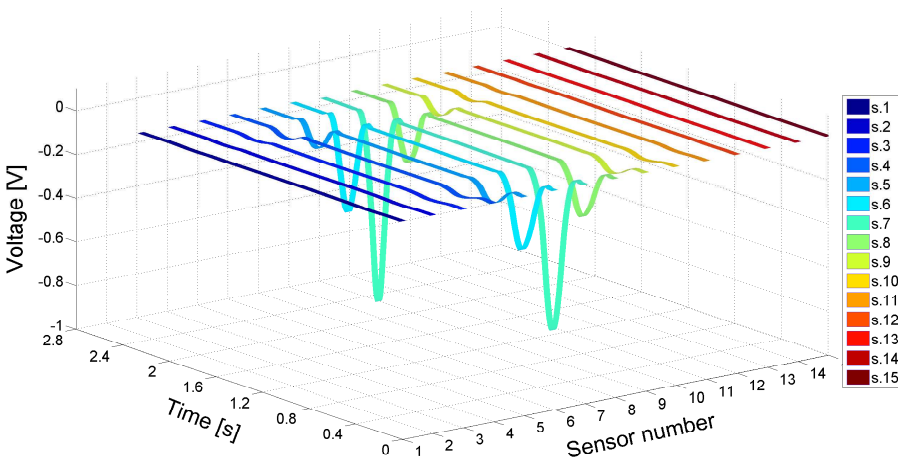


Figure 2.32. An example of the axle signals measurements obtained while calibrations of the device: vehicle velocity 3.5 km/h, wheel later position 68 cm.

In order to calibrate the device two-axle vehicles were used. The axle loads front  $AL_{FM}$  and rear  $AL_{RM}$  were statically measured. The testing vehicle was motorcycle with relatively small foot print. Therefore, the identification procedure might be based on the signals peak values. The following formulas were used,

$$AL_{Fi} = \sum_{i=1}^n \beta_i a_{ij}, \quad (2.10)$$

$$AL_{Ri} = \sum_{i=1}^n \beta_i b_{ij}, \quad (2.11)$$

where  $a_{ij}$  – the amplitude of front axle load signal produced by the  $i$ -th sensor during the  $j$ -th pass,  $b_{ij}$  – the amplitude of rear axle load signal produced by the  $i$ -th sensor during the  $j$ -th pass,  $\beta_i$  – the calibration factor for  $i$ -th sensor,  $AL_{Fi}$  and  $AL_{Ri}$  – the identified front and rear axle loads.

The objective of the calibration process is to determine the calibration factors  $\beta$  for all of the sensors making them identically sensitive. The considered system of equations is overdetermined i.e, the sensor number is lower than the number of passes. The calibration procedure utilizes the method of least squares. There is searching vector  $\beta$  which minimizes the difference between the observed values i.e., determined by Eq. (2.10), Eq. (2.11) and the expected values, i.e.,  $AL_{FM}$  and  $AL_{RM}$ . The procedure can be presented by following formula:

$$\left\| AL_{FM} - \sum_{i=1}^n \beta_i a_{ij} \right\|^2 + \left\| AL_{RM} - \sum_{i=1}^n \beta_i b_{ij} \right\|^2 \rightarrow \min. \quad (2.12)$$

The calibration results are shown in Fig. 2.33. Figure 2.33(a) illustrates the primary percentage change for each of the passes in regard to the mean value for all of the passes before sensor calibration. Figure 2.33(b) presents the results after applying obtained calibration factors. The significant decrease of the discrepancy was obtained after sensors calibration (notice different scales in Fig. 2.33).

### Tests of the plate-shape device precision

The precision of the plate-shape device was tested. The methodology based on the axle signal peak values tuned by the sensors calibration factors (see Eq. (2.10)) was used. The preweighed vehicle was used for test. It passed over the device several times with the different lateral positions. The examples of the sensor signal time and amplitude responses are shown in Fig. 2.34. It corresponds

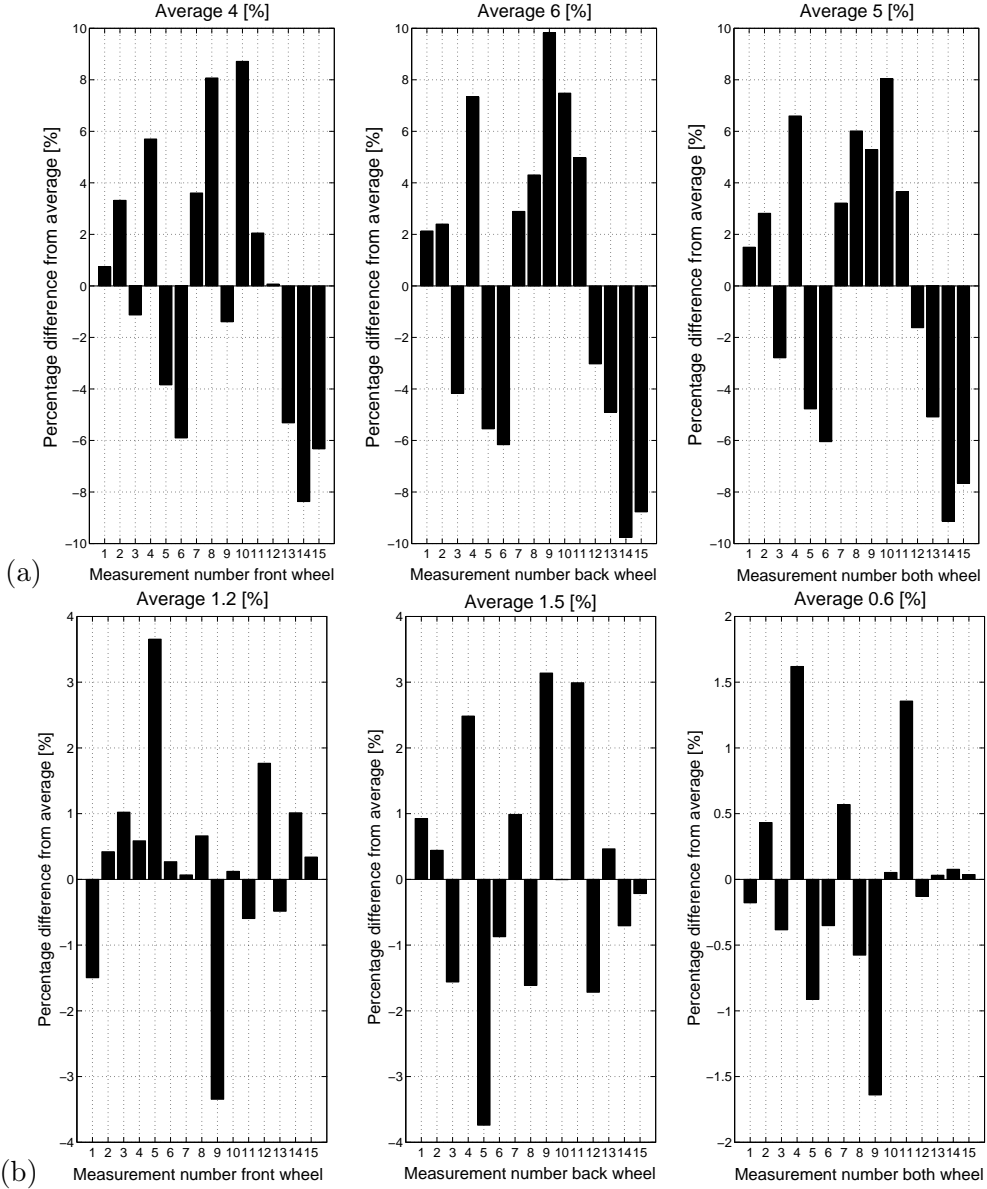


Figure 2.33. Average percentage precision: (a) without calibration, (b) after applying the obtained calibration factors.

to the motorcycle wheels passing over the device with approximate 40 km/h. The bigger signal amplitudes corresponding to the back wheel is clearly observed, see Fig. 2.34(b).

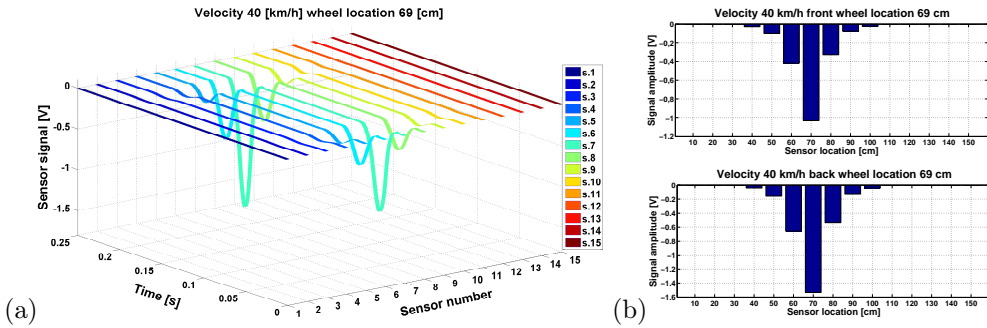


Figure 2.34. Sensor signal: (a) time-domain response, (b) amplitude response.

The performed trials enable to check the device precision. Figure 2.35 presents the percentage accuracy of identified values by the device with respect to the accurate (statically measured) axle loads for many trials. Obtained results enable to conclude that the precision of the plate-shape device was better than 10%. Therefore, it was approximate two time higher than in case of the beam-shape device.

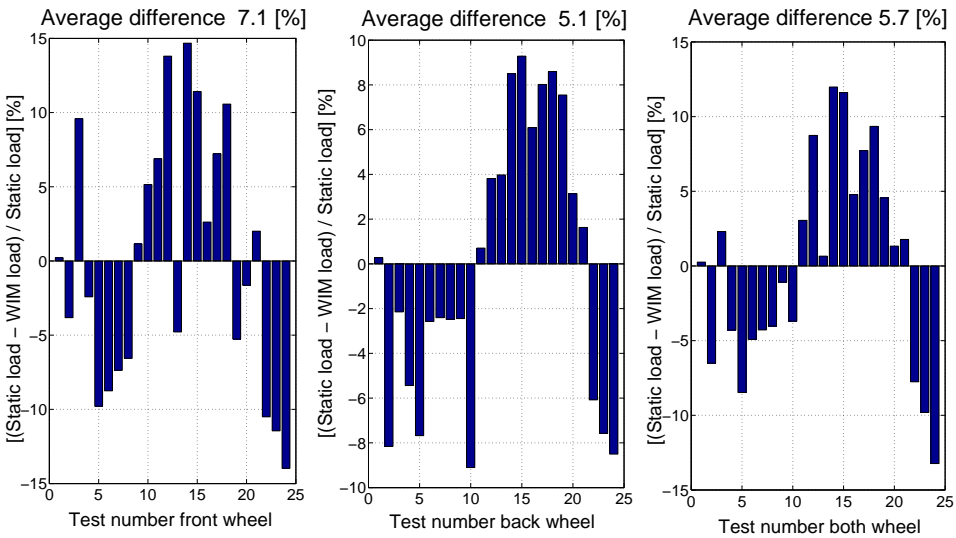


Figure 2.35. Precision of axle loads identification.

### Velocity tests

As the final step of the research, the velocity effect was tested. The vehicle was passed over the device with different speeds in the range of 20–80 km/h. The maximal one was limited by the safety reason, i.e., location of the device in urban areas. The results examples are shown in Fig. 2.36 in order to quantitatively present the velocity effect. The graph presents the voltage signal obtained from the strongest responding sensor, i.e., the closest one to the excitation (passing wheel of vehicle). The four velocity variants are shown. Contrary to the beam-shape, unprofitable vibration of the plate-shape device was not observed. Compare Fig. 2.25 to Fig. 2.36 where the signal shape was similar for all used velocities. The author of this thesis believes that even for higher velocities (more than 100 km/h) the axle load identification of vehicle passing over plate-shape device would be feasible, this was proved by modal analysis of the plate (see Appendix E). The measurements performed by the plate-shape device shows that the increase of velocity leads to change of the front and back wheel signals proportions (see Fig. 2.36). This could be caused by an air resistance effect acting on motorbike or an effect of applied acceleration. To find it out, more thorough research is needed.

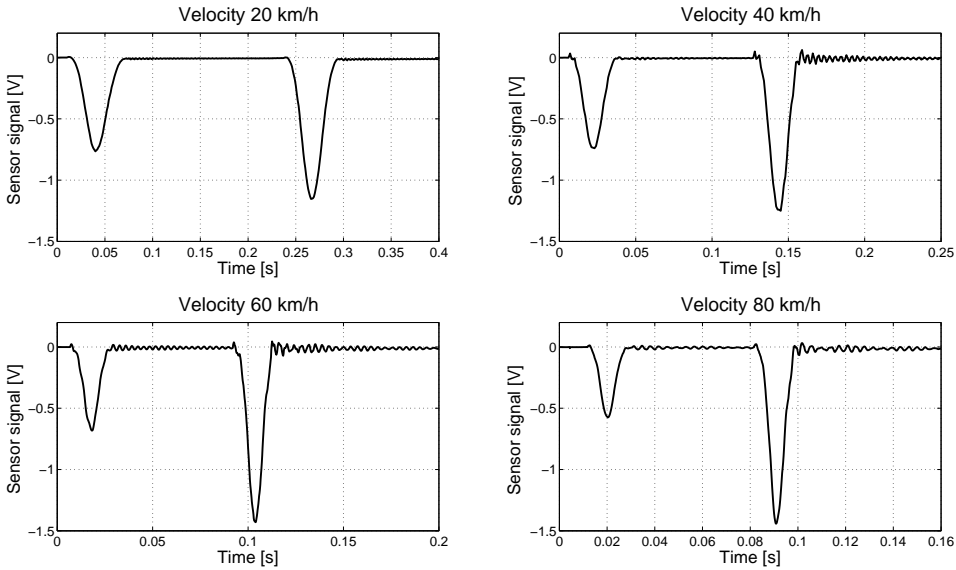


Figure 2.36. Velocity effect.

## 2.5 Final remarks

The analysis presented in this chapter proved the feasibility of application of the proposed Weigh-in-Motion devices. The methodology utilizing beam-shape device enables to identify the axle load with  $\pm 20\%$  accuracy while the plate-shape one shows the precision in range of  $\pm 10\%$ . The precision can be increased using more devices located parallelly in order to detect the axle load few times. The accuracy of the presented methodologies strongly depends on the quality of the measurements and calibration process precision.

The beam-shape device shows its high sensitivity to the velocity. For the higher velocities strong beam vibrations were observed. As a consequence, the velocity operation limitation is an important disadvantage of this idea. Contrary to the plate-shape device, no velocity limitation in the measured range was noticed.

Crucial for the proposed inverse problem algorithm dedicated to beam-shape device is the scrupulous preparation of the map of the calibration factors of the sensors signals in terms of various excitation conditions. This map can be also obtained numerically. It was checked that the beam-shape device algorithm should consider few parameters: the load position in terms of the length of the beam, velocity of the vehicle and width of its tire affecting on the device.

The piezoelectric sensor distribution density and plate width were found to be important factors for load identification precision. The increase of sensors number results in smaller fluctuation of the summarized sensors signal in terms of load position. The plate width increase results in smaller sensitivity of the structure to load distribution shape.

It was proved that the peak values of the signal cannot be the accurate representation of the vehicle weight, since the tire footprint is considerably larger than the width of the WIM detector. In this case the axle signal integration procedure is needed. As a consequence, the precise vehicle velocity identification is required since the axle signal is approximately inversely proportional to the speed.

It was found out that in case of using the piezoelectric sensors for measurements, it is very important to use proper amplifiers in the measurements set-up. It was proved that the considerably better results can be obtained by application of charge amplifiers instead of the voltage ones.



# Weigh-in-Motion system for the railway transport

## 3.1 Introduction

The previous chapter considered the dynamic load identification using the Weigh-in-Motion technology for the road transport. The current one is strongly related to this subject. The WIM technology for the railway transport is taken into account. The state of the art of the dynamic weighing systems for railways is presented at the beginning of the chapter. The main considerations are focused on the development and practical implementation of a new WIM system for railways, which constitutes a part of a larger Structural Health Monitoring (*SHM*) system dedicated to railway truss bridges. The chapter presents results of measuring sessions carried out *in situ* by means of a few kinds of sensors. A velocity and train load effects were considered while the realization of an experimental tests. An algorithm of indirect identification of load based on the analysis of strain histories in the rail has been proposed. A numerical model of wheel-rail-support has been calibrated to experimental data. Numerical simulation has pointed out important factors, that need to be considered in order to obtain proper values of the identified dynamic forces exerted by a running train on the rail.

## 3.2 A review of the existing railways WIM systems

The need to monitor and control the dynamic influence of trains on railway track has emerged from the infrastructure administrators as a consequence of separation from the train operators (carriers) and establishment of free-market relations between them. Since then, the administrators have started to charge the carriers for using the railway track.

In general two approaches to determination of dynamic traffic load are possible: either use a railway car equipped with sensors [6, 99, 100] or perform measurements by means of external sensors fixed to the infrastructure outside the train. The first method is not frequently applied and it seems to be less effective from the practical point of view. Hence, the second approach has been more deeply reviewed here.

In the past one of the first techniques of identification of train load was successfully applied using an instrumented bridge [101, 102]. This approach mentioned in the previous chapter is also applicable in road transport and consequently named Bridge Weigh-In-Motion (B-WIM). Most frequently, standard strain gauges [103] are used as sensors in such WIM applications. Recently however, the fibre optic sensors have been gaining more and more attention, especially for newly constructed huge bridges. In existing structures, the fibre optic sensors can be mounted on the surface of the bridge deck [81]. For newly designed bridges, the fibres are usually embedded inside the structure [104, 105] at the stage of its construction. It allows for permanent monitoring of such bridges from the very beginning of their exploitation.

At the time, there are a few types of commercially available WIM systems for railways. One of the method is the indirect measurement of the vertical force exerted on the rail and further transmitted to the track support. This methodology requires a special preparation of the track by equipping it with a solid foundation. The foundation has to be well integrated with the railway track, therefore installation of such systems is both time- and cost-consuming. In this application, strain gauges are mounted on the foundation not on the rails themselves. The main advantage of the mentioned methodology is a high precision of the identified load values. The price to pay for the precision is however a strict velocity limitation for trains during measurements [106, 107], which should be in the narrow range 3–8 km/h [108]. This is due to the fact that the foundation should not be subjected to excessive vibrations in order to collect high-quality measurements. This can be regarded as a disadvantage of the system.

In order to overcome the velocity limitations, the accuracy of results must be sacrificed. One can propose load identification methods utilizing the measurements of rail strains using various sensors. As the rail is in direct contact with the train wheels, the methods are able to provide estimations of relatively many parameters like: individual wheel and axle loads, gross weight of each railway car, the number of railway cars, total train weight, velocity, direction of movement, even the state of the wheel e.g., possible polygonization.

The variety of the identified parameters and the lack of velocity limitations during measurements are the main advantages of the mentioned methods. Nevertheless they are characterized by poorer precision of the parameter estimation (practically  $\pm 5\%$ ), which can be considered as a drawback.

The classification of the mentioned WIM systems for railways can be performed on the basis of the type of used sensors and also on the location of their mounting. One of the first systems was utilizing strain gauges [109] welded to the neutral axis or mounted on rail foot [110]. Recently, the growing competition for the strain gauges are optical fibers. They can be mounted either to the side of the rail [111], or to the foot of the rail with the help of special clamps [112] as shown in Fig. 3.1 (a). A great advantage of the optical fibres over strain gauges is their insensitivity to electromagnetic disturbances.

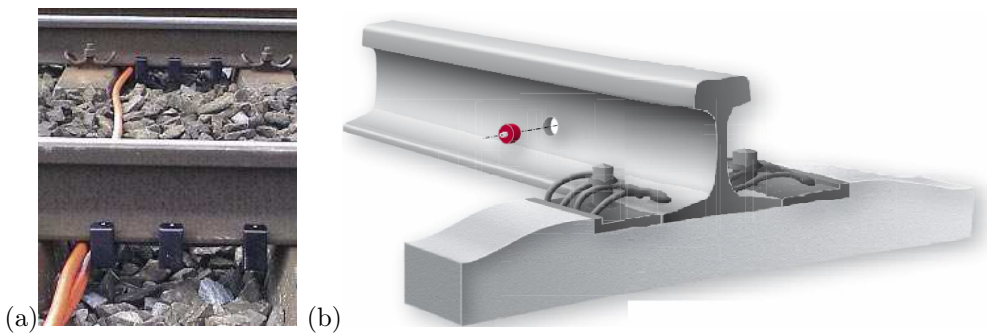


Figure 3.1. Example of WIM application railways: (a) optic fibers sensors Gotcha [112], (b) intrusive quartz sensor Kistler [113].

There are also intrusive solutions of WIM applications for railways. The idea is to bore a small hole in the rail web and insert a sensor into it. One option is a quartz force sensor of cylindrical shape [113] as shown in Fig. 3.1 (b), another one is a sleeve equipped with strain gauges from inside [114]. The direct measurement of force in the case of railway transport is practically difficult to perform because of high magnitudes of train loads, which would mean the use of force sensors of considerable dimensions. Hence the indirect methods i.e., strain measurements are more often applied.

### 3.3 The proposed WIM system

It should be emphasized that all of the described solutions in the existing rail-WIM applications involve a considerable cost. One of the motivations of the

author is to propose an alternative to the existing solutions, characterized by similar reliability and accuracy at an affordable cost. Another motivation is to integrate the proposed WIM solution with the damage monitoring block of the mentioned SHM system which is schematically presented in Fig. 3.2.

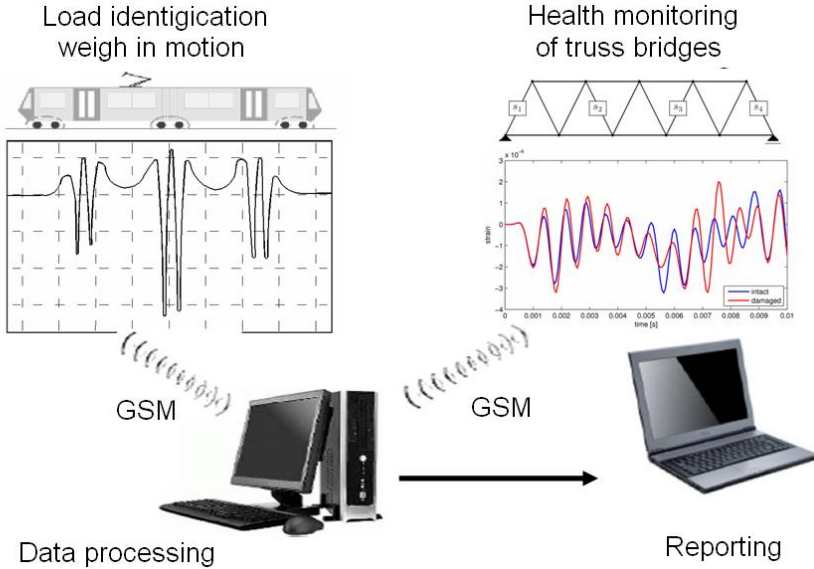


Figure 3.2. General scheme of the system for SHM of truss bridges integrated with the rail-WIM system.

### 3.3.1 General idea of the WIM system for railways

The proposed solution relies on a nondestructive way of recording histories of strains evolving in the rail due to train motion. The strains are collected by piezoelectric sensors mounted on the bottom part of the rail foot in between the sleepers as schematically shown in Fig. 3.3, depicting major elements of the proposed system.

In the majority of applications, piezoelectric sensors are used as accelerometers. In this work however, they measure strains similarly to strain gauges and optical fibres. Two kinds of piezoelectric sensors are considered – the popular ceramic ones and the more sophisticated fibre-based ones. The performance of both types of sensors is similar. They are able to cover an extremely wide range of frequencies (0.1 Hz – 100 MHz) due to high stiffness of piezoelectric materials. Similarly, the measurement range in terms of voltage magnitude (signal

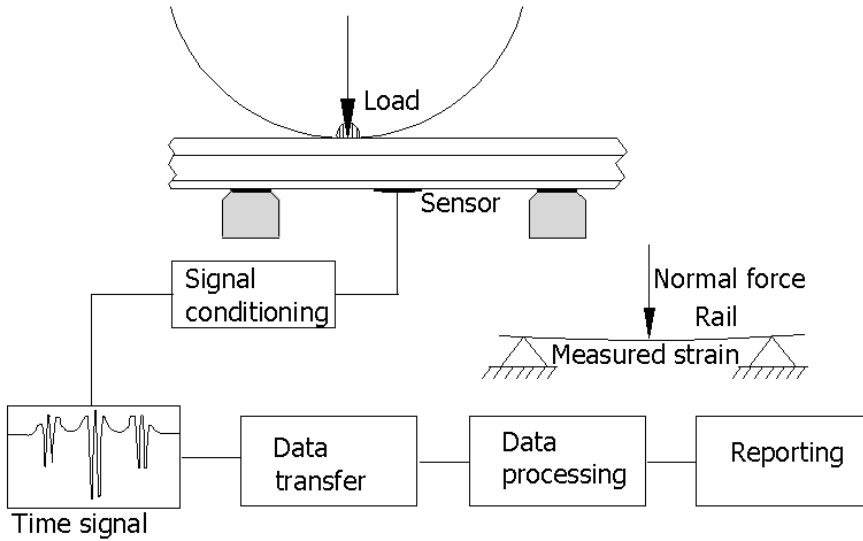


Figure 3.3. Scheme of data acquisition and processing for the proposed WIM system.

strength) reaches up to 100 million for piezoelectric sensors, which is absolutely distinctive compared to other sensors. Other advantages include e.g. less laborious surface polishing compared to strain gauges or lower cost of driving electronics compared to optical fibres. The piezo-fibre-composite (PFC) sensors are more durable as they consist of piezo fibres embedded in polymer which makes them waterproof and insensitive to electromagnetic noise. However the PFCs are much less attractive than the ceramic piezo-sensors as far as price is concerned. Therefore the author believe that the ceramic piezo-sensors, well-protected against environmental factors on site, are a cost-effective alternative for the other strain sensors.

The electric signal (proportional to strain) from the piezo sensor is first preconditioned by amplifying, filtering and digital sampling operations. The objective of this signal processing is to have the signal in its optimal form before sending it to a remote centre using wireless transmission. For security reasons, it is planned to use an encrypted transmission using available internet cryptographic protocols, e.g., Transport Layer Security (TLS). When the data is captured by a remote server, it is first archived and then analyzed. It is planned to make the results of the analysis available to the user via an internet browser with password protection.

In order to improve the reliability and accuracy of the proposed WIM system, some extra sensors should be applied. It is planned to mount sensors in pairs on both rails. It is also important to design such a way of sensor mounting, which makes the devices well hidden in the railway track in order to avoid devastation. An important issue is to mount the sensors in reasonable time without much interference with the existing infrastructure, not to expose the rail traffic to serious disturbances.

An important aspect of hardware is to supply power for the system in a reliable manner. In order to make the system independent, the power will be supplied by accumulators permanently charged by photovoltaic modules. For the sake of energy saving, the system will be active only during the ride of the train over the WIM measuring point. When the train is gone, it will switch to a passive mode. Additional sensors, operating in a standby mode to detect the coming train, are needed to realize this energy saving idea.

### 3.3.2 Proposed methods of dynamic load identification

The load identification problem belongs in general to the class of inverse problems presented in [6, 12, 115]. One way to solve such a problem is a pattern recognition approach. Roughly speaking, it consists in comparing an analyzed pattern with a set of already existing patterns and specifying the most similar one from the set.

In the proposed system, the pattern recognition scheme has been adopted as the first option of the methodology employed to solve the inverse problem. In the mentioned method the crucial task is to prepare a data base containing a collection of strain histories for diversely loaded railway cars weighed in various operational conditions. A component  $i$  of the data base may be a strain history  $\varepsilon_i$  which is a function of essential factors e.g., magnitude of load  $Q$ , number of axles  $n_a$  in a car bogie, train velocity  $v$ , outside temperature  $T$ , etc., influencing the signal shape in time  $t$

$$\varepsilon_i = f(Q, T, t, v, n_a, \dots). \quad (3.1)$$

The biggest problem is where to take the data from to fill in the data base. The data can be obtained from experiments using many railway cars of known load distribution but this way is inefficient due to the time and cost involved. An alternative is to build a numerical model. This is a much more friendly approach, provided however that the model is conformable with measurements, which again implies some experimental work in a limited range to tune the model to experiments.

The pattern recognition method consists in comparing the actual single measurement  $\varepsilon_{actual}$  with the  $i$  ones previously stored in the data base. The point is to retrieve the most similar (in a defined norm) case [26] with the assigned characteristic parameters ( $Q, T, t, v, n_a$ , etc.) from the data base. Thus the procedure identifies such a value of load  $Q_{id}$  which is a result of the following problem of optimal case search:

$$Q_{id} = \operatorname{argmin}_i \left[ \varepsilon_{actual}(Q, T, t, v, n_a) - \varepsilon_i(Q, T, t, v, n_a) \right]^2. \quad (3.2)$$

In order to facilitate the process of data retrieval, one can use sets of in-advance prepared amplitude variations of the measured signal depending on just one driving parameter and keeping the other ones constant. However this is also quite laborious because numerous cross-relations need to be established and some parameters should be known beforehand.

Due to the problems with building a reliable data base, another option of load identification considered by the author is a calibration of the measured signal in the on-line mode. The idea is to scale the measured signal for every passing train individually, knowing the mass of the locomotive corresponding to a reference load level  $Q_{ref}$ . Good news is that freight trains are usually towed by standard locomotives of electrical drive, whose mass is quite stable, not influenced by the amount of fuel. For instance Polish Railways usually use the ET-22 locomotives of 120 tons with possible mass deviation of  $\pm 1.5$  tons, which opens up the potential for auto-calibration. For all freight trains it is feasible to find a scaling coefficient  $R$  between the reference signal  $\varepsilon_{ref}$  measured for the locomotive and the corresponding value of a priori known load  $Q_{ref}$ :

$$R = Q_{ref} \cdot \varepsilon_{ref}^{-1}. \quad (3.3)$$

When the relation for the locomotive is established, it is possible to determine the load of other railway cars  $Q_{id}$  by means of the following equation:

$$Q_{id} = R \cdot \varepsilon_{actual} \cdot A_d(n_a). \quad (3.4)$$

The proposed on-line calibration seems to be indifferent to environmental influences such as temperature or condition of the railway track. It is caused by the fact that the parameter  $R$  includes these influences. It may reach different values for the same train in different seasons of year, for instance, but we do not look for a constant coefficient. The role of  $R$  is to provide a reference point for rescaling the signal regardless of environmental conditions. One important factor however should be taken into account, the locomotive bogie and the

freight car bogie usually do not have the same number of axles. This implies that the load distribution exerted by the bogies on the track will be different. Hence the influence of the axle distribution coefficient  $A_d(n_a)$  on the identified train load must not be neglected, as can be noticed in Eq. (3.4). Results of numerical analysis, presented further in this Chapter in Fig. 3.18, show that the coefficient  $A_d(n_a)$ , unlike  $R$  (cf. Fig. 3.7), varies in a non-linear way.

Except for the magnitude of dynamic load  $Q_{id}$ , other useful information from the strain history can be also determined. One of such parameters is the train velocity  $v$ . The easiest way of its calculation is to use responses from two sensors mounted in a known distance  $D_S$  on the same rail. It is a reasonable solution because the additional piezosensors may also serve as extra WIM sensors providing more data for averaging. The ratio of the distance  $D_S$  to the time delay  $\Delta t$  between two signals generated by two successive sensors allows for trivial calculation of the train velocity. However it must be assumed that the train velocity on the section  $D_S$  is constant. It is a justified assumption as the distance  $D_S$  does not exceed a few meters in practice.

The proposed method of WIM measurements enables to determine the loads from individual axles by Eq. (3.2) or Eq. (3.4) and the train velocity by simple calculation. The type of a railway bogie may also be roughly identified by looking at time intervals corresponding to subsequent bogie axles. This allows for calculating the distances between the axles and comparing the values with catalogue dimensions for standard railway cars.

A more challenging analysis is the identification of wheel damage, especially polygonization. Irregularities in wheel shapes would cause repeated high frequency components in the recorded signal. Knowing the wheel diameter and parameters of the ride, it should be possible to identify the wheels in which the effect becomes manifest.

In order to make the identification easier, the measured signals should be pre-conditioned. A low-pass filter is applied to extract the principal contents of the signal corresponding to the car mass while a high-pass filter is used to provide a good representation of signal oscillations accompanying the wheel irregularities. In practice it might be a reasonable compromise to apply a band-pass filter with a variable frequency range e.g. dependent on the train velocity.

### 3.4 Pioneer installation of the proposed WIM system *in situ*

Measuring sessions were carried out since 2007 till 2010 in a location selected together with Polish Railways. The SHM system mentioned in 3.3.1 was

mounted on a typical truss railway bridge spanning a channel in Niepořet near Warsaw. The accompanying WIM system was installed on rails ca. 40 m away from the bridge. A scheme of the integrated SHM system with the location of WIM sensors is depicted in Fig. 3.4. The investigation described later in the chapter is focused on identification of the dynamic load only.

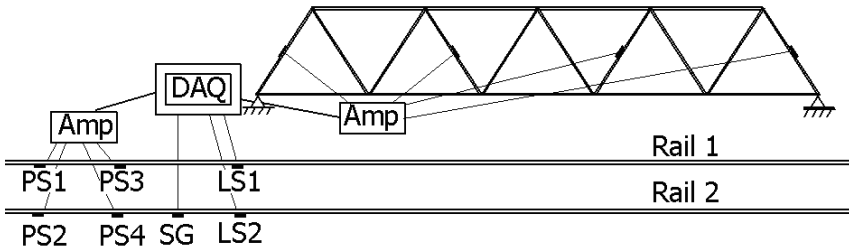


Figure 3.4. Components of the proposed WIM system during *in-situ* tests:  $PS1$ ,  $PS2$ ,  $PS3$ ,  $PS4$  – piezoelectric sensors,  $SG$  – strain gauge,  $LS1$ ,  $LS2$  – laser sensors recording displacements,  $AMP$  – amplifier,  $DAQ$  – data acquisition unit.

### 3.4.1 Experimental tests of the piezo-based WIM system

Two types of piezoelectric sensors were used in experimental tests – piezoelectric fibre composite  $PFC$  sensors shown in Fig. 3.5(a) and sensors made of the piezo ceramic material  $PZT-7$  shown in Fig. 3.5(b). For comparison, strain gauges in the half-bridge configuration were used, see Fig. 3.5(c). Additionally, laser sensors for measuring vertical displacements were mounted beneath the rail foot, see Fig. 3.5(d).

Figure 3.6 illustrates a time signal collected by the piezo-sensor during a passage of a freight train at approx. 40 km/h. The wheels can be identified as significant peaks of the signal. The positive signal values are observed between the axle peaks. Each train bogies running over the WIM measuring point can be recognized by characteristic separated groups of peaks. The first part of the signal (approx. 3 s) corresponds to a locomotive with two three-axle bogies, the rest to cars with two-axle bogies. It can be noticed that the first seven towed cars were lighter than the last four ones.

The basis for identification of train loads are the peak values of the time signal. In order to scale the signal in terms of mass, a reference level  $Q_{ref}$  is needed. This must be set in a calibration procedure e.g., the on-line calibration described in Section 3.3.2. The mass of a car is calculated as a sum of peak values from all axles belonging to this car. In order to improve the reliability of

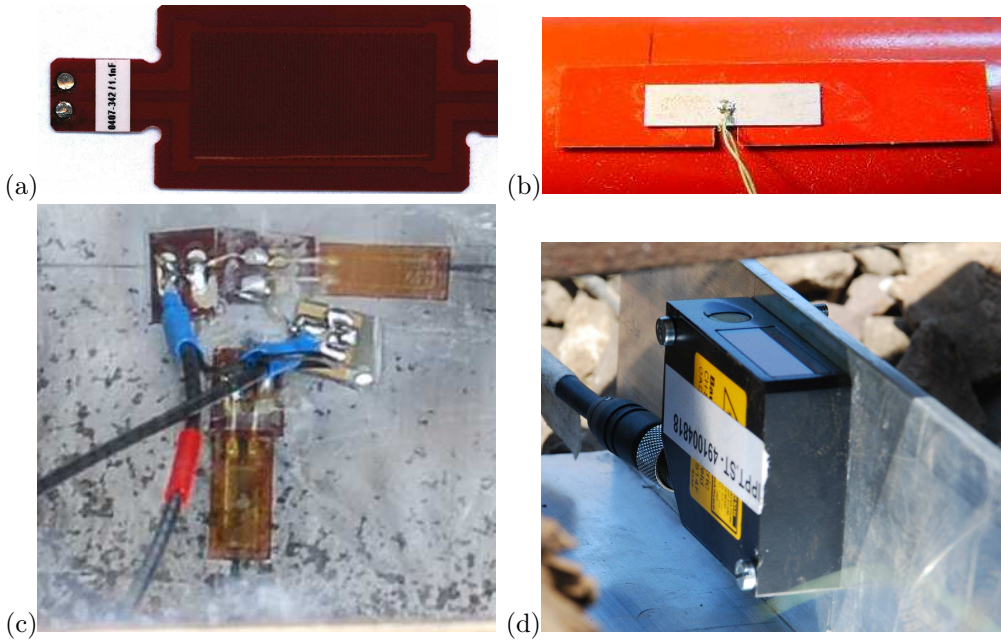


Figure 3.5. Sensors used in experimental tests: (a) piezoelectric fibre composite sensors *PFC*, (b) piezoceramic sensors based on the *PZT-7* material, (c) half-bridge configuration of strain gauges, (d) laser displacement sensor.

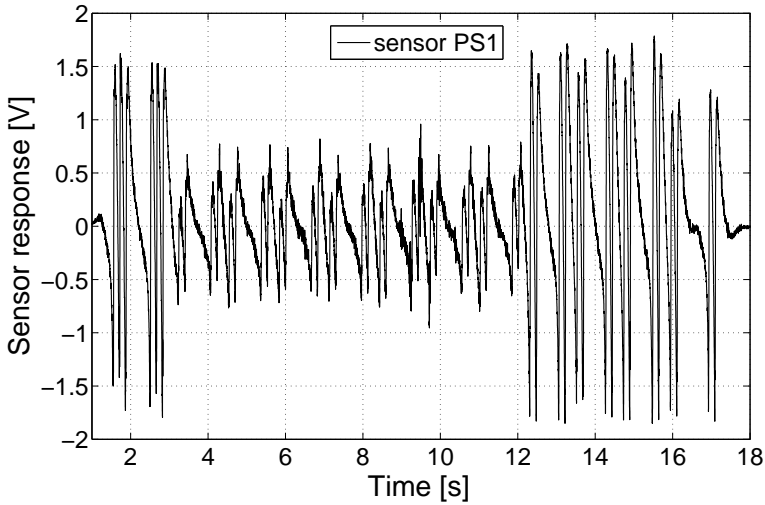


Figure 3.6. Time signal from the piezo-sensor as a response to passage of a freight train.

identification, one spare sensor should be mounted in each location. Then the calculation can be performed by means of pairs of sensors. If both the sensors work fine an average value can be calculated, if not – a measurement from just one sensor, providing trustworthy responses, should be considered.

Calibration of the proposed dynamic WIM system may be performed by a quasi-static (at 5 km/h) weighing system using strain gauges. Knowing the mass of a locomotive and each car in the train from quasi-static measurements, a relation between mass and voltage recorded by piezo-sensors of the proposed WIM system at regular train speed can be found. The results of such operation are presented in Fig. 3.7. It can be observed that the relation between measured mass and recorded voltage is linear despite generally poor condition of the railway track in the place of installation of the WIM system.

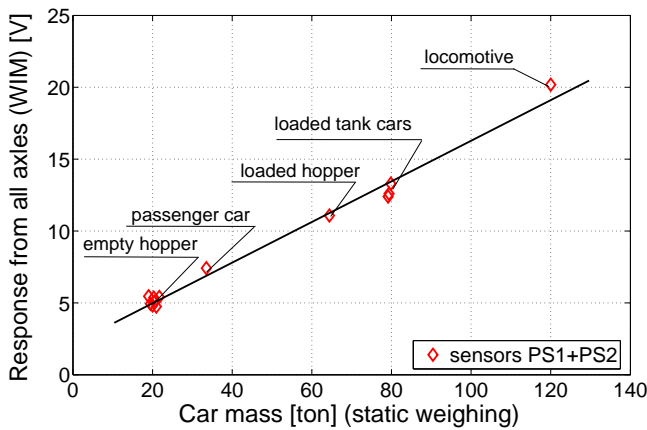


Figure 3.7. Mass-voltage relationship obtained on the basis of calibration from static weighing.

During the passage of the train with known masses, vertical displacements of the rail were measured (see Fig. 3.8). The results correspond to the ones presented in Fig. 3.6, picturing a different quantity (voltage) for the same train passage. In the displacement plot, the whole bogies rather than separate axles can be recognized. The lighter and heavier cars can be clearly distinguished. The displacement measurements were not used for weighing trains. They were rather carried out for having as much data as possible at the stage of tuning the numerical model to experiments, which will be discussed later. In general, the track in the WIM area was in a very poor technical condition. The rail displacement was about one order of magnitude higher than cited in the literature [116, 117] and recommended by design standards.

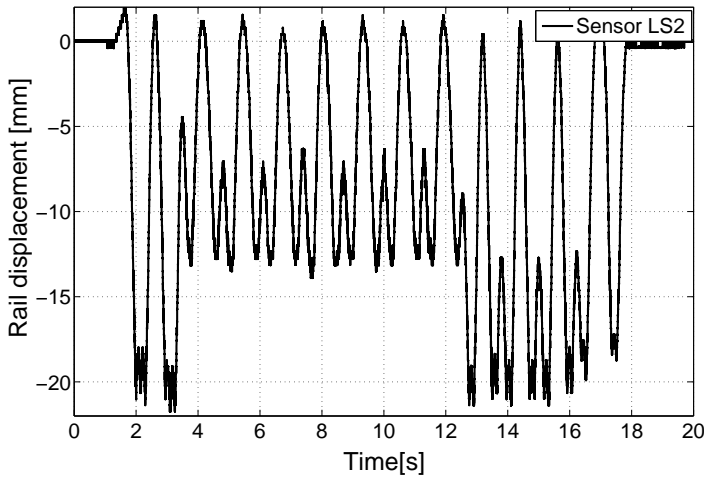


Figure 3.8. Vertical displacements of rail recorded by the laser sensor.

### 3.4.2 Performance comparison of piezo-sensors and strain gauges

One of the objectives of the section is to compare the performance of the piezoelectric sensors and strain gauges. Both the measurements, corresponding to the passage of the locomotive ET-22 at the velocity 40 km/h, are presented in Fig. 3.9(a). The curves match in the lower part and vary in the upper one. Analyzing the problem further, both the signals after their normalization were transferred to the frequency domain by the Fast Fourier Transform (FFT) as shown in Fig. 3.9(b). It is clear that signal spectra are not the same. In the range of low frequencies, the strain gauge response dominates, contrary to the high frequency range in which the piezoelectric responses are of higher values. It is caused by the fact that voltage amplifiers were used to process the signals from piezoelectric sensors. Unfortunately they acted as high-pass filters due to the effect of charge drift [48]. This effect can be minimized by applying a charge amplifier for collecting piezoelectric responses, because this equipment is suitable for quasi-static (0.1 Hz) measurements [54] as well. Another advantage is that the output of the charge amplifier does not depend on the input capacitance [48]. It means that the electronics operated by a charge amplifier is insensitive to cable length. Finally, the responses collected by strain -auges and piezo sensors were filtered by a high-pass filter (over 1.3 Hz). As a result, quite good agreement between both types of sensors was obtained as demonstrated in Fig. 3.9(c).

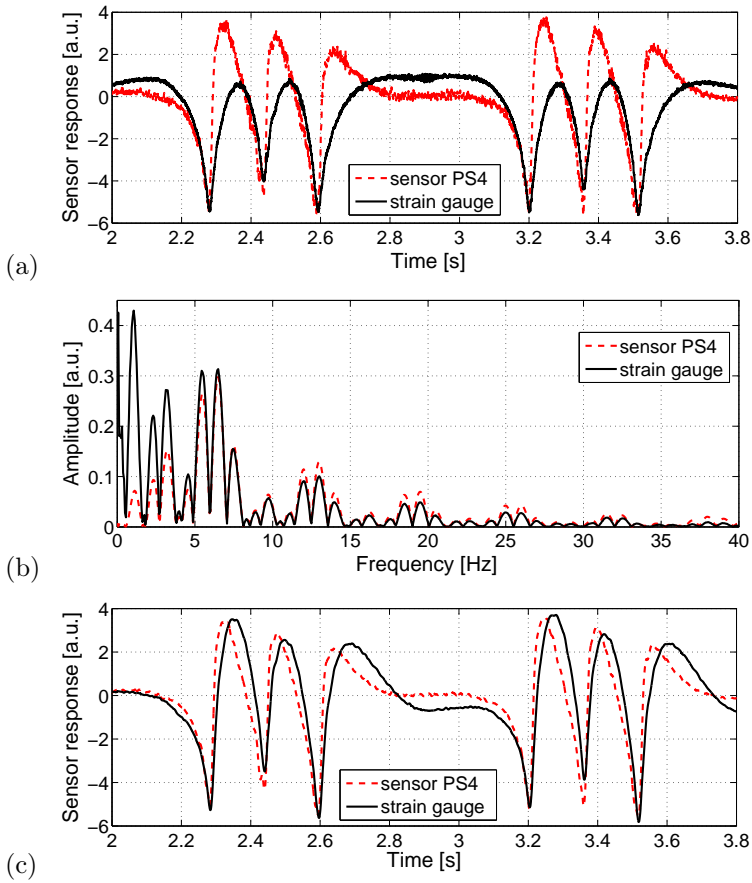


Figure 3.9. Signals from two kinds of sensors due to the passage of the ET-22 locomotive: (a) direct measurements in the time domain, b. spectra in the frequency domain, (c) filtered signals in the time domain.

The other experiments were performed for the testing the different electronics dedicated to piezoelectric sensors measurements. The two kind of the amplifiers i.e., charge and voltage were used. The locomotive passage measurements taken by the piezoelectric sensors and additionally strain gauges are shown in the Fig. 3.10(a). The measurements conducted via the strain gauges and piezoelectric sensors with charge amplifier are analogical in contrary to the signals measures via voltage amplifiers. In was found out the voltage amplifier results are not represents the “real” deformation of the rail caused by mentioned its high pass filtering effect. It can be observed in the example of passenger car passage measurements taken by different piezoelectric electronics shown in the Fig. 3.10(b).

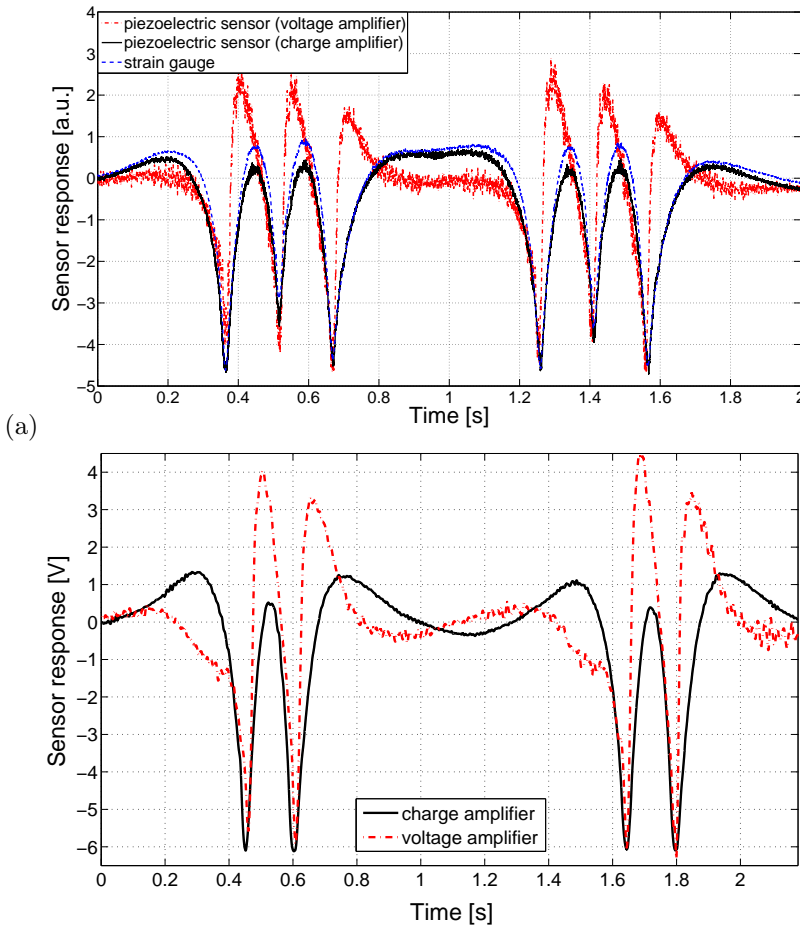


Figure 3.10. Measurements by different electronics: (a) locomotive passage, (b) passenger car passage.

It should be emphasized that only the signal amplitudes in the lower part (below zero) of strain histories are analyzed by the proposed WIM algorithms. Therefore the differences in upper parts of the plots due to the use of various types of sensors (cf. Figs. 3.9(a,c)) or to use different driving electronics (cf. Fig. 3.10(b)) are negligible from the practical point of view.

Another *in situ* test was aimed at examining the repeatability of the time signal at various velocities of the ET-22 locomotive running over the WIM measuring point back and forth. The runs were repeated for four velocities i.e., 20, 40, 60, 80 km/h. Figure 3.11 (a,b,c) present the selected peak levels of the signal

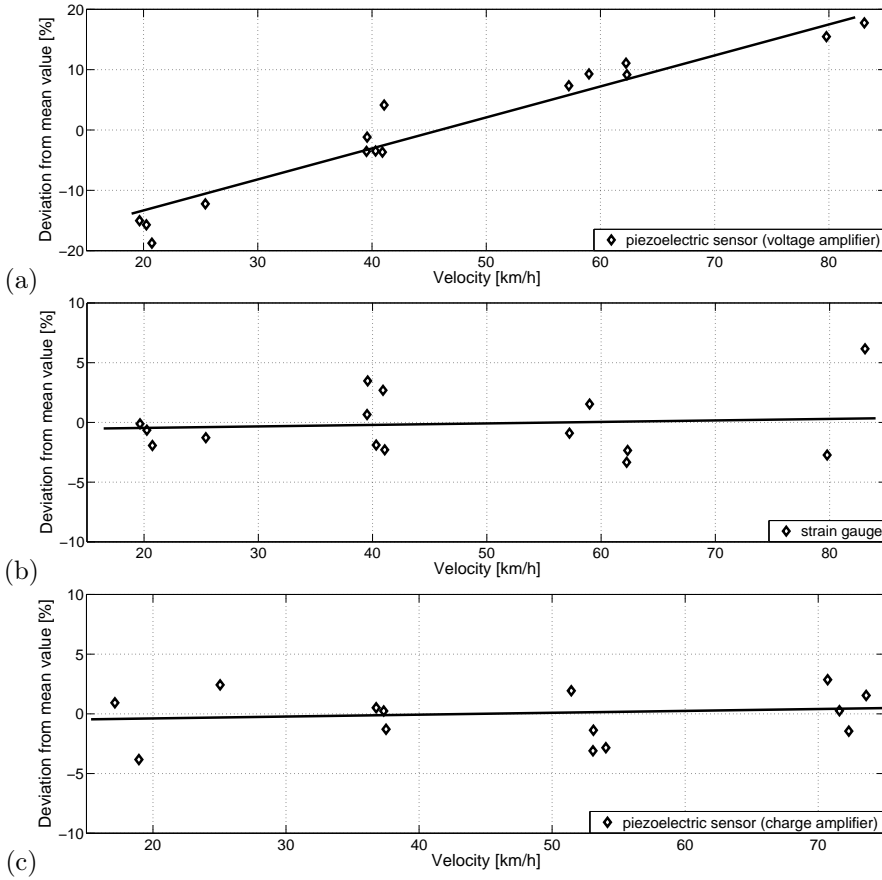


Figure 3.11. Velocity effect on the measured signal: (a) piezoelectric sensor (voltage amplifier), (b) strain gauge, (c) piezoelectric sensor (charge amplifier).

as a function of velocity for piezoelectric sensors (voltage and charge amplifier) and strain gauges, respectively. The velocity effect in the case of strain gauge and piezoelectric sensor with charge amplifier measurements seems to be insignificant in the selected range of velocities. The same conclusion was drawn by other researchers [117]. The variability of repeated strain gauge and piezoelectric sensor with charge amplifier measurements conducted for the selected range of velocities (20–80 km/h) is about  $\pm 5\%$ . On the contrary, the influence of velocity can be clearly observed in responses collected by the piezoelectric sensors with voltage amplifier, which is again likely to be caused by the drift effect in this kind of amplifier. The use of the customized charge amplifier resolves this problem as can be seen in Fig. 3.11(c).

### 3.5 Numerical model vs. experiments

The numerical simulation presented in this section aims at determination of the factors influencing the dynamic response of the rail, e.g., the number of axles per bogie or sleeper-ballast interaction. The main objective of the analysis is to obtain the calibration factors in order to assure the precision of the load identification algorithm.

#### 3.5.1 A review of railway track models

Several railway track models are available in the literature. A comprehensive review of this subject can be found in [118–120]. The earliest modelling of the railway track was reported by Winkler (1867). In his work, the Euler-Bernoulli model was used to define an infinitely long beam resting on a uniform elastic foundation representing the support (i.e., sleepers and ballast) [121]. The track structure can be modelled as being either finite or infinite in length. The wheel/rail system can be proposed as a discrete mass-spring-damper model [122]. Both frequency and time domain models are in use [123]. The most common way of the rail modelling is to apply the beam model proposed by Timoshenko. Nevertheless the Euler-Bernoulli beam is still in use.

The supports can be modelled as a continuous elastic foundation [124] or discrete beams [116]. The supports can be considered as massless spring-damper systems [125] or models in which the mass of the sleepers, ballast and also the stiffness of paddings and damping coefficients are considered [126].

The most common way of modelling is to analyze a half of the track only, justifying this simplification by an assumption of the symmetric load distribution. Nevertheless the full track model can be also used [127].

Another problem is an appropriate application of the wheel/rail interface in the model. The simplest way is to use a stationary load but a moving load (or moving mass) simulating the effect of dynamic load of the train is much more closer to reality. The most realistic method modelling the vertical load resulting from the wheel-rail contact is that of moving mass (wheel) rolling on the track as presented in [125]. This way is not commonly used because it is time consuming.

In general, the complexity of the model depends on the objectives of the analysis to be performed and according to [128] “the model should be as simple as possible and as accurate as necessary”.

### 3.5.2 Description of the proposed model

For verification of the *in situ* measurements and determination of the calibration factors, a numerical model of the rail-sleeper-ground interaction was proposed. Taking advantage of the experience in modelling of the WIM system for road transport (see Sections 2.3.3 and 2.4.2), the railway track was modelled using the same FE package *ADINA*. A scheme of the model is shown in Fig. 3.12. The track and loading are assumed to be symmetric with respect to the centerline between the two rails. Therefore only half of the track is modelled in order to shorten the computational time.

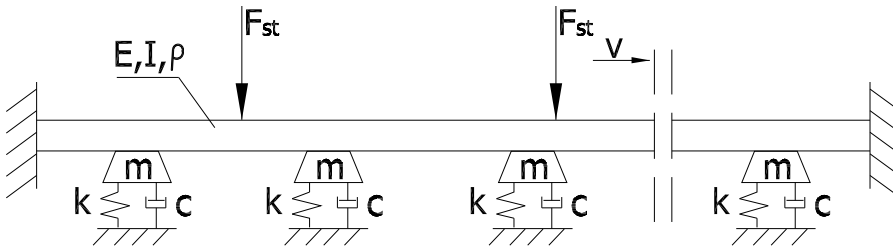


Figure 3.12. Model of the rail-sleeper-ground interaction.

The considered model includes a section of 60 sleepers supporting a rail with the clamped-clamped boundary conditions. The spacings between the sleepers are 60 cm. The analysis is focused on the middle part of the model (20 middle sleepers) to eliminate the influence of the boundary conditions on results. The two-node Hermitian beam (based on the Euler-Bernoulli beam theory, corrected for shear deformation effects [95]) with proper geometry and material data is used to model the real *S60* rail. The Kelvin-Voigt model is employed to model the interaction between the sleepers of mass  $m = 100$  kg and the ground. The parameters of all the modelled sleepers are identical which is some simplification in view of the results presented in [119]. The rail pad is not additionally modelled which can be justified by the poor condition of the investigated real track. The loading is applied as vertical force vectors moving along the rail with a constant velocity.

#### Selection of coefficients for the Kelvin-Voigt model

The stiffness  $k$  for the Kelvin-Voigt model was determined thanks to the *in situ* measurements. The displacement measurements presented in Fig. 3.8 are the basis for generation of the experimental force-displacement characteristic

of the track depicted in Fig. 3.13(a). The poor condition of the real track was manifested by a very low stiffness at the first phase of rail deformation, in which the sleepers had no contact with the eroded ballast beneath. In order to reflect this behavior of the real track, a bilinear characteristic shown in Fig. 3.13(b) was adopted in the model. The magnitude of force at 20 mm downward displacement was adjusted in Fig. 3.13 (b) thanks to multiplication of the *in situ* measured force (100 kN cf. Fig. 3.13(a)) by the ratio of distance between sleepers (0.6 m) to mean distance between bogie axles (1.5 m). This basically means that a large portion of the force from the axle of a railway car standing over the WIM measurement point is balanced by reactions of the two neighbouring sleepers. Accordingly, the stiffness coefficient is low, i.e.,  $k = 0.25$  MN/m if 10 mm downward displacement is not exceeded and high, i.e.,  $k = 4$  MN/m otherwise.

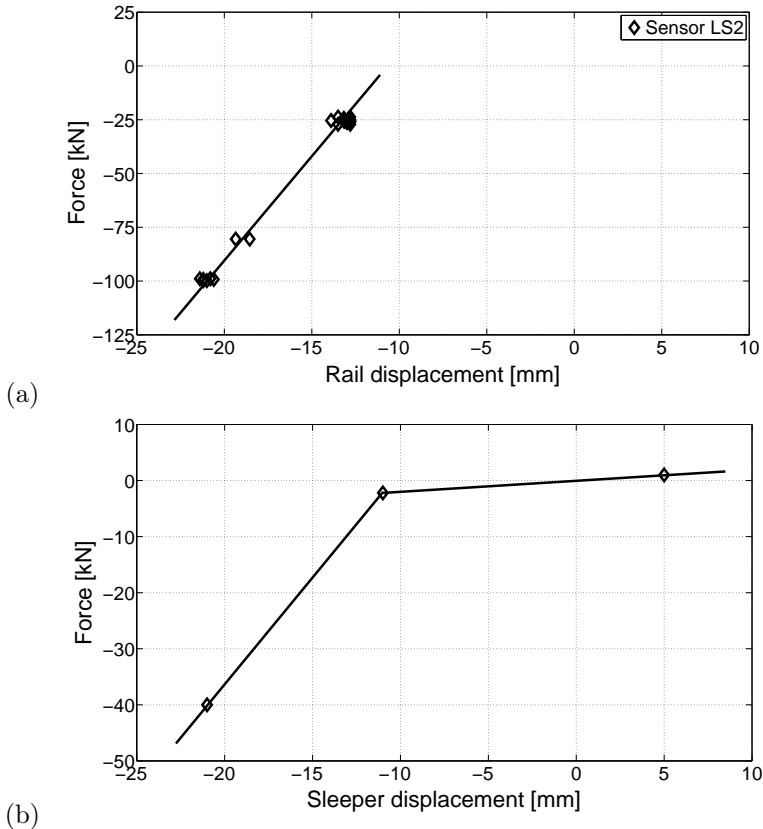


Figure 3.13. Force-displacement characteristic of the track: (a) measured *in situ*, (b) used in the model.

The viscous damping coefficient  $c$  was assumed on the basis of literature analysis. As the starting point, the research performed in the Railway Scientific and Technical Centre [129] was studied. A new type of steel sleepers embedded in the ballast layer was tested on the laboratory testing stand shown in Fig. 3.14. The track was periodically loaded (frequency approx. 2.8 Hz) by hydraulic jacks. The vertical force  $F$  acting on the sleeper and its vertical displacement  $x$  were measured. The measurement results and the viscous damping parameters of the track are shown in Fig. 3.15. An area corresponding to the potential energy  $W$  of the system was determined. The hysteresis area  $\Delta W$  which illustrates the level of energy dissipation per one load cycle was observed.



Figure 3.14. View of the testing stand for a new type of railway track [129].

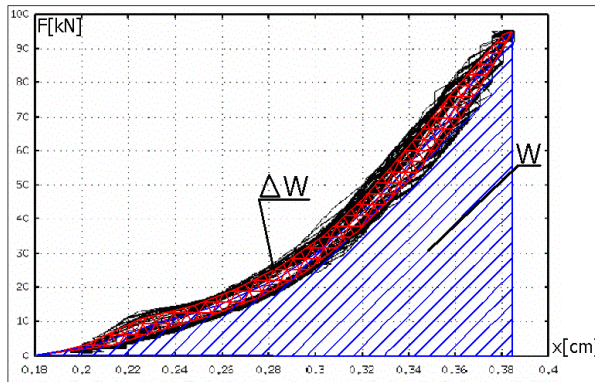


Figure 3.15. Vertical force versus displacement after a long period of track testing [129].

For harmonic excitation the energy dissipated by the structure during one cycle of load can be described by Eq. (3.5):

$$\Delta W = \oint F \cdot dx = \oint c \cdot \dot{x} \frac{dx}{dt} \cdot dt = \int_0^{\frac{2\pi}{\omega}} c \cdot \dot{x}^2 \cdot dt. \quad (3.5)$$

The displacement and velocity can be determined from Eq. (3.6) and Eq. (3.7)

$$x(t) = A \cdot \cos(\omega t - \varphi), \quad (3.6)$$

$$\dot{x}(t) = -\omega A \cdot \sin(\omega t - \varphi). \quad (3.7)$$

Hence, substituting Eq. (3.7) into Eq. (3.5), Eq. (3.8) can be obtained [130]

$$\Delta W = c \cdot \omega^2 \cdot A^2 \int_0^{\frac{2\pi}{\omega}} \sin^2(\omega t - \varphi) \cdot dt = \Pi \cdot c \cdot \omega \cdot A^2. \quad (3.8)$$

Finally, the viscous damping coefficient  $c$  can be found from Eq. (3.9):

$$c = \frac{\Delta W}{\Pi \cdot \omega \cdot A^2}, \quad (3.9)$$

where  $A$  – the amplitude of the vertical displacement of the track,  $\omega$  – the angular frequency.

Hence, substituting the measured data (see Fig. 3.15) into Eq. (3.9), the viscous damping is equal to:

$$c = 2 \cdot 10^5 \text{ N s/m.}$$

It should be noticed that the above-calculated value corresponds to measurements of a new type of the track [129]. Relatively high viscous damping was obtained. In [116], the viscous damping coefficients for the rail pad  $c = 1.5 \cdot 10^4$  N s/m and for the sleepers  $c = 3.1 \cdot 10^4$  N s/m were used respectively. The value of  $c = 1.44 \cdot 10^4$  N s/m was applied in the model presented in [125]. The damping coefficient reported in [131] was related to the unit of length (along sleeper) and equal to  $c = 6 \cdot 10^4$  N s/m<sup>2</sup>. Relatively big scatter of damping parameters can be found in the literature. It is related to various configurations of practically applied ballasts and sleepers.

The track model developed by the author should correspond to the response of the real track which is in a relatively poor technical condition. Hence, in the proposed numerical model, a rather low value of damping was assumed i.e.,

$$c = 3 \cdot 10^4 \text{ N s/m.}$$

### Validation of the track model

The numerical results obtained from the built model were confronted with the experimental measurements for a passage of the 120 ton ET-22 locomotive. Histories of vertical displacements of the rail at the WIM measuring point and corresponding stresses in the rail foot are depicted in Fig. 3.16, evidencing a decent conformity of numerical and experimental data.

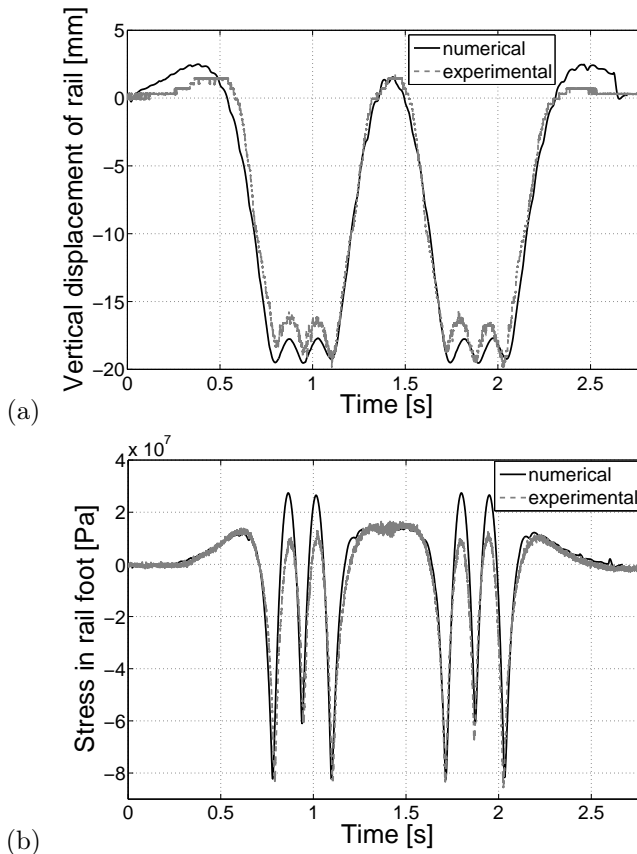


Figure 3.16. Numerical vs. experimental results: (a) vertical displacements of the rail, (b) stresses in the rail foot.

As already mentioned, the identification of load parameters by the proposed WIM system is performed using the downward peaks of the strain/stress evolution in time. In the lower part of Fig. 3.16(b), the agreement between the numerical model and experiment is excellent. Discrepancies in other parts do not influence the quality of load parameter identification.

### Effect of stiffness of the track support

The parameters that may change, while the proposed WIM system is in use, are certainly the support conditions of the sleepers. Stiffness of the track can be affected by environmental factors, e.g., low temperature in winter or maintenance issues, e.g., replacement of ballast. Hence it is important to estimate the influence of the support conditions on the extent of rail deformation. Using the numerical model, an analysis of various support conditions was performed.

Under the assumption of constant load distribution and constant velocity, the influence of the support stiffness  $k$  on the strain response of the rail was estimated. The obtained results are presented in Fig. 3.17. The graph presents a relative change of the rail strain as a function of the ratio of the support stiffness to base stiffness. The base stiffness was assumed to be equal to track stiffness identified on the basis of *in situ* measurements. The highest stress in the rail foot was observed for the most flexible supports. The obtained relation is strongly non-linear. The support condition was found to be an important factor influencing the stress response of the rail. Hence it is necessary to take account of the support conditions in the proposed load identification algorithm based on pattern recognition, because it is dependent upon environmental factors.



Figure 3.17. Rail stresses as a function of support stiffness.

### Effect of load distribution

Railway cars may have a different number of axles per bogie. The most common bogies have two axles [106]. Nevertheless non-typical cars with one, three, four or eight axles per bogie [132] are also in use. Hence the load distribution effect must be taken into consideration. In the analysis, the same total load value acting on the track was distributed on a different number of axles. The axle spacing was averaged from a set of typical freight cars and locomotives. Constant train velocity and support conditions were assumed. The obtained results are shown in Fig. 3.18, which presents a relative change of rail strain as a function of the axle number with the load distribution for a three-axle bogie serving as reference.

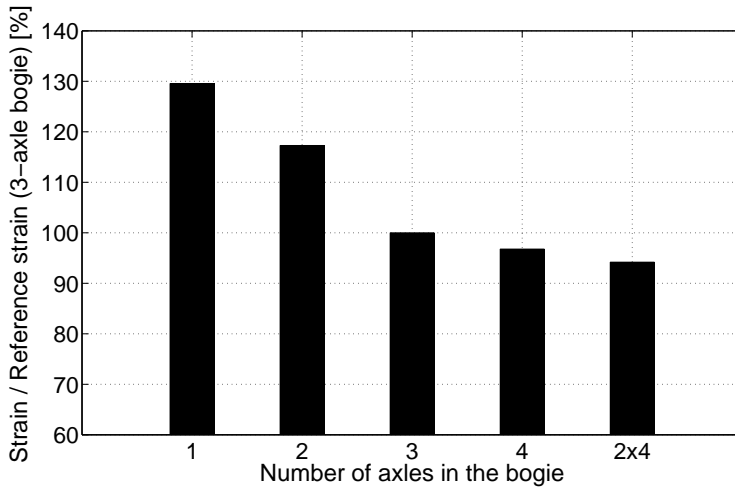


Figure 3.18. Rail strains as a function of load distribution.

The results shown in Fig. 3.18 confirm that the load distribution effect must not be neglected. Otherwise the cars with a smaller number of axles might be identified as heavier than in reality. Hence a correcting factor should be taken into account in the load identification algorithm. This factor is especially important if the on-line calibration method (with the locomotive serving as a reference), mentioned in the Section 3.3.2 will be applied. The need of such correction comes from the fact that locomotives usually run on three-axle bogies while freight cars on two-axle ones.

### 3.6 Final remarks

This chapter presents numerical and experimental investigations of a new WIM system developed for the railway transport. The system is supposed to identify the dynamic loads generated by a train passing over piezoelectric sensors mounted to the rails. The WIM proposition is meant to be a part of an integrated SHM system dedicated to health monitoring of railway truss bridges.

The general idea of the proposed WIM system and the methods employed for the identification of moving train load have been explained. The accompanying hardware and data transfer issues have been discussed. Two algorithms of load identification have been considered. The method based on the on-line calibration which makes the measurements insensitive to environmental conditions seems to be much more practical.

Responses from *in-situ* measuring sessions registered by piezoelectric sensors and strain gauges have been presented. Both types of sensors proved to be applicable to dynamic weighing of trains. Moreover the test of two kind of piezoelectric sensors (e.g., piezo-ceramic and piezo-fiber) were conducted. The results were very similar despite the very different cost of the sensors (piezo-fiber one are approximate 10 time more expensive to piezo-ceramic one). A linear relation between the identified load and sensor responses was obtained. The velocity effect was apparent for measurements recorded by the piezoelectric sensors and processed by the voltage amplifier. Strain gauge and piezoelectric sensors with charge amplifier results seem to be insensitive to this effect.

The experimental data have been successfully verified by a FE numerical model. An analysis of the factors influencing the load identification was performed experimentally and numerically. The effects of load distribution and support conditions were found essential for interpretation of results by the load identification algorithm.

The thorough investigation of the system accuracy and durability issues will be the subject of further tests.

# Impact load identification

## 4.1 Introduction

The objective of this chapter is strongly related to the concept of *Adaptive Impact Absorption* (AIA) [4, 5, 133]. An AIA system is a structure equipped with control devices that modify its local structural properties (e.g., local stiffness) in real-time in order to adapt the structure to the actual dynamic loading. The initial challenge is to invent technologies applicable to the above-mentioned control devices. One option deals with the concept of structural fuses with elasto-plastic type of overall performance and the controllable yield stress level, where the control mechanism can be based on various types of actuators, e.g., electromagnetic, piezoelectric, magnetostrictive or magneto-SMA [134–136]. Shock absorbers based on magneto-rheological fluids or piezoelectric valves can be successfully utilized for AIA in case of repetitive, exploitative impacts, for example in adaptive landing gears [4]. Another type of AIA systems are *Adaptive Inflatable Structures* (AIS) [137] composed of chambers filled with compressed gas and equipped with high performance valves which control release of pressure during impact. Finally, *Micro Pyro-technique Systems* (MPS) can be used for detaching (in real-time) selected structural joints in order to improve structural response in emergency situations (e.g., in crash of vehicles) [138].

In general, the AIA system should be designed for random, impact multi-loads, which creates new research challenges due to optimal forming of structural geometry and location of control devices. Examples of engineering applications for AIA systems are as follows: protective road barriers [139, 140], automotive longitudinal members [141, 142] bumpers and head-rest [143], so-called multi-folding protective systems [144], adaptive landing gears [57, 145], pneumatic offshore structures [146] and adaptive airbags for emergency landing [147]. The general overview of the AIA concepts developed in IFTR can be found in [148]. In all mentioned applications, the development of the optimal adaptation strategy requires information about the characteristics of the impact loading and the

value of the impact energy which has to be dissipated. Therefore, the initial step of the adaptive impact absorption should be identification of the impact loading. Moreover, an efficient methodology for the possibly precise and fast (real-time) identification of the impact loading is required.

Due to the fact that identification of the actual impact scenario constitutes prerequisite for the functioning AIA systems, it should be performed fast enough to enable control the energy dissipation process [149]. The dead-line condition is to identify the impact parameters at the very beginning of the process, i.e., before the time instant when the acceleration of the colliding object achieves its optimal value (the constant value that enables to use the full stroke of the controllable absorber).

The objective of this chapter is focused on the problem of real-time identification of impact load (i.e., the impacting mass and its initial velocity). The idea is to determine this two parameters when no sensor used for identification is installed on the impacting object. However, the different case was considered in the Appendix F. The identification considered in this chapter will be performed by mean of specially invented device, the so-called impactometer (patent pending [58]) which is equipped with a force sensor (and/or accelerometer) and tuneable gas-spring. It is assumed, that the impactometer is located on the structure protected by an AIA system and is exposed to impact of an object of unknown mass and velocity.

Many techniques were developed in order to identify parameters of impact and dynamic excitations. Most often this problem deals with identification of the impact force value [11] its location [150] or both [151]. In the paper [115] a brief review of methods used in the case of the indirect impact force identification is presented. This article considers a variety of approaches for measuring time history of the impact force, its direction and location. The authors of the paper [24] give detailed overview of the on-line load identification techniques. Moreover, the paper introduces four time-domain methods and discusses advantages and disadvantages of the particular approaches. A comparison of these techniques leads to the conclusion that all of them have their own limitations and drawbacks. The literature review shown that none of the methods is able to identify both falling mass and its kinetic energy during the initial milliseconds of impact. The motivation for the author is to fill this gap.

Taking into account the objective of this thesis, the crucial issue for developed identification techniques is operation time criteria (i.e., the time required to identify parameters of the impact load) which has to fulfill the deadline condition. Contrary to off-line identification techniques [20], which usually make use of a numerical model of structure and require long computational time, the

identification techniques considered in this chapter have to be performed in a few milliseconds to allow triggering of the AIA control procedure in real-time. This is the reason, why the identification procedure should be based upon a locally operating simple hardware device rather than on a sophisticated software and distributed sensor system.

The layout of the chapter is as follows. First part of the paper includes a general formulation of a problem and motivation for performed researches. In the Section 4.3 the laboratory set-up for drop tests is demonstrated. In the Section 4.4 numerical model for simulation of the dynamic response of the impactometer device is developed. Results of the experimental tests and numerical simulations for the series of various impact scenarios are presented in Section 4.5. In the following Section 4.6, an analytical algorithm for impact load identification is formulated and verified numerically as well as experimentally. Finally, in Section 4.7 another algorithm, based on response map approach is presented and verified. The plans for implementation of the impactometer concept are described in Section 4.8 while the concluding remarks are drawn in final Section 4.9.

## 4.2 Impact load parameters characteristics

The chapter is devoted to identification of impact parameters of object colliding in to structure. Contrary to the reference [29, 115] the impact force identification is not main subject of interests. It is assumed that for triggering impact energy dissipation process via AIA devices in order to minimize the unprofitable effect of collision the mass and the parameters of motion of colliding object are needed. Figure 4.1 shows schematically how the impacting object (i.e., its mass ( $m$ ) and its impact velocity ( $v$ )) effect to the impacted cantilever structure. The curves mark the different impact scenarios characterized by the same kinetic energy ( $E_k$ ) of colliding object.

Two characteristic areas can be determined in the mass-velocity domain:

- “*Fast dynamics*” (area 1) corresponds to small mass impacting with high velocity and results in local structural deformations and damages in vicinity of the impact point.
- “*Slow dynamics*” (area 2) corresponds to heavy mass impacting with low velocity, which causes quasi-static structural deformation. In the case of the cantilever beam shown in Fig. 4.1, the overloaded parts are in the vicinity of the supports.

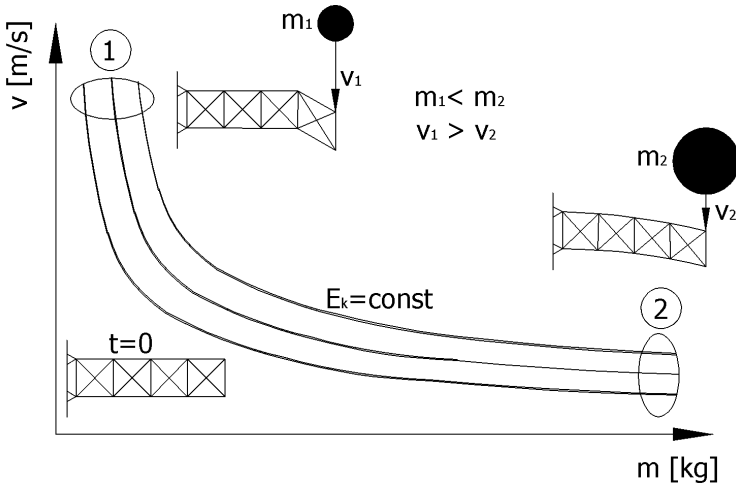


Figure 4.1. Influence of falling mass and impact velocity on structural response.

Exemplary numerical simulations of structural response to two different impact loads with the same impact energy are shown in Fig. 4.2, where the case (a) corresponds to “*slow dynamics*” (larger mass and smaller impact velocity), while the case (b) corresponds to “*fast dynamics*” (smaller mass and larger impact velocity). Qualitatively, different structural response in both cases is observed. As a consequence it is assumed further that the impact load identification indicates identification of two parameters (apart from its localization): (1) mass of the impacting object, and (2) its impact velocity. Real-time determination of these two parameters allows for predicting the further development of the impact scenario and triggering the optimum structural adaptation via AIA system.

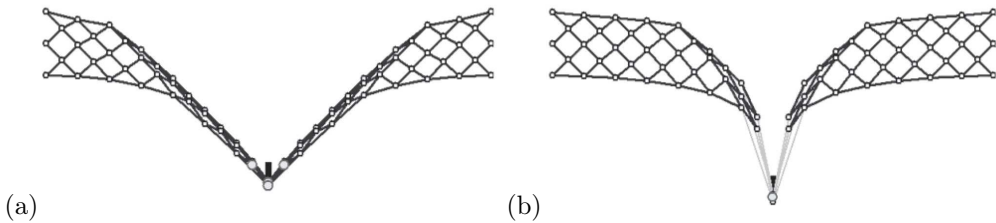


Figure 4.2. Numerical simulation of truss structure responses affected by the same impact kinetic energy [152]: (a) “slow dynamics” case with high mass/velocity ratio, (b) “fast dynamics” case with small mass/velocity ratio.

### 4.3 Experimental test stand

Impact tests have been carried out making use of the experimental free-fall drop test stand constructed at the Institute of Fundamental Technological Research (see Fig. 4.3). The set-up allows to generate initial impact energy up to 1.5 kJ by mass of 100 kg dropped from the height of 1.5 m. Pneumatic absorber equipped with sensors has been used as a prototype of impactometer device. Adjustment of initial pressure inside the cylinder was found to be an effective method of modification of the impactometer properties. Moreover, after having installed the controllable exhaust valve into the pneumatic cylinder, the impactometer can began to play a role of semi-actively controlled impact energy absorber with the capacity of relatively simple and fast modification of its characteristics.

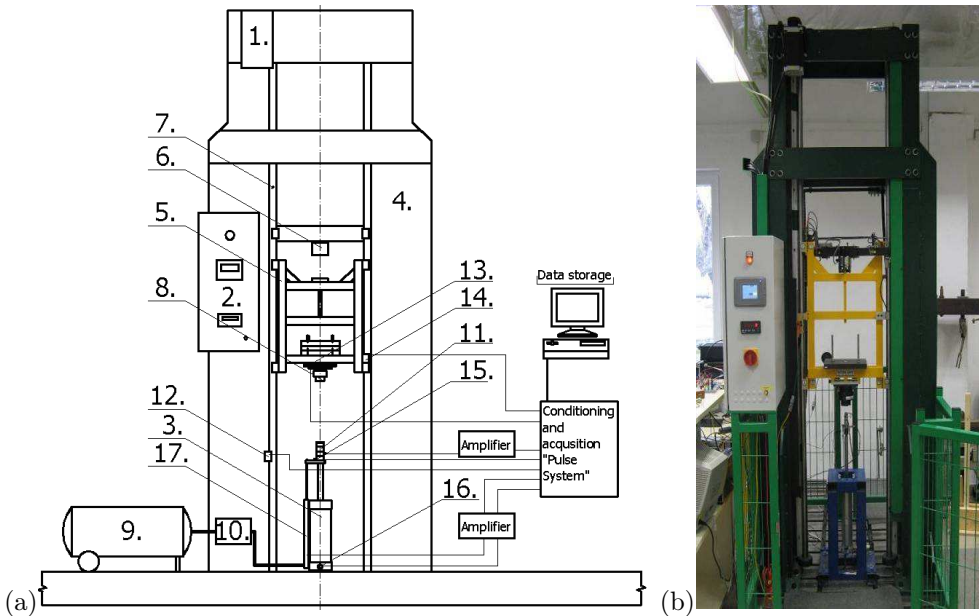


Figure 4.3. Experimental free-fall drop test stand: (a) a diagram of the experimental set-up, (b) a picture of the test stand.

The test-stand is equipped with electric motor (1) for lifting the mass and a control switch box (2) used to program a set of drop tests. The main parts of the set-up are the pneumatic cylinder (3) mounted in the vertical position (diameter 63 mm, maximum stroke 250 mm), the frame (4) and the carriage (5). The lift mechanism includes an electromagnet (6) used for releasing the impacting mass

fixed to the carriage (5), which is guided by the rail system (7) embedded in the frame. The mass is impacting onto the pneumatic cylinder via a rubber bumper (8). The compressor (9) enables to modify the initial pressure inside the pneumatic cylinder (3) via the regulator (10). The measurement system includes all necessary conditioning systems and amplifiers. The measured data are recorded by a Pulse (Brüel & Kjær) acquisition system enabling to acquire measurements with frequency of 50 kHz for all signals coming from:

- the piezoelectric sensor (11) fixed to the piston rod of the pneumatic cylinder, in order to measure the impact force-time history;
- the optical switch (12), which acts as a trigger and allows to determine the vertical velocity of the impacting mass just before the impact;
- the accelerometer attached to the carriage to determine deceleration of the falling mass (13);
- the magnetic linear sensor (14) to determine displacement of the falling mass;
- the accelerometer (15) attached to the piston rod of the pneumatic cylinder;
- the “fast” pressure sensor (16) mounted in the cylinder;
- the LVDT sensor (17) to determine displacement of the piston.

The experimental drop tests have been performed for a better understanding of the impact process and its dependency on particular parameters of impact. Then collected measurements have been used for validation of the numerical model and for testing the effectiveness of the impact identification algorithms. The developed methodologies make use of the force and acceleration sensor measurements only. Nevertheless, additionally applied sensors, as well as the analysis of high-speed camera film were utilized for the numerical model validation.

#### 4.4 Numerical model of the system<sup>1</sup>

The pneumatic absorber described above was modeled numerically in order to simulate its response to various impact scenarios, i.e., impact of the rigid object of various masses and initial velocities. Another purpose of numerical simulation was to estimate the influence of selected parameters of the pneumatic cylinder on the dynamic response of the system and further to choose optimal parameters of the impactometer.

---

<sup>1</sup>The numerical implementation of the pneumatic absorber model was done by Cezary Graczykowski [64].

The proposed basic model of pneumatic absorber subjected to impact loading is based on assumption that pressure, density and temperature of the gas enclosed in each chamber are uniform in every instant of time. Moreover, due to the fact that considered impact process is relatively short it is assumed that heat transfer through cylinder walls does not occur and process can be considered as adiabatic. The numerical model is schematically presented in Fig. 4.4(a), while the corresponding mechanical system is shown in Fig. 4.4(b).

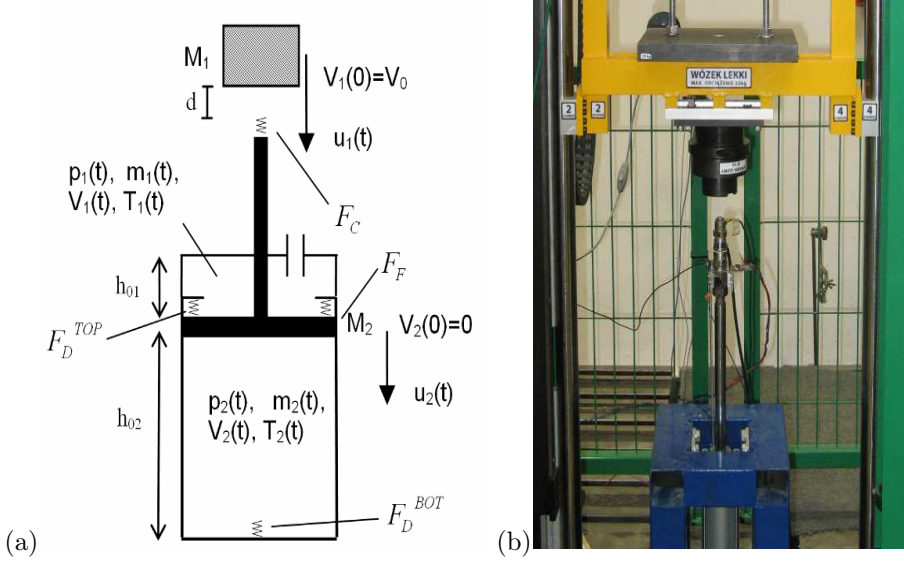


Figure 4.4. Considered mechanical system: (a) numerical model, (b) experimental set-up.

The considered system consists of two rigid objects, the falling mass and the piston, which in numerical model are represented by two mechanical degrees of freedom. Equations of motion take the form:

$$M_1 \frac{d^2 u_1}{dt^2} - M_1 g + F_C = 0, \quad (4.1)$$

$$M_2 \frac{d^2 u_2}{dt^2} - M_2 g - F_C + F_P + F_F - F_D^{TOP} + F_D^{BOT} = 0, \quad (4.2)$$

where  $M_1$ ,  $M_2$  are the mass of falling object and the mass of the piston, respectively, while  $u_1$ ,  $u_2$  indicate their displacements, and  $g$  is the gravitational acceleration. Equations (4.1) and (4.2) are coupled by the component indicating contact force which arises during collision of the falling mass with the piston rod. The definition of the contact force depends on colliding objects material

properties and moreover, it is influenced by the geometry and shape of contact surfaces. Models of the unidirectional contact proposed in the literature usually include some combination of springs with stiffness  $k$  and dampers [153] with viscous damping  $c$ . Let us recall here the following classical models described by Eqs. (4.3a)–(4.3c) where initial distance between bodies is denoted by  $d_0$ :

- linear visco-elastic proposed by Kelvin-Voigt:

$$F_C = k(u_1 - u_2 - d_0) + c(\dot{u}_1 - \dot{u}_2), \quad (4.3a)$$

- linear spring, nonlinear dashpot model by Walton [153]:

$$F_C = k(u_1 - u_2 - d_0) + c(u_1 - u_2 - d_0)(\dot{u}_1 - \dot{u}_2), \quad (4.3b)$$

- general model based on combination of nonlinear spring and nonlinear dashpot described by the equation:

$$F_C = k(u_1 - u_2 - d_0)^n + c(u_1 - u_2 - d_0)(\dot{u}_1 - \dot{u}_2)^m. \quad (4.3c)$$

A thorough analysis of contact force models will be presented in Section 4.6.2 that concerns the “peak-to-peak approach”, since the assumed contact model will be crucial for the identification procedure.

Apart from the contact force  $F_C$  the equation of piston motion contains terms indicating the pneumatic force  $F_P$ , the friction force  $F_F$  and two delimiting forces  $F_D^{TOP}$  and  $F_D^{BOT}$ . The pneumatic force  $F_P$  is defined as a difference of pneumatic forces acting on both sides of the piston which are the results of pressures  $p_1$  and  $p_2$  acting on upper and lower piston area ( $A_1$  and  $A_2$ ). In case when falling mass is not in contact with the impacted object the definition of the pneumatic force additionally contains term indicating ambient pressure  $p_A$  acting on the area of the piston rod:

$$\begin{aligned} F_P &= p_2 A_2 - p_1 A_1 \quad \text{if } F_C \geq 0, \\ F_P &= p_2 A_2 - p_1 A_1 - p_A (A_2 - A_1) \quad \text{if } F_C < 0. \end{aligned} \quad (4.4)$$

The friction force  $F_F$  is the results of friction which occurs between piston and cylinder walls. Two models were considered: the Coulomb friction which depends only on the direction of the piston movement, namely:

$$F_F := -F_F \quad \text{if } \frac{du_2}{dt} < 0 \quad \text{and} \quad F_F := F_F \quad \text{if } \frac{du_2}{dt} > 0, \quad (4.5)$$

and the velocity-dependent friction described by the friction coefficient  $c_F$ :

$$F_F = c_F \frac{du_2}{dt}. \quad (4.6)$$

In order to confine the piston movement to the range determined by the cylinder geometry, top delimiting force  $F_D^{TOP}$  and bottom delimiting force  $F_D^{BOT}$  were used. Top delimiting force confines upward displacement of the piston and provides initial equilibrium of the piston in case when initial pressure is higher than ambient pressure. On the contrary, bottom delimiting force is activated at final part of the stroke (displacement larger than  $u_2^{crit}$ ) to protect the piston against hitting the cylinder's bottom. Both forces are defined in the simplified form of linear spring with the stiffness  $k_D$ :

$$\begin{aligned} F_D^{TOP} &= -k_D u_2 \quad \text{if } u_2 < 0 \quad \text{and} \quad F_D^{TOP} = 0 \quad \text{if } u_2 \geq 0, \\ F_D^{BOT} &= k_D(u_2 - u_2^{crit}) \quad \text{if } u_2 > u_2^{crit} \quad \text{and} \quad F_D^{BOT} = 0 \quad \text{if } u_2 \leq u_2^{crit}. \end{aligned} \quad (4.7)$$

The following part of the numerical model is related directly to thermodynamics of the system. The basic equation describing gas in both chambers is the ideal gas law:

$$\begin{aligned} p_1 V_1 &= m_1 R T_1 \quad \text{where} \quad V_1 = A_1(h_{01} + u_2), \\ p_2 V_2 &= m_2 R T_2 \quad \text{where} \quad V_2 = A_2(h_{02} - u_2), \end{aligned} \quad (4.8)$$

where  $V_1, V_2, T_1, T_2$  volumes of the chambers and its temperature,  $R$  is gas constant,  $m_1, m_2$  are air masses while  $h_{01}, h_{02}$  are initial lengths of the chambers. The flow of the gas between the upper chamber and environment can be described by a simple formula which relates mass flow rate of gas into the upper chamber and the pressure difference between this chamber and environment:

$$\Delta p = p_1(t) - p_A = -c_V(t)\dot{m}_2 - c_H(t)\dot{m}_2 |\dot{m}_2|, \quad (4.9)$$

where  $c_V, c_H$  are the flow resistance coefficients. Other, more sophisticated analytical models of the gas flow can be found in the classical literature [154, 155]. However, let us note that precise modelling of flow of the gas to the upper chamber of the cylinder is beyond the scope of this thesis. The inflow of the gas could be totally blocked or totally opened with no significant influence on further considerations and conclusions concerning impact identification.

Balance of internal energy of gas enclosed in each chamber has to be considered in a full form containing gas internal energy, global work done by external forces, and enthalpy of the gas added/removed from the system (cf. [156]):

$$dm_{in}\bar{H}_{in} - dm_{out}\bar{H}_{out} = d(m\bar{U}) + dW. \quad (4.10)$$

Specific gas enthalpy  $\bar{H}_{in}$ ,  $\bar{H}_{out}$ , specific gas energy  $\bar{U}$  and work done by gas  $W$  are defined as follows:

$$\bar{H}_{in} = c_p T_{in}; \quad \bar{H}_{out} = c_p T; \quad \bar{U} = c_v T; \quad dW = p dV; \quad (4.11)$$

where  $c_p$  and  $c_v$  indicate specific heat at constant pressure and constant volume, and  $T_{in}$  indicates temperature of the gas which enters the chamber. Due to the fact that lower chamber remains closed the term describing enthalpy of the added gas vanishes.

Initial conditions for the system concern initial position and velocity of falling object and the piston, and initial parameters of the gas inside the cylinder:

$$\begin{aligned} u_1(0) = u_1^0; \quad \frac{du_1}{dt}(0) = V_1^0; \quad u_2(0) = u_2^0; \quad \frac{du_2}{dt}(0) = 0; \\ p_1(0) = p_A; \quad T_1(0) = T_1^0; \quad p_2(0) = p_2^0; \quad T_2(0) = T_2^0. \end{aligned} \quad (4.12)$$

Equations (4.1)–(4.12) fully define the problem of double chamber pneumatic cylinder subjected to the impact loading. The resulting system of differential algebraic equations can be easily transformed into a system of four differential equations by incorporating ideal gas law and definition of forces into other equations. The variables for which equations are solved (chosen among  $u_1, u_2, m_1, m_2, p_1, T_1, p_2, T_2$ ) and corresponding initial conditions can be chosen arbitrarily. The final system of differential equations was implemented in mathematical software MAPLE and solved numerically by the fourth-order Runge-Kutta method.

## 4.5 Impact scenarios

This section presents examination of the impact process for considered mechanical system. The objective is to analyze the structural response under impact excitation with regard to collision parameters as well as impactometer properties. The considerations are performed on the basis of the experimental and numerical results.

### 4.5.1 Experimental tests of impact scenarios

The considered impact types are limited to the collinear central collision between the rigid bodies (i.e., falling mass and the piston rod of pneumatic absorber). A variety of impact scenarios of this kind have been tested. The impact scenarios were defined by three parameters: the impacting mass value,

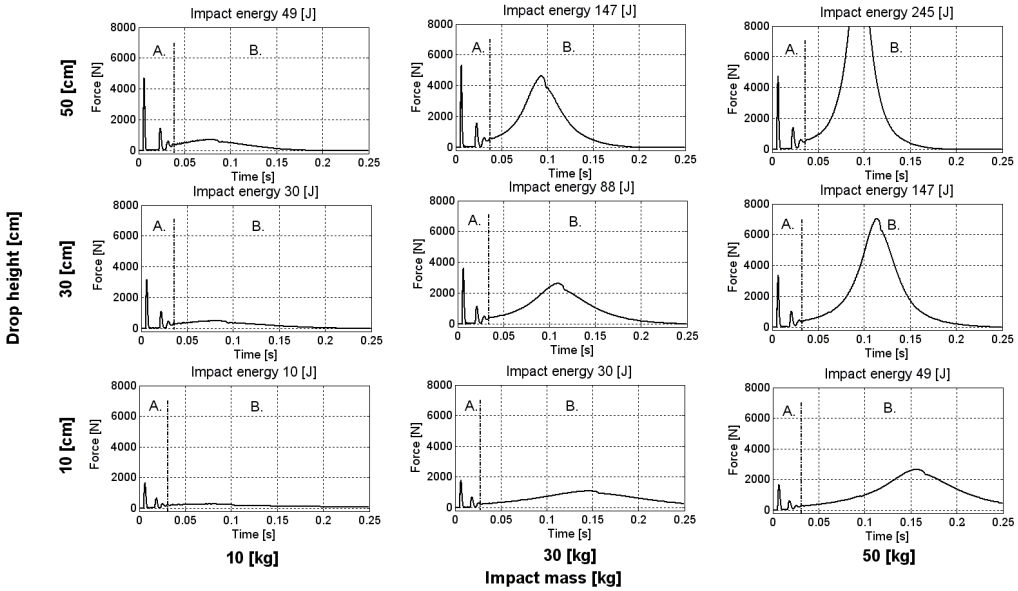
the velocity of the colliding object and the initial pressure inside the pneumatic absorber. The range of the impacting mass was 10–55 kg, while the relative impact velocity was adjusted by the drop height, which was confined to the range of 0.05–0.5 m. The pressure was modified in the range of 0–400 kPa where 0 is understood as the atmospheric pressure.

The chosen cases of collision scenarios are presented in Fig. 4.5. The graphs illustrate the experimental measurements of the contact force acting between the impacting mass and the piston rod. Each group of nine graphs corresponds to a different initial pressure in the cylinder of pneumatic absorber, namely: a. 20 kPa, b. 200 kPa.

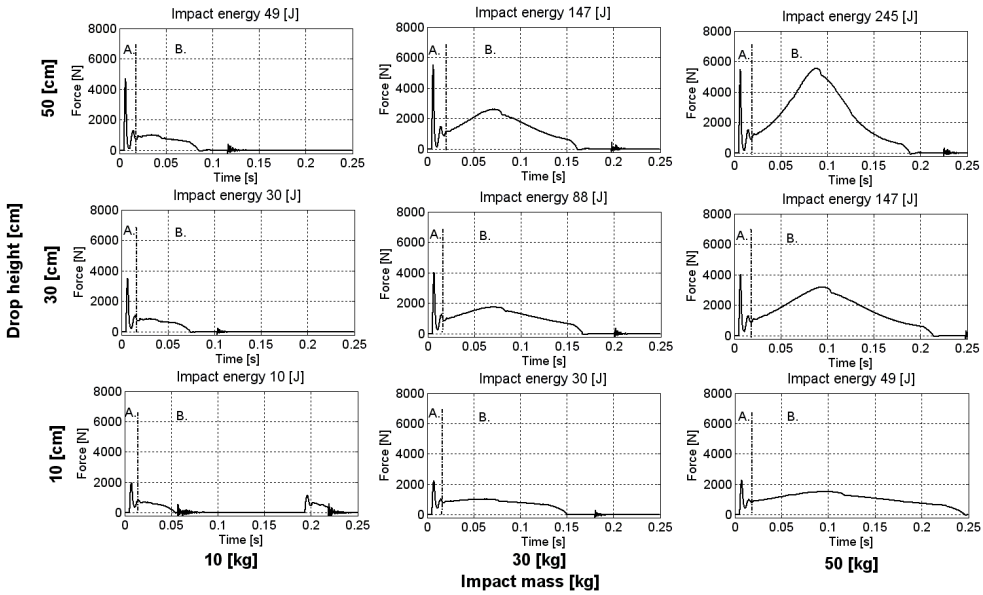
Characteristic change of contact force observed in the experiment allows to distinguish division of the impact process into two separate stages (i.e. *A*, *B*) which were marked in Fig. 4.5:

- the first one i.e., stage *A* when the piston rod rebounds from the falling mass and large oscillations of the contact force occur,
- the second one i.e., stage *B* during which falling mass is moving downwards together with the piston which results in smooth change of the contact force.

The total duration of the stage *A* was approx. 20–40 ms (mainly depending on the initial pressure), while the duration of an average force peak was approx. 5 ms. The phenomenon of the initial piston rebounds in stage *A* is the consequence of relatively small value of force acting on the bottom part of the piston at the beginning of process. Each of the considered impacts can be characterized by the number of rebounds between the falling mass and the piston rod observed in the stage *A* of the process. For the employed range of impact conditions (mass-velocity-initial pressure) it was found that the number of the rebounds was between 0–2. It might be concluded that the most important factor for occurrence of the rebounds was the initial pressure. In general, the maximum number of rebounds was observed in case of the smallest initial pressure. The number of rebounds, characteristic successive reduction of contact force peaks amplitudes and time between rebounds were insensitive to used impact mass and velocity but depends on initial pressure. Generally, the stage *A* of the process reveals the strong sensitivity to impact velocity but appears to be slightly dependent on the mass of the hitting object. The first peak of the contact force increases together with the impact velocity which is the result of the explicit dependency of the contact force on velocity of the impacting object (cf. Eqs. (4.3a), (4.3b)).



(a)



(b)

Figure 4.5. The effect of impact mass and velocity on the contact force history: (a) initial pressure 20 kPa, (b) initial pressure 200 kPa.

The rebounds of the piston are damped either as a result of dissipative properties of the contact material or due to the friction force acting between the cylinder walls and the piston. Along with an increase of initial pressure, the distance between the initial peaks in stage *A* is decreasing and simultaneously, the height of the peaks (value of contact force) is slightly rising. When the initial pressure is large, the contact force between the peaks is not reduced to zero, which means that the piston and the falling mass are not separated from each other, see Fig. 4.5(b). Let us note that the phenomenon of initial rebounds of the piston is a typical feature of the considered pneumatic absorber and for instance it does not occur in typical hydraulic absorbers.

The first stage of the impact process was also analyzed on the basis of the coefficient of restitution (see Appendix G). The analysis enable to conclude that the observed impact process is rather the elastic than the plastic.

In further part of the process (i.e., stage *B*), the falling mass is moving downwards together with the piston. The stage *B* is significantly sensitive to both impact velocity and mass of the hitting object. Some of the collisions presented in Fig. 4.5 are characterized by the same impact energy, for example (10 kg – 50 cm and 50 kg – 10 cm). In these cases, very different structural responses were observed, as defined by the force time-history in both impact stages. The impact of the same energy caused by an object with a larger mass results in a higher value of the contact force in the second stage of the impact. It is mainly caused by the impacting object vertical movement and the effect of change of its potential energy via the absorber compression.

An additional comment should be made on the dissipative properties of the considered system. The main process that governs its performance is compression of the air chamber located below the piston. Therefore, in the first approximation, the system can be treated as a nonlinear elastic spring which does not dissipate kinetic energy of the hitting object. However, a more strict analysis reveals several mechanisms of energy dissipation: i) damping of the contact material, ii) friction of the piston and cylinder walls, iii) inflow of the gas from the environment to the upper chamber of the cylinder. The experimental results indicate that dissipative properties of the system in the presented form are rather insignificant. In the case of a high initial pressure the decompression of the gas spring causes an upward rebound of the falling mass. It is manifested in the form of oscillations of the contact force which occur when the piston achieves its top extreme position (see for example Fig. 4.5(b)).

The objective of the considered problem of impact identification is to utilize the measurements performed during stage *A* to obtain the desired impact parameters. This would allow the stage *B* of the impact process to be controlled

in order to reduce the impact force and the acceleration of the colliding objects (the so called Adaptive Impact Absorption, cf. [5]). The proposed methodology requires that the maximal value of the contact force in stage *A* is lower than the maximal value of contact force in stage *B*. The above condition was examined for presented experimental data and it results in contour lines shown in Fig. 4.6. For each value of the initial pressure, the plane defined by the impact parameters (impacting mass and drop height) can be divided into several areas defined by ratio of the maximal force in first and second stages of the process. It can be concluded that for the experimentally tested impact conditions low initial pressure is more profitable for the proposed methodology of combined impact identification and absorption.

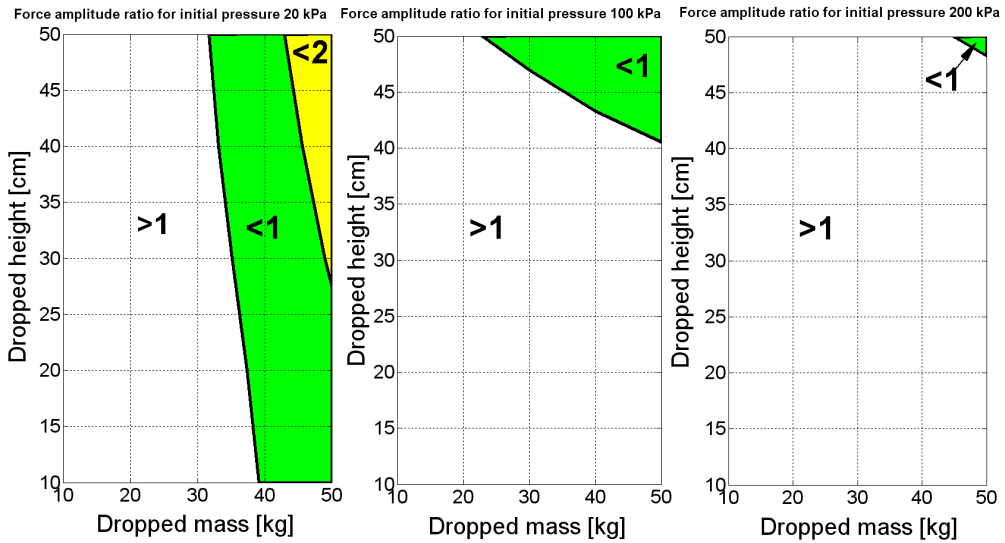


Figure 4.6. Ratio of maximal forces in two stages of the process in the mass velocity area for different initial pressures: 20 kPa (left), 100 kPa (middle), 200 kPa (right).

### Impact process visualization

Chosen tests were filmed with a high-speed camera in order to make visualization of the impact process and to perform the measurements validation. Figure 4.7 shows a sequence of frames with 10 ms interval, starting from the very beginning of the impact process, taken for the mass 30 kg falling from the 20 cm and the initial atmospheric pressure. The rebound between the falling mass and the piston rod is clearly seen in this figure.

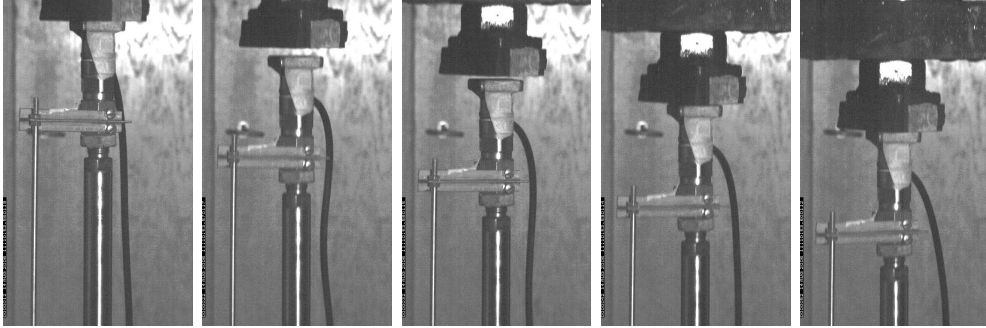


Figure 4.7. High-speed snapshots of impact process (drop height 20 cm, mass 30 kg, initial pressure 0 kPa): 0 ms, 10 ms, 20 ms, 30 ms and 40 ms.

The movies were analyzed by the use of Tema software which enables tracking of the chosen point of the observed picture. The objective of movie analysis was to confirm the falling mass and piston rod accelerometer measurements. The indirect determination of colliding bodies velocity has been used to validate measurement. Both velocities were obtained either by differentiation of the displacement from high-speed camera or alternatively by integration of the acceleration measured by accelerometer. An example of obtained results is shown in Fig. 4.8. Both indirect techniques led to similar results, although the differentiated displacement was noisier and required filtering, while the integration smoothed down the noise effect.

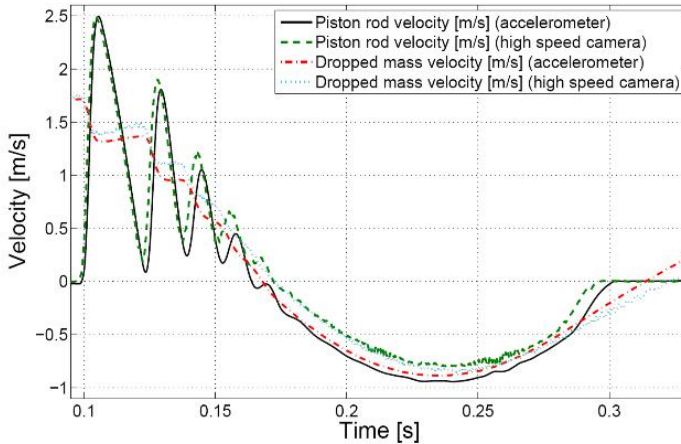


Figure 4.8. An example of indirect measurement of velocities (from the accelerometer and the high speed camera).

The determination of the velocity of the object impacting into the absorber is important with respect to further impact energy dissipation. The identification is possible with the accelerometer sensor located on the falling mass, however for integration the initial condition i.e., initial velocity must be known. Hence, for considered phenomena it is necessary to save the acceleration of the falling body from the very beginning when the velocity equals zero. Theoretically it is feasible. Nevertheless, from the practical point of view at least few difficulties tend to appear. First of all, long time of measurement lead to increase the error in the velocity identification due to for instance the effect of aliasing [157]. Another disadvantage is the necessity to sensor location on the impacting object which is very often impossible. In order to overcome mentioned problems another techniques will be proposed later on.

#### 4.5.2 Numerical simulation of impact scenarios

The parameters of the so called “*impactometer*”: i.e., properties of the bumper located between the colliding objects, mass of the piston rod and friction between the cylinder and the piston have a large influence on impact characteristics and further process of impact identification. However, none of these parameters can be easily modified on the experimental drop testing stand. On the other hand, the analysis of the impact scenarios should be extended to the cases of larger impact energies which also cannot be easily performed experimentally. Therefore, discussion of the influence of the mentioned “*impactometer*” parameters and larger impact energies will be conducted on the basis of numerical simulation.

#### Numerical model validation

Comparison of the numerical results obtained on the basis of the model described in Sec. 4.4 and the experimental measurements, is presented in Fig. 4.9. Although the results are in good qualitative agreement, the exact quantitative compatibility for the wide range of impact scenarios is difficult to obtain. The main reasons are complex and difficult to estimate mechanical properties of the rubber bumper used in the experimental set up (hiper-elastic material properties including Mullins and Payne effects [158, 159]). Another problem is precise determination of the friction force acting between the piston and cylinder walls. In general, the complexity of the model should depend on the objectives of the analysis to be performed. Let us note here that the model was used mainly to examine the qualitative influence of selected parameters. The attention for the

numerical model validation was especially focused on the stage *A* of the impact process when the identification process is going to be performed.

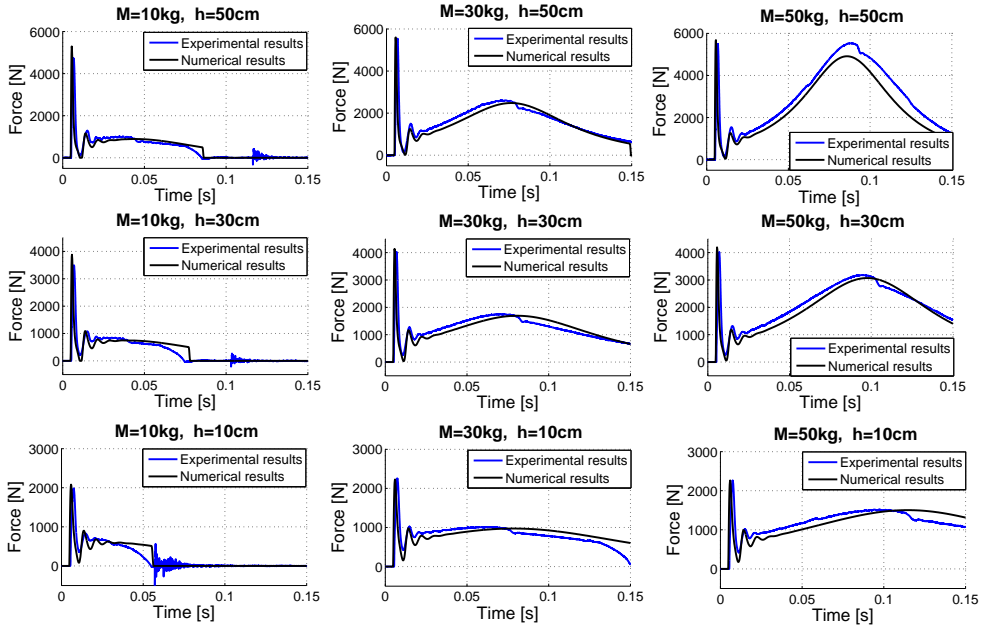


Figure 4.9. Comparison of experimental and numerical results of contact force in time domain (initial pressure equal 200 kPa).

#### Sensitivity analysis of selected parameters

The developed numerical model was used to investigate the sensitivity of the dynamic response of the system. The following parameters were analysed:

- stiffness of the bumper located between the falling mass and the piston rod,
- damping coefficient of the bumper,
- mass of the piston,
- friction between piston and cylinder walls.

The influence of stiffness and damping parameters is especially manifested in the first stage of the impact process. Increase of the stiffness of the contact

element increases the ratio of the stiffness term to the damping term. The first peak value as well as the rebound number increase together with the stiffness (see Fig. 4.10(a)). On the other hand, the maximal value of force during the second stage of impact grows insignificantly. The increase of the damping coefficient decreases the ratio of the stiffness term to the damping term. Therefore, an increase in damping causes a similar effect as a decrease of stiffness (compare Fig. 4.10(a) and Fig. 4.10(b)).

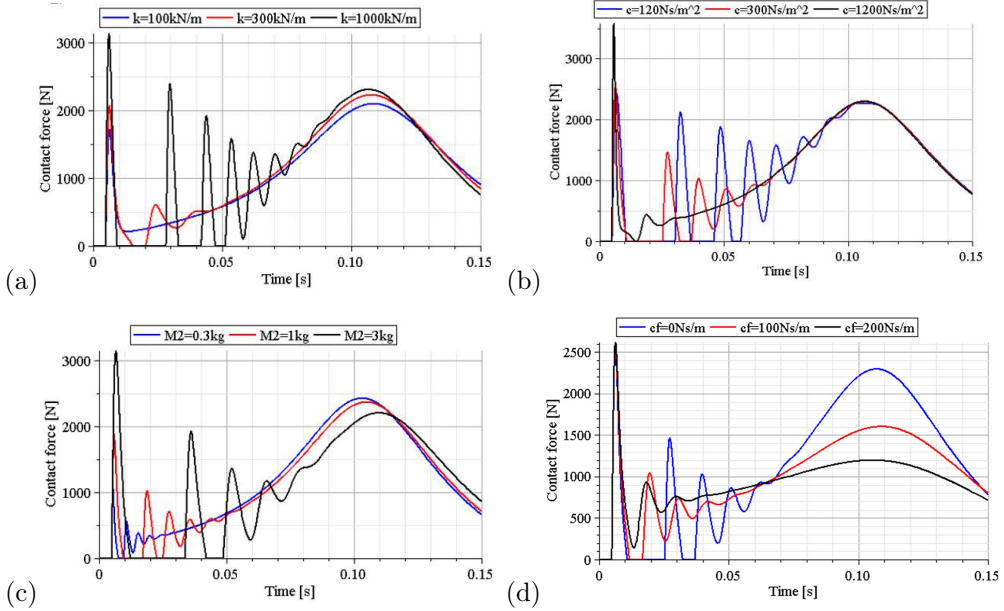


Figure 4.10. Contact force for various: (a) stiffness of the contact element, (b) damping coefficients of the contact element, (c) masses of the piston, (d) friction coefficients.

If the piston mass is increased, the initial peaks of the contact force tend to be more distinct and separated from each other (cf. Fig. 4.10(c)). Due to the fact that more energy is dissipated in the initial stage of impact, the peak force during the second stage of impact is reduced.

The friction force was simulated according to the velocity-dependent model where  $c_F$  was assumed as friction coefficient (cf. Eq. (4.5)). On a contrary to the parameters analysed before, the friction coefficient almost does not influence the first peak of force (see Fig. 4.10(d)). Nevertheless, friction significantly influences the further part of the impact process. An increase of the friction coefficient causes a reduction of the rebound number of the piston and a reduction of force in the second stage of impact.

### Extension to higher impact energies

Another purpose of the numerical model was an examination of the dynamic responses of the pneumatic system subjected to the excitation with higher impact energies. The range of the considered impact scenarios was extended with respect to the experimental section to the mass range 10–190 kg and height range 10–190 cm. The results of the analysis for selected impact scenarios are presented in Fig. 4.11.

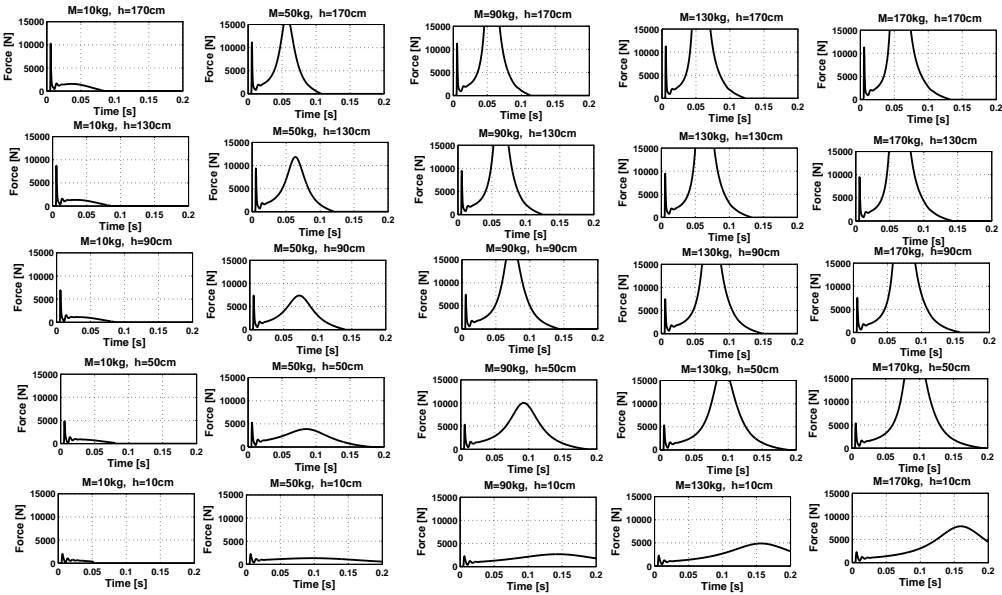


Figure 4.11. Effects of impact mass and velocity on the contact force time-history (initial pressure 100 kPa).

The most important conclusion from the conducted numerical analysis is that an increase of both the impacting object mass and the drop height (i.e., impact velocity) causes the ratio of the peak contact force in stage *B* to that in stage *A* to increase. This ratio is presented in Fig. 4.12 in the form of a contour plot in terms of impacting mass and drop height. The good quantitative agreement with the experimental plot (see Fig. 4.6) was obtained. For high impact energies the ratio is even greater than five which indicates that an application of the proposed system of impact identification is justified.

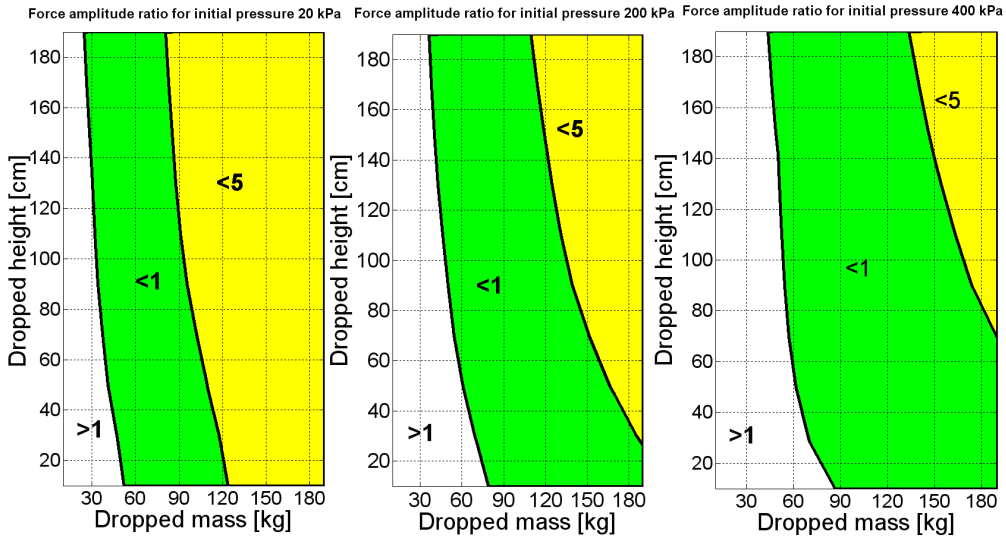


Figure 4.12. Ratio of maximal forces in two stages of the process in dependence on the impact mass and velocity for different initial pressures: 20 kPa (left), 200 kPa (middle), 400 kPa (right).

### 4.6 Impact identification based on “Peak-to-peak” approach

The methodology presented in this section is based on well-known mechanical principles. It utilizes measurements from two sensors: force sensor and accelerometer. Alternatively, the identification is feasible with measurements from one sensor, however then a well-tuned model of the absorption system is required.

#### 4.6.1 The idea

As described in a previous section, the impact process begins with several rebounds of the piston and the falling mass. The rebounds are separated by short time periods during which both objects remain in contact. During these periods certain instants of time must occur, when the velocities of both colliding objects are equal. This phenomenon is schematically shown in Fig. 4.13, where a simplified two degrees of freedom system is presented. The instants of time shown in Fig. 4.13 are also marked in Fig. 4.14(a).

The main idea of the proposed method of impact identification is based on computing the integral of the equation of motion of the impacting mass over time in the range defined by the time instants when the relative velocity of colliding

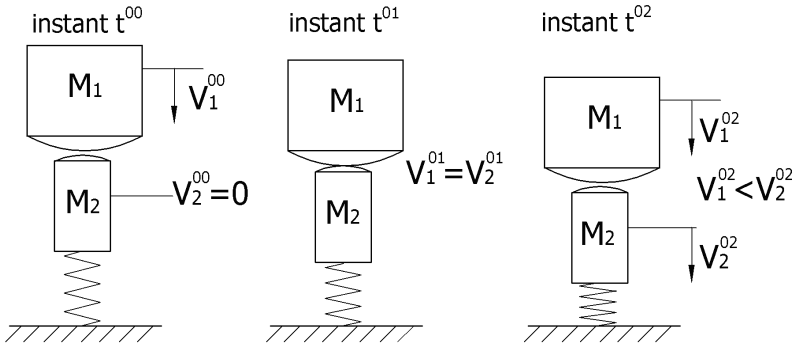


Figure 4.13. Different stages of impact: (left) beginning of the compression stage, (middle) time instant when both velocities are equal, (right) end of the restitution stage.

objects vanishes. Let us denote these characteristic time instants by  $t^{01}$  and  $t^{11}$  (see Fig. 4.14). In the equations presented in this section the upper indices represent the instant of time while the lower ones correspond to the colliding objects. Integration of the equation of motion of the falling mass yields:

$$M_1 \int_{t^{01}}^{t^{11}} \ddot{u}_1 dt - \int_{t^{01}}^{t^{11}} M_1 g dt + \int_{t^{01}}^{t^{11}} F_C dt = 0 \quad (4.13)$$

and therefore

$$M_1 = \frac{\int_{t^{01}}^{t^{11}} F_C dt}{\int_{t^{01}}^{t^{11}} (\ddot{u}_1 - g) dt} = \frac{\int_{t^{01}}^{t^{11}} F_C dt}{(V_1^{11} - V_1^{01}) - g \Delta t}. \quad (4.14)$$

Taking the advantage of the fact that in the considered time instants the velocities of both objects are equal, the velocities and accelerations of the falling mass can be replaced by the velocities and accelerations of the piston:

$$M_1 = \frac{\int_{t^{01}}^{t^{11}} F_C dt}{(V_2^{11} - V_2^{01}) - g \Delta t} = \frac{\int_{t^{01}}^{t^{11}} F_C dt}{\int_{t^{01}}^{t^{11}} (\ddot{u}_2 - g) dt}. \quad (4.15)$$

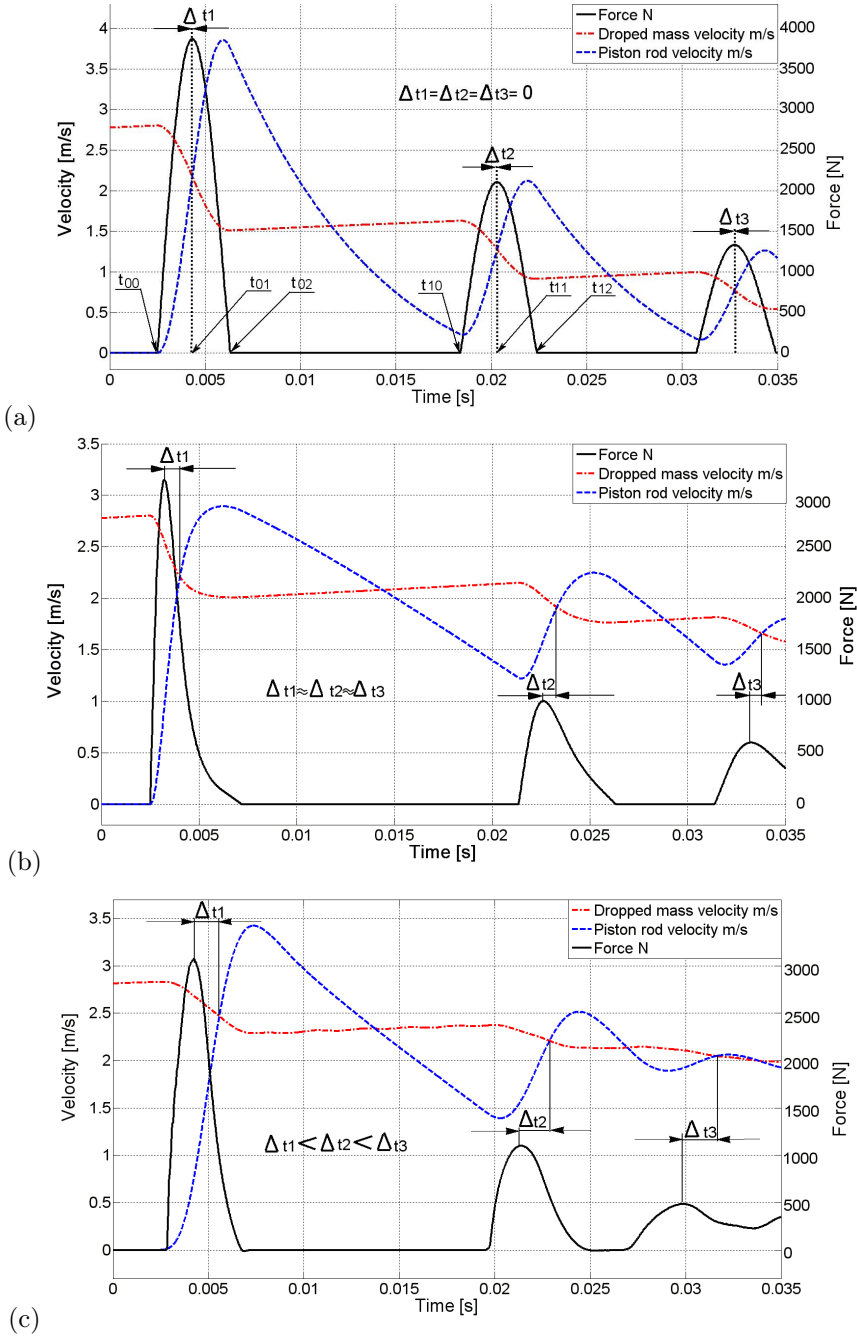


Figure 4.14. Contact force and colliding object velocities in time domain for different models of the contact material: (a) elastic contact force, (b) contact force with damping component, (c) experimental results.

The velocity of the impacting object at time instants  $t^{01}$  and  $t^{11}$  is simply determined based on the condition that both velocities are equal. Hence the following equations can be introduced:

$$V_1^{01} = V_2^{01} = \int_{t^{00}}^{t^{01}} \ddot{u}_2 dt, \quad (4.16a)$$

$$V_1^{11} = V_2^{11} = \int_{t^{00}}^{t^{11}} \ddot{u}_2 dt. \quad (4.16b)$$

The formulae (4.15), (4.16a) and (4.16b) can be utilized directly, if both the contact force and the acceleration of the piston are measured. Alternatively, these formulae can be expressed in terms of forces only. Integration of the equation motion of the piston yields:

$$M_2 \int_{t^{01}}^{t^{11}} \ddot{u}_2 dt - \int_{t^{01}}^{t^{11}} M_2 g dt + \int_{t^{01}}^{t^{11}} F_R dt - \int_{t^{01}}^{t^{11}} F_C dt = 0, \quad (4.17)$$

where  $F_R$  is the global force generated by the absorber. Equation (4.17), allows to define the impacting mass and impact velocity in terms of the contact force  $F_C$  and the force generated by the absorber:

$$M_1 = -M_2 \frac{\int_{t^{01}}^{t^{11}} F_C dt}{\int_{t^{01}}^{t^{11}} F_R dt - \int_{t^{01}}^{t^{11}} F_C dt}, \quad (4.18)$$

$$V_1^{01} = \frac{\int_{t^{00}}^{t^{01}} F_R dt - \int_{t^{00}}^{t^{01}} F_C dt}{M_2} + g \Delta t. \quad (4.19)$$

The force  $F_R$  generated by the absorber contains pneumatic and friction components and therefore it is difficult to be directly measured. Taking the advantage of short duration of the contact and high values of the contact force with respect

to other forces acting on the structure (i.e., friction, pneumatic), the simplification of  $F_R = \text{const.}$  might be used for approximate identification of the impact parameters. An alternative approach to impact identification utilizes measurement of the contact force only and the following definition of force generated by the absorber:

$$F_R(u_2, \dot{u}_2, t) = F_P(u_2, t) + F_F(u_2, \dot{u}_2) + F_D^{TOP}(u_2). \quad (4.20)$$

which can be applied in Eq.( 4.18) and Eq. (4.19) in order to determine the mass and velocity of the colliding object. Alternatively, the definition of the force  $F_R$  can be introduced into the differential equation of the piston motion:

$$M_2\ddot{u}_2 - M_2g + F_R(u_2, \dot{u}_2, t) = F_C(t). \quad (4.21)$$

The above equation allows to compute piston acceleration which can be further used in Eq. (4.15) and Eq. (4.16b) in order to identify the mass and velocity of the impacting object.

#### 4.6.2 Determination of time instants when colliding objects relative velocity vanishes

In order to apply the methodology presented in the previous part of this section, it is important to determine the instants  $t^{01}$  and  $t^{11}$ . In ref. [153] it is asserted that the relative velocity of contact points vanishes when the compression phase terminates and the restitution begins. In the classical impact theory (see ref. [160]) it is assumed that it occurs when the maximum contact force of colliding objects is observed. It might be thus concluded that the time instants, in which the velocities of the colliding bodies become equal, occur when the relative distance between the centers of gravity of the falling mass and the piston rod achieves the minimum value between the rebounds. Nevertheless, for the statement mentioned in the beginning of this section to be true the following conditions have to be fulfilled:

- the contact force must increase in terms of displacement,
- the contact force must be mostly a function of the elastic deformation of colliding bodies and should be independent or negligibly dependent on other factors like velocity.

In general, the method of determination of time instants at which the velocities of both objects are equal depends on the properties of the contact element

located between the falling mass and the piston. The three following cases will be considered separately:

- elastic model of contact force,
- model with viscous damping,
- real rubber applied in the experiment.

#### Elastic model of contact force

The assumption of contact force being purely elastic is often applied in the classical impact theory [153]. In such a case, the contact force arising between the falling object and the piston is a function of the distance between the centers of both bodies, i.e.

$$F_C = kx^n, x = u_1 - u_2 - d_0 \text{ if } x > 0, \quad (4.22)$$

where  $d_0$  indicates the initial distance between both objects while  $u_1, u_2$  represent their displacements. The condition of the extremum of the contact force is defined by the equation:

$$\frac{F_C}{dt} = kn(u_1 - u_2 - d_0)^{n-1}(\dot{u}_1 - \dot{u}_2). \quad (4.23)$$

The above formula indicates that the velocities of both objects are equal exactly at the instant of time when the contact force reaches its extremum (i.e., maximum or minimum), see Fig. 4.14(a). Therefore, in case of elastic definition of the contact force the characteristic time instant, which have to be applied in the proposed method, can be determined very easily. An advantage of this method is that, except for the fact that the contact force is elastic, neither the exact knowledge of the constitutive relation nor the knowledge of exact value of the stiffness coefficient is required.

#### Contact force with the viscous damping component

In a more general case the contact force is a linear combination of stiffness and damping:

$$F_C = kx + c\dot{x}, x = u_1 - u_2 - d_0 \text{ if } kx + c\dot{x} > 0. \quad (4.24)$$

Differentiation of the definition of the contact force over time yields:

$$\frac{F_C}{dt} - k \frac{d(u_1 - u_2 - d_0)}{dt} - c \frac{d^2(u_1 - u_2)}{dt^2} = 0. \quad (4.25)$$

At time instants in which the relative velocity vanishes, the second term of Eq. (4.25) is reduced to zero. By utilizing the equation of motion of the falling mass we obtain Eq. (4.26), which allows the mentioned time instants to be determined in terms of the mass of the hitting object. The whole system of equations for solving the identification problem reads:

$$\frac{dF_C(t)}{dt} - c \left( -\frac{F_C(t)}{M_1} + g - \ddot{u}_2(t) \right) = 0 \text{ for } t = t^{01}, t = t^{11}, \quad (4.26)$$

$$M_1^{id} = \frac{\int_{t^{01}}^{t^{11}} F_C(t) dt}{\int_{t^{01}}^{t^{11}} (\ddot{u}_2(t) - g) dt}, V_2^{id} = V_1^{01}. \quad (4.27)$$

A typical solution of the problem involves:

- assuming of the mass  $M_1$ ,
- calculation of the time instants  $t^{01}$ ,  $t^{11}$  from Eq. (4.26) and calculation of identified mass and velocity from Eq. (4.27),
- repeating procedure with the determined value of the mass.

Due to a large difference in masses of piston and falling object (and their accelerations), the influence of the term dependent on  $M_1$  is insignificant. As a result, the convergence of the proposed procedure is very fast and the impact parameters can be usually identified after a few iterations.

The contact model which involves both elastic and damping terms was examined numerically and exemplary results are shown in Fig. 4.14(b). On the contrary to the model with a purely elastic contact force, the colliding objects velocities do not equalize at the time instant when the contact force reaches its maximum but slightly later, which is in agreement with Eq. (4.25). The time shifts  $\Delta t_1$ ,  $\Delta t_2$ ,  $\Delta t_3$  were found to be almost insensitive to impact scenario, but they increased together with the viscous coefficient used in Eq. (4.24).

### Real rubber contact material properties

The rubber contact element used in the experiment is characterized by a complex mechanical behavior of rubber briefly described in Section 4.5.2. Precise modeling of rubber requires a three-dimensional model of the considered system as well as the Arruda-Boyce or the Ogden-Roxburg [161] constitutive models.

The alternative approach proposed here does not require a numerical model and is based on experimental results only. The performed measurements indicate that the time instants at which the relative velocity vanishes can be determined with respect to the contact force peaks.

The characteristic features of the process were observed:

- time shifts (i.e.,  $\Delta t_1$ ,  $\Delta t_2$ ,  $\Delta t_3$ ) were different for the first, second and third peaks of the contact force, cf. Fig. 4.14(c),
- mentioned time shifts were almost independent on impacting mass and velocity.

The second of these features enables a straightforward application of the proposed method based on Eq. (4.15) and Eq. (4.16b) since the duration of the time shifts are determined in advance.

### 4.6.3 Verification of the method

The proposed “*peak to peak*” identification method was verified experimentally and numerically. Equation (4.15) was applied in order to perform the mass identification. The experimental verification makes use of measurements from two sensors (i.e., force sensor and accelerometer attached to the piston rod). The initial experimental tests enable to obtain the average lengths of the time shifts  $\Delta t_1$  and  $\Delta t_2$  for the preselected set of impacts. They were further used during the stage of method verification for determination of the time instants  $t^{01}$  and  $t^{11}$ .

The impact mass identification was tested for a vast variety of impact scenarios defined by impact mass, velocity and initial pressure. Exemplary results of identification in the case of the initial pressure of 100 kPa are shown in Fig. 4.15. The graph presents in each case the exact value of the mass and the identification error (i.e., the relative difference between the identified and actual values).

The results presented in Fig. 4.15 show a large diversity of identification errors. It is a consequence of the strong sensitivity of the method to measurements inaccuracy which is especially apparent for small initial pressure and large mass of the impacting object.

The identification of the velocity was experimentally tested using integration of the piston rod acceleration (see Eq. (4.16b)). The method uses the assumption of the equality of velocities of the colliding objects at time instants  $t^{01}$  and/or  $t^{11}$ . For verification purposes the instant  $t^{11}$  was used, since then the impacting object mass is already identified. The determination of the actual velocity was

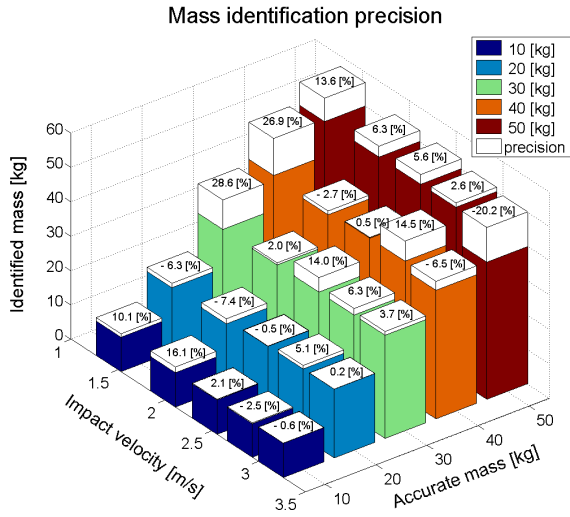


Figure 4.15. Mass identification, experimental results (initial pressure 100 kPa).

performed by an analysis of a movie taken by the high-speed camera as shown in Section 4.5.1. The identification results are shown in Fig. 4.16. The accuracy is consistently better than 2 % and no significant influence of the initial condition was observed.

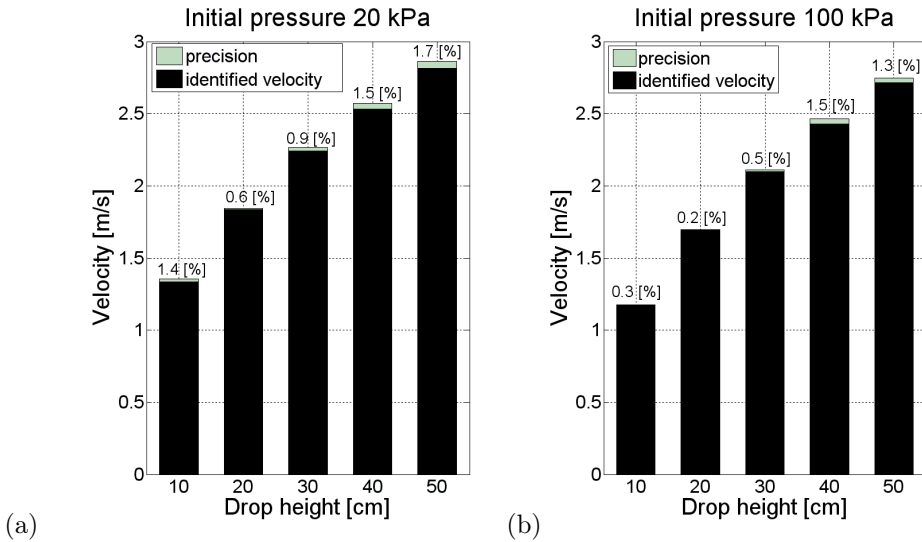


Figure 4.16. Velocity identification, experimental results: (a) initial pressure 20 kPa, (b) initial pressure 100 kPa.

The numerical model presented in Section 4.4 was used to perform a statistical analysis of mass identification error and to investigate the influence of selected parameters. The analyses were focused rather on qualitative than quantitative effects. In order to obtain more representative results, the average identification error for 125 impact cases (impact mass 10–50 kg, impact velocity 1–3 m/s, initial pressure 20–400 kPa) was calculated.

The proposed methodology turns out to be sensitive to impact conditions. Figure 4.17 presents the influence of impact mass, velocity and initial pressure on the mean identification error. More accurate results were obtained for smaller masses of the impacting object, which can be explained by an analysis of the ratio of the falling mass to the piston rod mass. A smaller ratio leads to a larger velocity change of the dropped mass in the first phase of the impact process. As a consequence, the identification procedure seems to be less sensitive to measurements noise in the case of small impacting masses. The second aspect noticed from the statistical analysis is that a higher initial pressure in the pneumatic absorber leads to more accurate results. In general, a full rebound between the impacting object and the piston rod is undesired, since it leads to a small change of the relative velocity in the first stage of the impact and a larger identification error as a consequence. Contrary to the mentioned parameters, the velocity effect was not significant, even if the precision slightly increased together with the impact velocity. The general conclusions mentioned in this section correspond to the analysis presented in the Appendix H.

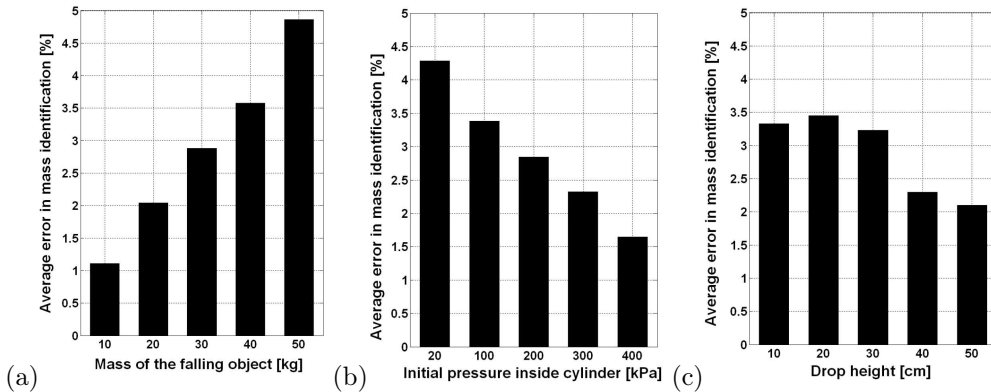


Figure 4.17. Average error of mass identification in dependence on: (a) falling mass, (b) initial pressure, (c) impact velocity.

The experimental results are often corrupted by the measurements noise. The sensitivity of the proposed methodology to these disturbances has been analyzed. In the numerical experiments, the noise-free simulation results were disturbed by random Gaussian noise in the range of 0–10 %, which was defined as the root mean square value of the original signal. The results are presented in Fig. 4.18, where the force, acceleration and both quantities were disturbed. Each point in the graph presents the mean identification error for 125 impact cases (defined by various masses, velocities and pressures). Despite the large number of tests, apparently random values of identification errors were obtained. However, an obvious conclusion might be drawn that larger disturbances in measured signal lead to a larger error of identification. The noise in the force signal was found to have a larger influence on mass identification error than the noise in the acceleration signal. It was noticed that the crucial task is the proper determination of the instants  $t^{01}$  and  $t^{11}$ , which are obtained based on the force signal. Hence, disturbances in the force signal lead to inaccurate determination of  $t^{01}$  and  $t^{11}$  and as a consequence, to errors in mass identification.

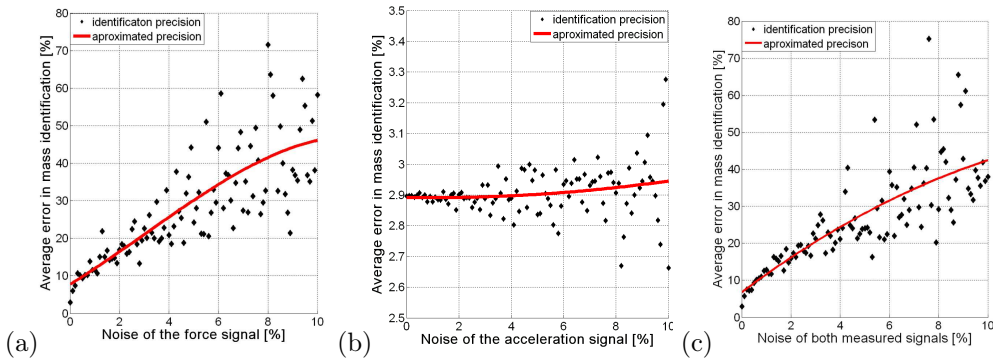


Figure 4.18. Average error of mass identification as a function of signal noise: (a) force signal noise, (b) acceleration signal noise, (c) both signals noise.

Finally, the influence of sampling frequency on the identification error has been analyzed. The results presented in Fig. 4.19 clearly reveal the importance of this parameter. As expected, higher sampling frequency enables to obtain more accurate results. Good results (i.e., mean error below 5%) are obtained for the sampling frequencies exceeding 30–40 kHz. Unfortunately, even in this case extreme outliers (i.e., approx. 20%) can be observed. A general conclusion might be drawn that the methodology requires a high sampling frequency of 50 kHz or more.

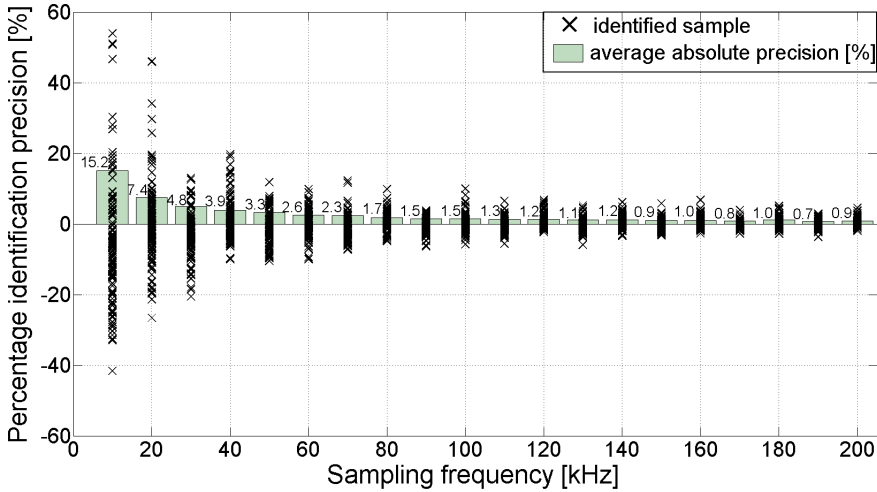


Figure 4.19. Error of mass identification as a function of sampling frequency.

## 4.7 Response map approach

The methodology proposed in this section is focused on the maximum simplicity of the data acquisition set-up, i.e., application of an algorithm which utilizes measurements from one sensor only. Besides, the aim was to decrease the computational cost, which is crucial, as the device has to respond immediately in order to fulfill the deadline condition.

### 4.7.1 The idea

The proposed method can be classified into the group of pattern recognition techniques. The identification is performed based on a formerly prepared database of measured dynamic responses caused by various impact scenarios applied to the considered structure. The actually measured dynamic response is compared with the responses stored in the database. The methodology can be classified as model-free because the structural model is not required in the identification stage.

The objective of identification is to determine the impact parameters (mass and initial velocity of the impacting body) for which the structural response is the most similar to the actually measured response. The identification is based on a pre-fetched database (called the response map) which gather selected

characteristic parameters of the measured structural response  $Y_1, Y_2, \dots, Y_m$  (e.g., signal amplitude, its period etc.) that correspond to various parameters of the applied loading  $x_1, x_2, \dots, x_n$  (e.g., mass, impact velocity, etc.). General dependency of the structural response on impact parameters is defined by the following relations:

$$\begin{aligned} Y_1 &= Y_1(x_1, x_2, \dots, x_n), \\ Y_2 &= Y_2(x_1, x_2, \dots, x_n), \\ &\dots \\ Y_m &= Y_m(x_1, x_2, \dots, x_n). \end{aligned} \quad (4.28)$$

The approach consists of two main steps. In the first step, the database is generated, which can be performed either via a calibrated numerical model of the structure [162] or by experimental tests. The second step is the actual identification. Measurement of the actual response is performed and compared with the measurements stored in the database.

The proposed approach leads to an optimization problem in which the discrepancy between the actually measured response  $Y_i^M$  and the stored responses  $Y_i$  is minimized. With the normalized least squares discrepancy measure, the objective function to be minimized takes the following form:

$$L(x_1, x_2, \dots, x_n) = \sum_{i=1}^m \left[ \frac{Y_i^M - Y_i(x_1, x_2, \dots, x_n)}{Y_i^M} \right]^2 \quad (4.29)$$

and the corresponding optimization problem relies on minimization of the objective function over impact parameters  $x_1, x_2, \dots, x_n$ . The number of parameters to be identified, denoted by  $n$ , is limited by the number  $m$  of the parameters used for identification:  $m \geq n$ .

In the considered case two parameters (i.e., falling objects mass  $M_1 \equiv x_1$  and its impact velocity  $V_1 \equiv x_2$ ) had to be identified based on a single measurement from the force sensor. Therefore, in order to construct the response maps, at least two characteristic quantities had to be extracted from each single measurement. As an example, Fig. 4.20 shows in the mass-velocity space the two parameters ( $Y_1, Y_2$ ) used to construct the response map.

For the given response maps, the impact identification procedure utilizes the error function defined as:

$$f(M_1, V_1) = \left[ \frac{Y_1^M - Y_1(M_1, V_1)}{Y_1^M} \right]^2 + \left[ \frac{Y_2^M - Y_2(M_1, V_1)}{Y_2^M} \right]^2, \quad (4.30)$$

where  $M_1$  and  $V_1$  are the impact parameters to be identified,  $Y_1(M_1, V_1)$  and  $Y_2(M_1, V_1)$  are obtained from the response maps for the specific values of  $M_1$  and  $V_1$ , while,  $Y_1^M$  and  $Y_2^M$  denote the actually measured values.

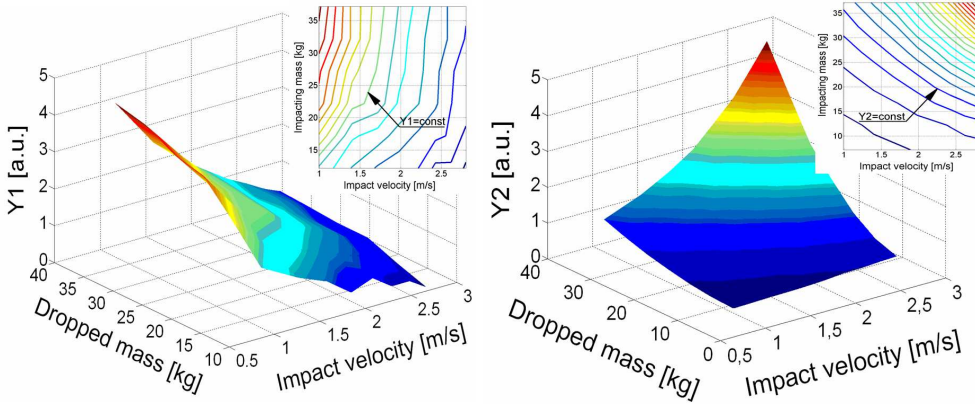


Figure 4.20. Examples of experimental response maps: (left)  $Y_1$ ; (right)  $Y_2$ .

The identification problem can be presented graphically. Consider two contour lines of the response maps, which correspond to the actually measured values  $Y_1^M$  and  $Y_2^M$ . The intersection point defines the identified impact parameters, which is shown schematically in Fig. 4.21, see the analogy to the contour line plot presented in Fig. 4.20.

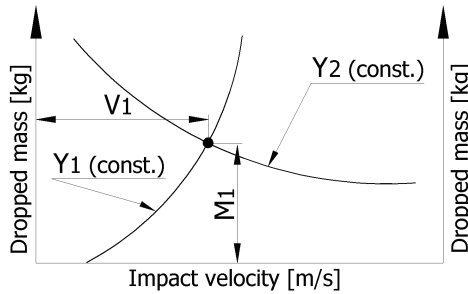


Figure 4.21. Graphical interpretation of the identification process.

### 4.7.2 Selection of parameters for the response maps

An important task is the extraction of the characteristic features of the measured response to be stored in the database. Appropriate choice of these parameters (signal features) facilitates the identification and leads to more accurate results.

The response map is prepared based on the experimental measurements of the contact force. The choice of force sensor was motivated by its location (i.e., fixed to the absorber) and signal properties (smooth and not requiring filtering). However, the procedure can use other sensor, if its measurements is sensitive enough to the impact parameters.

Since the procedure utilizes contact force as a main quantity for the identification, its sensitivity on impacting mass and velocity is crucial for the effectiveness of the methodology. The analysis (see Section 4.5, Fig. 4.5 and Fig. 4.11) conducted via the experimental measurements and numerical simulation proved strong dependence of the contact force on hitting object velocity during the whole period of impact. On the contrary, the dependence on mass of the impacting object is noticeable only in the second stage of impact. It indicates that in the first impact stage it is easier to identify the impacting object velocity than its mass.

As an example, the first parameter of the response ( $Y_1$ ) can be defined as the first peak value of the contact force, and the second parameter ( $Y_2$ ) as its integral in a certain period of time ( $t_0, t_{end}$ ):

$$\begin{aligned} Y_1(M_1, V_1) &= \max F_C(M_1, V_1, t), \quad t \in (t_0, t_{end}), \\ Y_2(M_1, V_1) &= \int_{t_0}^{t_{end}} F_C(M_1, V_1, t) dt, \end{aligned} \quad (4.31)$$

$$Y_1^M = \max F_C^M(t), t \in (t_0, t_{end}); Y_2^M(t) = \int_{t_0}^{t_{end}} F_C^M(t) dt. \quad (4.32)$$

The parameters defined by (Eq. 4.31) correspond to the values stored in the database while the parameters defined by (Eq. 4.32) are extracted from the actual measurement.

The shape of the objective function (cf. Fig. 4.22) was strongly dependent on the length of the time interval used to determine the second parameter  $Y_2$ . If only the initial stage of the impact was considered ( $t_{end} = 10$  ms), the objective function depended mainly on the impact velocity (a long valley along the mass parameter, see Fig. 4.22(a)). As the length of the time period increased, the objective function became dependent also on mass of the hitting object. It indicates that mass identification is easier when the measurement of the response is performed over a longer time period.

The choice of proper parameters of the response for preparation of the response map is also motivated by practical aspects. The selected values have to

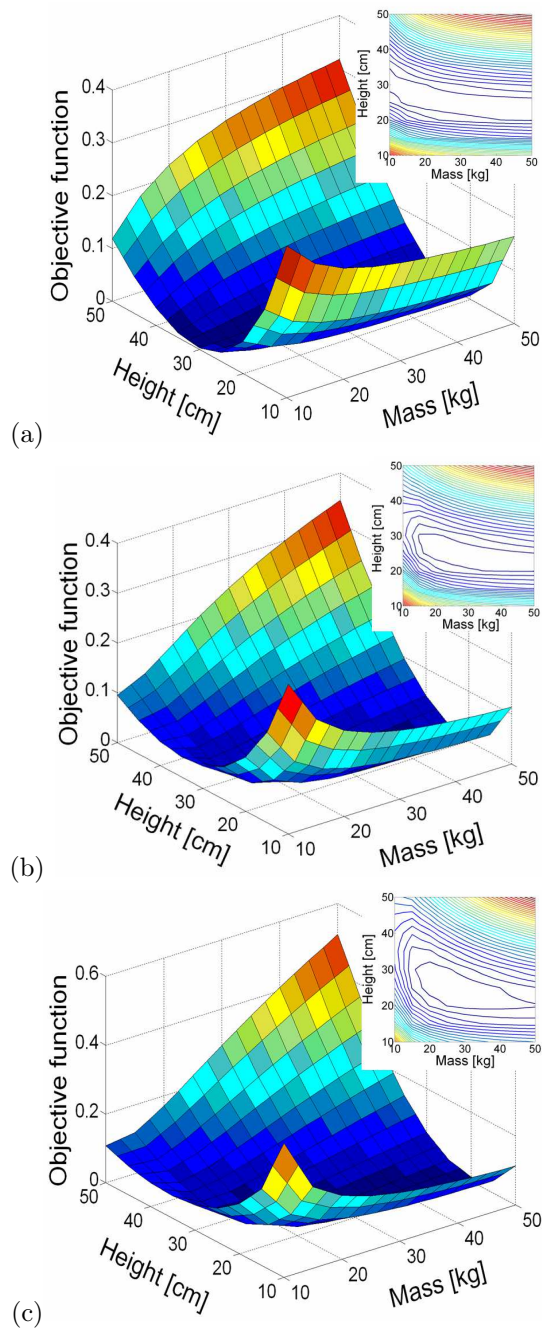


Figure 4.22. Dependence of the objective function on the time interval used for identification: (a)  $t_{end} = 10$  ms, (b)  $t_{end} = 40$  ms, (c)  $t_{end} = 60$  ms.

be characteristic for the impact process, that is it should be possible to unambiguously determine them from the measured signal (without neglecting the deadline condition). Hence, the objective is to find characteristic parameters of the response which exist at the beginning of the impact process (stage *A*). Another important aspect is the reduction of dimensionality of the response maps, as pattern recognition classifiers become in general less effective as the dimensionality of the feature space increases [163]. Moreover, the computational cost is significantly lower in case of a small-dimensional database. Sampling of the parameter space might be uniform or non-uniform. If a region of more frequent cases can be determined, the probability density functions are used [162] for sampling of the parameters space. In the considered case it is assumed that each impact scenario is equally probable and a uniform sampling is used.

Finally, taking into account all the above indications, the selected parameters were either the amplitudes of the two first peaks of the force signal or the force maximum value and integral in the considered time interval.

#### 4.7.3 Verification of response map approach

The verification of the method was focused on the sensitivity analysis and it was performed on the basis of numerical simulations. Two parameters were considered: identification error and computational cost.

The response map was built using the results obtained for 100 different impact scenarios (10 impacting masses 10–50 kg and 10 impact velocities determined by the drop height 5–50 cm), while the initial pressure was not altered. Hence, the database was originally of the size  $10 \times 10$  and utilized two parameters. The approach was tested using 10 randomly selected impacts. An important problem to be considered is the minimal size of the database which guarantees acceptable identification accuracy. The database density was numerically increased by interpolation. Nine databases ( $25 \times 25$ ,  $50 \times 50$ ,  $100 \times 100$ ,  $250 \times 250$ ,  $500 \times 500$ ,  $1000 \times 1000$ ,  $2000 \times 2000$ ,  $2500 \times 2500$ , and  $3000 \times 3000$ ) were obtained.

The graphs shown in Fig. 4.23 present the average identification error and the computational cost of identification of impacting mass Fig. 4.23(a) and impact velocity Fig. 4.23(b) as functions of the database size. Here, the first two peaks of the contact force in the first stage of the impact process were used as characteristic parameters. In each case, the accuracy of velocity identification turns out to be much higher (about 5–10 times) than the accuracy of mass identification. It is the result of the different sensitivity of the measured contact force on both parameters. In general, the accuracy of the response map approach increases together with the database size. Nevertheless, the compu-

tation time increases significantly as well. Hence, the identification process for large databases became impractical with regard to the deadline condition. For databases larger than  $3000 \times 3000$  ( $9 \cdot 10^6$  of mass-velocity variants) the computational cost exceeded 350 ms for a modern PC. As a consequence, the  $500 \times 500$  database has been used to guarantee an acceptable identification accuracy and to keep the computational cost low.

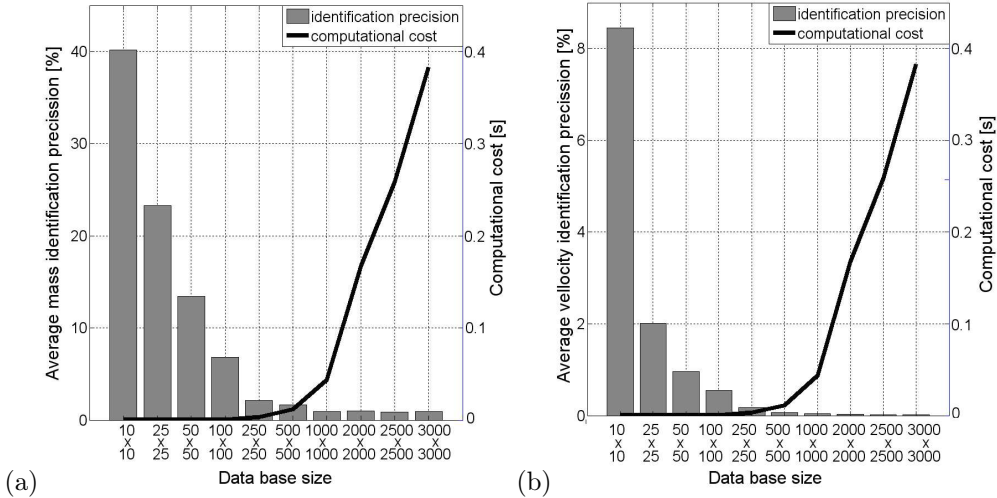


Figure 4.23. Average identification error and time as functions of database size: (a) mass identification, (b) velocity identification.

Next, the maximum value of the contact force and its integral in a certain time interval were used as characteristic parameters to build the database. A significant influence of the integration interval length on the identification error was found. The results obtained for the database  $50 \times 50$  are shown in Fig. 4.24. The accuracy increases together with the time interval, which is most significant for smaller databases. On a contrary, in the case of velocity identification, the obtained precision is insensitive to the length of the integration interval.

### 4.8 “Impactometer” device concept

The conducted research enables to propose a concept of the device which utilizes the developed on-line identification methods. Such a device contains a gas spring, which can be switched to a pneumatic absorber (via controlled opening of pressure release valve), and thus be capable of impact energy absorption in

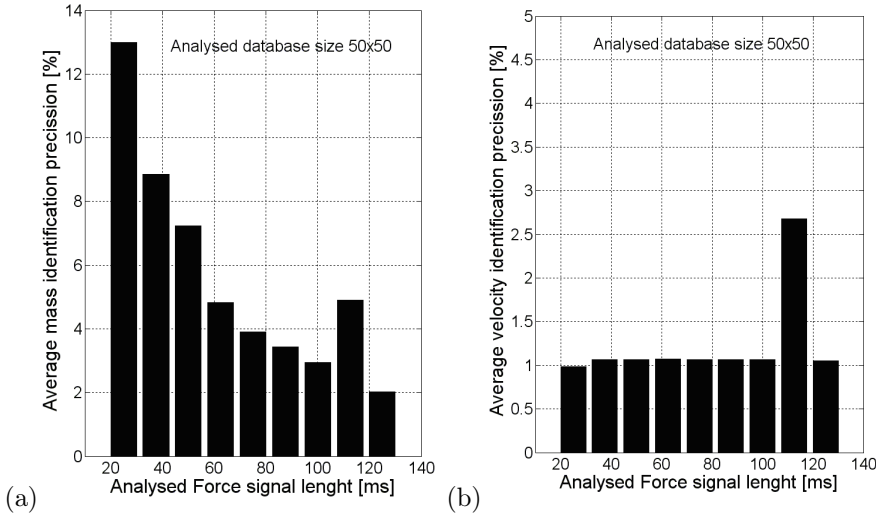


Figure 4.24. Identification error as a function of analysed force signal length: (a) mass identification, (b) velocity identification.

a controllable manner (patent pending). A simplified scheme of the impactometer together with the pneumatic AIA (Adaptive Impact Absorption) device is shown in Fig. 4.25(a). The force sensor  $F$  and the accelerometer  $A$  are used for the identification of impact parameters and together with the gas spring and the control system  $CS$ , are the main part of the impactometer. The pressure sensors  $P_1$  and  $P_2$  are used for the measurement of the pressure in the chambers  $V_1$  and  $V_2$  and together with the control system  $CS$  and controllable valve  $Z$  are the main parts of the AIA system.

The theoretical effectiveness of an AIA system which utilizes impactometer-based impact identification is shown in Fig. 4.25(b). Three force histories are presented: i) the case when the valve remains closed during the impact process, ii) the case with constant optimum valve opening and finally iii) the case with a real-time control of the gas flow. Both considered adaptation strategies enables to reduce the contact force observed in the second stage of collision and so to decrease the acceleration acting on the colliding object. The second of the applied strategies (real-time control of the gas flow) allows to obtain optimal constant level of the acceleration.

### 4.9 Final remarks

The chapter presents a thorough analysis of the process of a rigid body impact into a pneumatic cylinder. The impact drop tests were performed experimentally and a numerical model of the impact process was developed. A wide variety of impact scenarios have been tested and its range has been numerically extrapolated. Various properties of contact element in collision region were investigated. Two algorithms for real-time impact load (i.e., impact mass, velocity) identification have been demonstrated (in Sections 4.6 and 4.7). Both algorithms operate in real-time and enable identification of impact during the initial milliseconds. It makes them useful for potential future applications in adaptive impact absorbing systems since non of then do not required the sensors located in the impacting object.

The first of the proposed approaches (the “peak-to-peak” method) uses two sensors (contact force and piston acceleration) for a very fast identification, which is possible due to the simplicity of the procedure. On the other hand, the method requires high sampling frequency and almost noise-free measurement data. Precision of the identification was found to be sensitive to the internal parameters of the “impactometer”. An acceptable precision was obtained when the mass of the impacting object was comparable to the mass of the piston rod (within the range of one order of magnitude) and for high pressures inside the cylinder.

The second of the proposed methods (the “response-map” approach) is based on single measurement only (contact force), however it requires initial prepara-

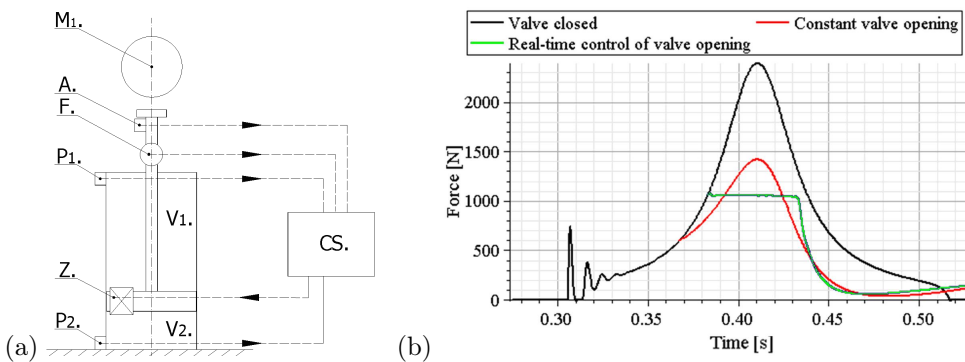


Figure 4.25. An adaptive impact absorption system equipped with the *Impactometer* device: (a) schema of the proposed system, (b) numerical example of an impact scenario.

tion of the database. It can be obtained either by multiple experimental tests or by numerical simulations. The “response-map” approach requires longer identification time than the “peak-to-peak” approach, but the results are more precise. The mean value of identification errors as well as their deviations decrease for larger databases, however at the cost of the identification time. It was proved that the precision is significantly improved by considering a longer contact force history, but it delays the identification process. Independently on the identification method, accurate velocity identification is much easier to perform than accurate mass identification.

In the next step, the “impactometer” will be realized and implemented. The problem of impact identification will be extended into two and three dimensional cases which is much more challenging and requires more advanced identification techniques.

# Concluding remarks

The concluding part of this thesis, firstly, presents a brief summary of the chapters content and in the following part, emphasizes the original achievements of the study.

## 5.1 Thesis summary

The main objective of the thesis was to develop techniques for dynamic load identification operating in real-time. To this end, two major tasks were undertaken, namely:

- development of a new class of cheap detectors, operating on the basis of piezoelectric strain sensors, suitable for real-time detection of loads generated by vehicles (i.e., a new type of WIM detectors dedicated for road and railway transport),
- development of a new class of impact detectors, appropriate for real-time impact load detection (i.e., the detection of impacting object's mass and velocity).

The thesis begins with a definition of the dynamic load identification problems and emphasize a motivation for the performed research. In the introductory part, a brief discussion of the load identification techniques in the form of literature review is also given. Special attention is paid to real-time systems and important notions relevant for this subject are explained. Since piezoelectric measurements were extensively utilized during the experimental research, the piezoelectric sensoric techniques are discussed and compared to other methods.

**Chapter 2** explores the area of road Weigh-in-Motion detectors. It starts with literature review which gives an overview of the already developed and available road WIM devices. Two new WIM detectors (i.e., beam-shape and plate-shape one), operating on the basis of the monitoring of the strain development in deformable body by use of piezoelectric strain sensors, were proposed.

Their development was supported by numerical modelling validated experimentally. It enabled to perform experimental and numerical investigations of factors important for moving load identification and to formulate algorithms. The research proved that, since the detector is considerably wider than the footprint area, no integration of the measured signal is necessary, and in principle, the signal amplitude can be taken as a load equivalent. As a consequence, the wider detectors are more precise what was shown in the thesis. Practical implementation of the beam-shape and plate-shape devices proved that the first one was more sensitive to the velocity effect of a vehicle passing over the detector. At higher velocities strong vibrations occur, and consequently, the beam-shape detector can be applied only for limited range of velocities (up to 50 km/h) contrary to the plate-shape one where no velocity limits were observed. Two times higher load identification precision achieved by the plate-shape device (better than 10 % of accuracy related to the static measurements) makes it more promising in practice. However, the beam-shape device requires smaller number of sensors than the plate-shape one which may be of importance in cases where the economical point of view is considered.

**Chapter 3** is devoted to the implementation of the Weigh-in-Motion detectors for railway transport. First, some existing WIM methods in the railway applications are reviewed. The main purpose of the research presented in this chapter was a practical implementation of a detector which operates on the basis of piezoelectric-strain measurements in the rail. The idea utilizes the recording of the strain evolving in rail due to the motion of train. The experimental research was carried out *in situ* and enabled to validate the numerical model of the rail-sleeper-ground system. The numerical and experimental research were focused on the analysis of the factors affecting the load identification using the developed idea. A linear relation between the identified load and responses obtained from sensors was observed. The train velocity effect was insignificant for signal amplitude measurements recorded by the piezoelectric sensors and processed by the charge amplifier in the tested range of velocity. The numerically investigated effects of load distribution and support conditions were found to be important for load identification. Two algorithms of load identification were proposed. The method based on the on-line calibration which makes the measurements insensitive to some environmental conditions seemed to be more practical. Despite the poor condition of the railway tracks in the measured area the developed device shown 5% of repeatability of sensor signals responses.

The research presented in the second and third chapters proved that the piezoelectric strain sensors can be used for the dynamic load identification. This kind of sensors is good alternative for more popular ones, like strain gauges

and/or fiber optics. However, it is crucial to use high quality electronics and proper calibration process. The usage of a proper amplifier in the measurement set-up was found to be of an uttermost importance. It was proved that considerably better results can be achieved when charge amplifiers were used instead of the voltage ones. Two types of piezoelectric sensors were used, namely, piezo-ceramic one and piezo-fiber one, for which similar results were observed despite a significant difference in their cost.

The research described in **Chapter 4** is of a more fundamental matter than the one presented in the previous chapters. The fourth chapter is focused on the development of the “*impactometer*” concept. First, a review of the so-called Adaptive Impact Absorption (AIA) is given since the AIA systems seem to be a potential area of application for the impactometer. The objective of this chapter is related to the problem of real-time identification of impact load (i.e., the detection of an impacting object’s mass and initial velocity). The conducted experimental research as well as numerical simulations led to development of two identification algorithms satisfying the following requirements: firstly, sensors used for the identification cannot be directly attached to the impacting object, and secondly, the identification should be attainable at the very beginning of the impact process. It was checked that the precision of mass identification depends strongly on the absorption properties of an AIA system; taking into account these absorption properties should allow for an improvement in identification. The impact velocity identification was found to be less challenging; in general, it was attainable with higher accuracy than the mass identification. Two different identification methods were compared. It was shown that each of them has its own merits, limitations and drawbacks.

## 5.2 Key achievements

The thesis in the author’s belief, is rather experimental than the theoretical one. It has already been mentioned that the main objective was development and practical implementations of all presented ideas. However, the experimental research was supplemented with many numerical simulations in order to expand the area of investigation.

In author’s belief, all assumed objectives of the thesis have been accomplished. In particular, the following original achievements can be distinguished:

- a inexpensive piezoelectric-sensor-based technology for train and road weight-in-motion devices was developed,

- laboratory and field tests of the new piezo-based road weight-in-motion concepts were conducted,
- algorithms for dynamic load identification dedicated for the original proposed road WIM devices were formulated and implemented,
- two prototypes of weight-in-motion devices dedicated for road transport (namely, the beam-shape one and the plate-shape one) were designed, manufactured and tested,
- the methodology capable of monitoring of the railway transport (based on the strain history measured in rail by piezoelectric sensors) was developed,
- the measurement algorithm for railway load detection as well as the procedure of on-line calibration for the rail WIM system was formulated,
- a prototype of weight-in-motion device dedicated for railway transport was designed, manufactured and tested,
- important factors for proper dynamic load identification used for WIM railway and road devices were determined,
- two real-time impact load identification procedures using sensors fixed to the impacted body (i.e., no sensors present on the impacting object) were developed.
- a concept of the “impactometer” suitable for real-time mass and velocity identification of impacting object was introduced.

Some parts of the presented research were used in patents pending, namely:

- patent pending for the railway weigh-in-motion system constituting a part of the structural health monitoring system dedicated for truss bridges [3],
- patent pending for the method and device for mass and kinetic energy identification of an object impacting onto barrier [58],
- patent pending for the pneumatic absorber and the method for impact energy dissipation [164].

# Finite element modelling of piezoelectric sensors

Load identification devices considered in this thesis utilize the sensors operating on the basis of piezoelectric effect. Models of the WIM devices i.e., road one (beam-shape and plate-shape) and rail one were created on the basis of the FE method. Thus, one of the crucial aspects for obtaining correct numerical results was precise modelling of piezoelectric strain sensors. The models were prepared by means of ADINA software, which is not directly equipped with the model of the piezoelectric material so this task was not trivial and a more in-depth explanation is needed.

The explanations presented in this appendix are particularly oriented for shell structures and thin wall 3D structures. Certain assumption were made. The piezoelectric patch has to be parallel to the mid-plane of the structure. The electric field and the displacement are assumed to be uniform across the piezoelectric sensor thickness and aligned on the normal to the mid plane [165]. Moreover, the sensors are thought to be homogeneous along the longitudinal and the transversal directions. As a consequence, the piezoelectric constants are equal ( $e_{31} = e_{32}$ ). Finally, the effect of the interaction between the sensor and the structure is neglected. The last simplification can be justified by the fact of relatively small dimension in comparison to the whole structure.

An example of a piezoelectric shell is presented in Fig. A.1. For a piezoelectric sensor, defined as a shell which satisfies the assumptions mentioned above, the following equation can be applied to calculate the value of the charge generated by means of the piezoelectric material [96]

$$Q = e_{31} \int_C \left( \vec{u}_0 \cdot \vec{n} + z_m \frac{\partial w}{\partial \vec{n}} \right) dl, \quad (\text{A.1})$$

where  $Q$  – the charge generated by piezoelectric sensor,  $e_{31}$  – the piezoelectric constant,  $\vec{u}_0 \cdot \vec{n}$  – the displacement normal to the contour,  $z_m$  – the distance

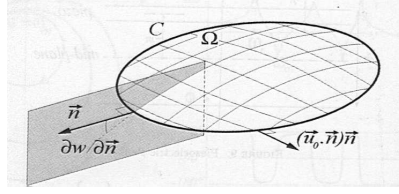


Figure A.1. View of the shell with parameters used in Eq. (A.1) [96].

between the mid plane of the model and the piezoelectric sensor (see Fig. A.2),  $\frac{\partial w}{\partial \bar{n}}$  – the slope.

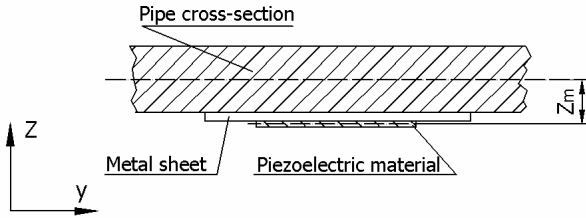


Figure A.2. Representation of the parameter  $z_m$  for thin wall structures.

The charge generated by means of the piezoelectric sensor depends on linear strains and this represents the first term of Eq. (A.1). Moreover, it is important to consider the bending slope of the sensor and this was included the second term in Eq. (A.1).

In the numerical model, the surface of the piezoelectric sensor is discretised using nodes. The density of the FE model mesh should be fit, so that the positions of the nodes correspond to the edge of the piezoelectric sensor. According to the paper [166], it was proved that the value of the response of modelled sensor does not depend on the number of the FE corresponding to the modelled sensor. Thus, the charge produced by the modelled transducer is equivalent to the sum of the displacements and rotations of the nodes located on the sensor edge. Since the piezoelectric strain sensor is a rectangular (this shape was used in experimental test), the value of the charge can be calculated from the following formula:

$$Q = e_{31} \left( \sum_{i=1}^n (u_i + z_m \varphi_i) + \sum_{j=1}^n (v_j + z_m \psi_j) \right), \quad (\text{A.2})$$

where  $u$  – node displacement in  $x$  detection,  $\nu$  – node displacement in  $y$  detection,  $\varphi$  – rotation of node around  $y$  axis,  $\psi$  – rotation of node around  $x$  axis,  $i$  – nodes on the edge located parallel to  $y$  axis,  $j$  – nodes on the edge located parallel to  $x$  axis.

It is recommended (if possible) to prepare the FE model in such a way to locate the piezoelectric sensor to be parallel to the coordinated system axis used in the FE program. This operation considerably simplifies the analysis. For instance, in case of the model presented in Fig. A.3, the modelled piezoelectric sensors were located on the bottom of the pipe. This position allows the analysis in two dimensional coordinate system  $(x, y)$ .

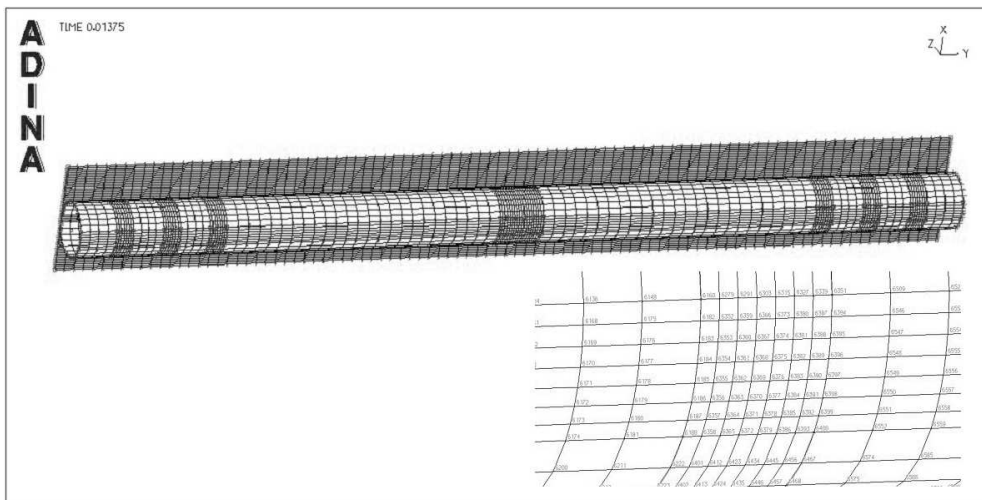


Figure A.3. Down view of the model.

The charge produced by a piezoelectric sensor is linearly proportional to the sensor deformation. Thus, it is advisable to measure the displacements and rotations of the nodes located on one edge in relation to the other parallel edge. It was practically conducted by calculating the displacements and the rotations in the opposite nodes using the opposite signs, as illustrated in Fig. A.4. To ease the analysis, the rotations and the displacements are presented in two drawings. Senses of the vectors presented in Fig. A.4(b) were chosen according to the “corkscrew rule”.

In practice, the values of the signals were calculated separately for the nodes located on the longer and on the shorter edge of the sensor. For the first case

the following formula was used:

$$Q_{\text{long}} = \sum_{i=1}^n (x_i + z_m \varphi_i), \tag{A.3}$$

where  $x$  – node displacement in the  $x$  detection,  $\varphi$  – rotation of the nodes around  $x$  axis,  $i$  – the nodes located on the longer edge of the modelled sensor.

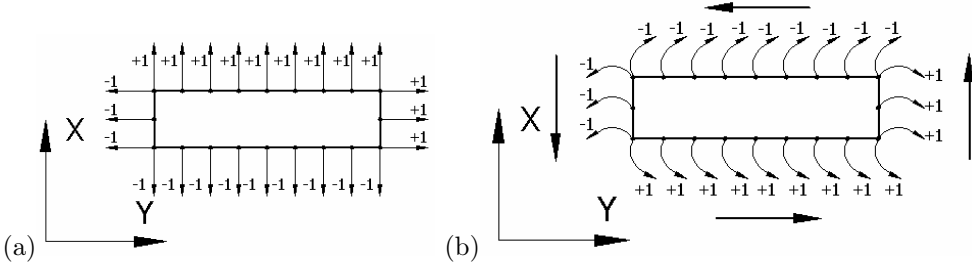


Figure A.4. Senses of the vectors used in calculation: (a) displacements, (b) rotations.

For the second case the signal was computed as follows:

$$Q_{\text{short}} = \sum_{j=1}^n (y_j + z_m \psi_j), \tag{A.4}$$

where  $y$  – node displacement in the  $y$  detection,  $\psi$  – rotation of the nodes around  $y$  axis,  $j$  – nodes located on the longer edge of the modelled sensor.

If the aim of analysis is more qualitative than quantitative, then the piezoelectric constant factor can be neglected in those formulas (A.3) and (A.4).

Finally, the signal generated by means of the sensor model is obtained by the sum of the values calculated from Eqs. (A.3) and (A.4). In order to achieve the quantitative validation of simulation, or to compare the numerical and experimental results, the piezoelectric constant must be considered. Moreover, the measured signals are most often stated in voltage. Hence the following formula may be useful:

$$V = \frac{Q_F}{C}, \tag{A.5}$$

where  $Q_F$  – the charge resulting from force  $F$ ,  $C$  – the capacitance of the device,  $V$  – the sensor voltage signal.

# B

## Small testing stand of the beam-shape device

Testing stand presented in Fig. B.1(c) has been built in order to perform a feasibility study of the proposed beam-shape WIM device. Moreover, the objective of the research was to develop an algorithm for the load identification (see Appendix C). The stand included a steel pipe symmetrically supported at the ends. The Amplified Piezoelectric Actuator APA60SM, see Fig. B.1(b), manufactured by the “Cedrat” company was used to generate the excitation. The oval shape of the actuator serves mechanical amplification of the deformation of the piezoelectric material which is usually up to about 0.1%  $1 \mu\text{m}/\text{mm}$  at typically 150 V [167]. Two piezoelectric patches, see Fig. B.1(a), located symmetrically on the surface of the pipe, were used to measure the parameters of the excitation.

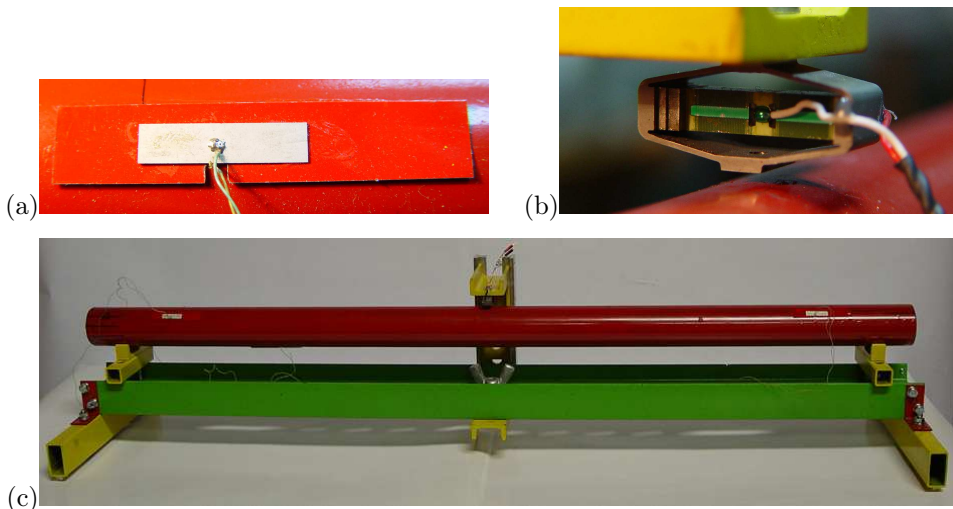


Figure B.1. Laboratory testing stand: (a) piezoelectric sensor, (b) actuator, (c) overall view.

The design of the stand enables the actuator to be put in different positions along the test pipe. In general, this feature has been used in order to simulate various location of excitation generated by car wheel (in the case of “real” structure). The location of the actuation is one of the considered variables. Electric signals of various shape, amplitudes and periods can be used to drive the actuator. A half-period sinusoidal signal was chosen to simulate the tire force exerted by a running car on the structure, because it is close to the real one (see Fig. 2.4). An example of a waveform of the driving signal is shown in Fig. B.2(a). The parameters labeled in Fig. B.2(a) have the following meanings:

- the period of the signal  $T'$  is equivalent to the car tire contact time with the analyzed structure,
- the amplitude of the signal  $A'$  is proportional to the axle-load of the car.

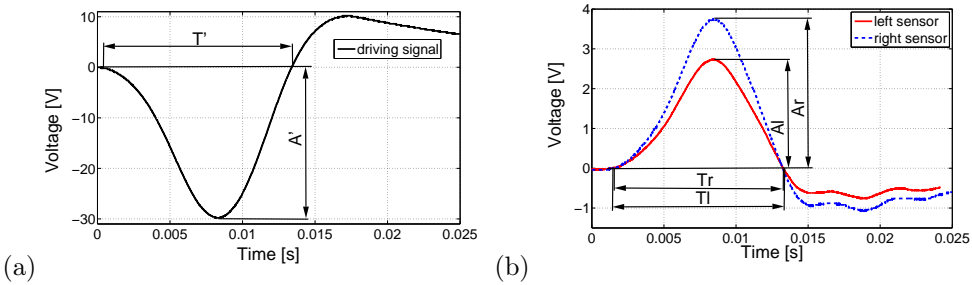


Figure B.2. Experimental signals: (a) the waveform of the signal driving the actuator, (b) the signal produced by the sensors mounted on the pipe.

In real road conditions, cars travel with different velocities, their weights as well as the positions of their wheels on the lane vary a lot. These three factors have to be taken into account while performing the research. Thus, the actuator has to be put in various locations during the experiments and various values of the excitation period and the amplitude have to be used.

When the pipe is bent, the piezoelectric sensors produce a voltage signal. Based on the signal generated by the piezoelectric patches, the investigated parameters (axle load and velocity) can be determined. Sample signals received from the piezoelectric patches are shown in Fig. B.2(b). The presented values correspond to:  $T_l$ ,  $T_r$  – the periods of the measured signals,  $A_l$ ,  $A_r$  – the amplitudes of the signals. Two sensors located symmetrically with respect to the supports of the deformable body are used: the symbol  $l$  marks the measurements coming from the left sensor while the symbol  $r$  marks the measurements coming from the right sensor.

# Simplified load identification algorithm

Presented load identification algorithm was developed on the basis of the laboratory experiments performed by use of the testing stand shown in Appendix B. The algorithm objective was to identify the dynamic excitation acting on the beam-shape structure based on the signals produced by the sensors.

Depending on the real road conditions, vehicles travelling over the WIM devices have various technical and motion parameters. Therefore, the algorithm should be sensitive at least to the quantities like:

- the vehicle axle loads values,
- the position of tire forces pressing the WIM structure,
- the velocity of vehicle.

The assumption of the linear dependence of the response on the excitation was introduced. In general it is confirmed in the literature [47, 168], where piezo-electric effect is related to the linear response theory. Moreover, the mentioned assumption can be justified by the fact that the deformable structure undergoes only small (i.e., linear) deformations.

In the first step, the algorithm should recognize the excitation position  $x$  in terms of the length of the structure. To achieve it, the following relation based on sensors signals amplitudes  $A_l$  and  $A_r$  (see Fig. B.1) is used:

$$X' = \frac{A_l - A_r}{A_l + A_r}. \quad (\text{C.1})$$

This relation is valid, if the considered structure is symmetric. If the load is applied in the middle of the tube, then  $X' = 0$ . If the load is applied closer to the left sensor, then  $X' > 0$ , and if it is applied closer to the right sensor, then  $X' < 0$ . For the laboratory structure (see Fig. B.1), the values of the  $X'$  parameter in terms of the load position  $x$  take the form of an injective function as it is illustrated in Fig. C.1. Hence, by means of  $X' = f(x)$ , the determination of the load position is feasible. Moreover, the task is simplified by the observed linearity of the dependence.

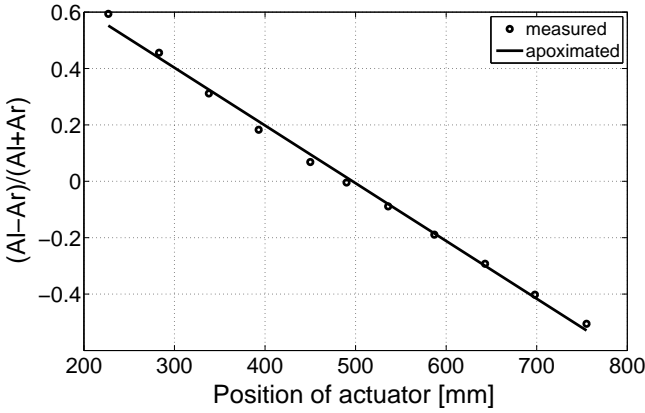


Figure C.1. Difference of amplitudes of the left  $A_l$  and right  $A_r$  sensors divided by their sum as a function of the position of the actuator.

Duration time of excitation  $T'$  is calculated as the average of the durations measured by the left  $T_l$  and right  $T_r$  sensors,

$$T' = \frac{T_l + T_r}{2}. \quad (\text{C.2})$$

Period  $T'$  is strongly related to the vehicle velocity and its footprint tire size. In general, if the vehicle velocity is higher and its foot print is smaller, the time duration  $T'$  is shorter. Therefore, the determined value of  $T'$  might be only used for preliminary estimation of vehicle velocity.

Finally, in order to perform load identification which acts on WIM device its calibration factor  $K$  is needed. The parameter  $K$  can be given by the following formula

$$K(x, T') = \frac{A'}{A_l + A_r}. \quad (\text{C.3})$$

The calibration factor  $K$  combines relation between the excitation position  $x$ , its duration  $T'$  and the proportion of input/output signal amplitudes. It generally depends on the electromechanical properties of the device. The parameter  $K$  might be obtained via experimental test of the device or its numerical modelling. The experimental result obtained for the structure shown in Fig. B.1 are illustrated in Fig. C.2.

The parameter  $K(x, T')$  can be obtained, for example, by means of interpolating the values presented in Fig. C.2, since the position and the time period

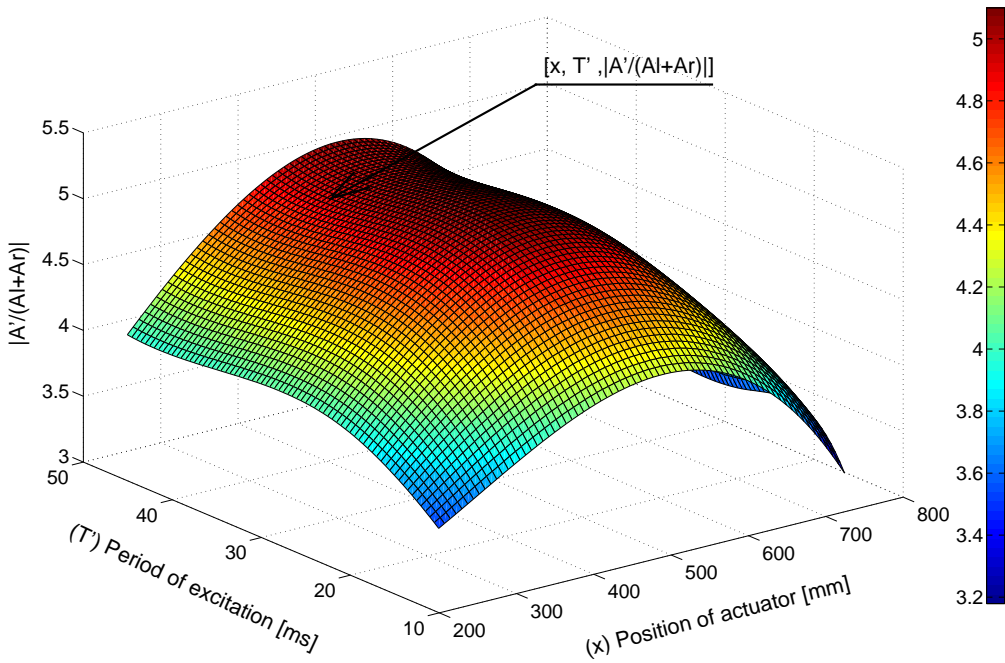


Figure C.2. Ratio of the excitation amplitude to the sum of the amplitudes measured by the left and the right sensor as a function of the actuator position and the excitation period.

of the excitation are known i.e. determined from measurements and by use of formulas (C.2) and (C.3). Finally, the load intensity  $A'$  affecting the beam-shape device might be calculated by the following formula:

$$A' = (A_l + A_r) \cdot K(x, T'). \quad (C.4)$$



## Full size testing stand of the beam-shape device

A full-size testing stand of beam-shape WIM device was prepared. The dimensions of the spherical shaped pipe used as bending element were: length 2000 mm, outside width 80 mm and 4 mm thickness of the wall. The pipe was equipped with six piezoelectric strain sensors in the form of piezoelectric patches of the same type as in the previous experiment presented in Appendix B. The general view of the setup is presented in Fig. D.1(a,b,c), while the piezoelectric strain sensors distribution is shown in Fig. D.1(d).

The steel pipe was symmetrically supported at the ends. The support conditions and pipe dimensions were analogical as it was planned to be used in later field tests. A pneumatic system was used to generate the excitation. The piston rod was equipped with a piezoelectric force sensor in order to measure force history. Three factors were taken into account in experimental study, namely:

1. in real road conditions the vehicles travel at different velocities,
2. the vehicles have different weights, and
3. the wheel positions on the lane can vary a lot.

Thus, the pneumatic piston rod had to be put in various locations along the pipe during the experiments and various values of the excitations time and amplitudes were used.

A valve system in the pneumatic cylinder enables the excitation to be modified by changing the pressure in the cylinder. The pressures of 8 bar, 6 bar and 4 bar were used, which were equivalents of the force values of 2200 N, 1650 N and 1100 N, respectively. The rise-time of the load was modified by changing the valve flow rate. As the rise-times (5–95% of the maximum load) of 216 ms, 328 ms and 673 ms were used in the performed test. The excitations type used in experiments are shown in Fig. D.2.

The measurement set up enables to perform the acquisition of generated signals by means of seven transducers (piston rod force sensor and six piezoelectric

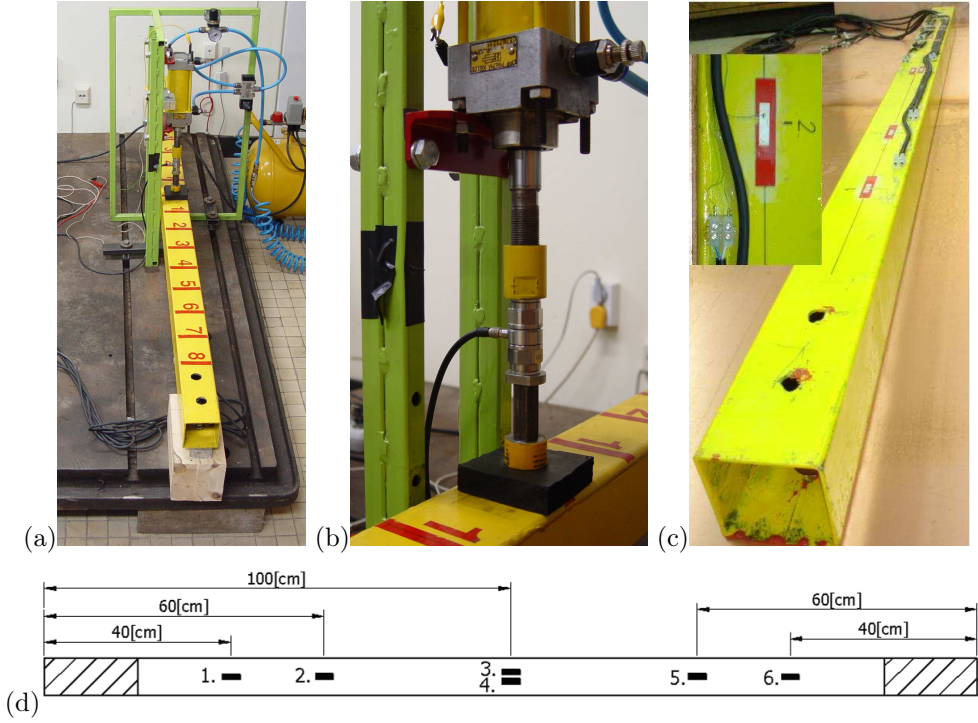


Figure D.1. Laboratory experiment: (a) an overall view of the testing stand, (b) the piezoelectric force sensor, (c) the piezoelectric strain sensors located on the bottom side of the pipe (d) the locations of the piezoelectric strain sensors.

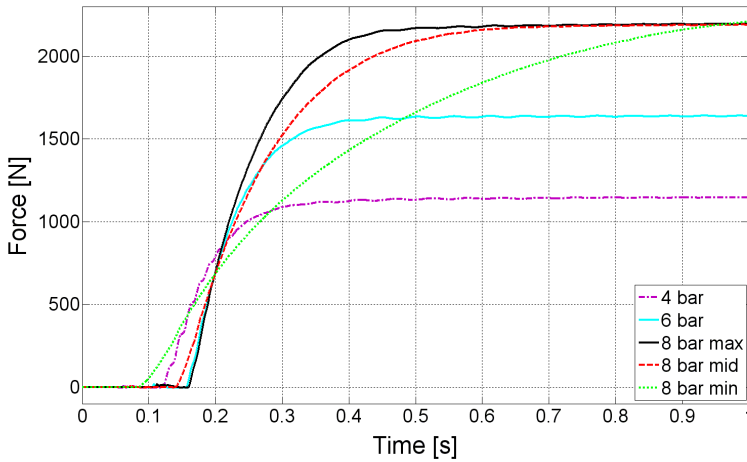


Figure D.2. An example of used excitation.

strain sensors). Figure D.3 presents an example of signals obtained for the excitation located 20 cm from the very center of the pipe. A characteristic charge flow for the measurement is observed (see Fig. D.3 and compare the signals generated by means of the force sensor and the piezoelectric strain patches). Drift effect is defined as any undesirable change of output signal in time which is not a function of measured variable [48]. This unprofitable feature is probably caused by use of voltage amplifier in the measurement set up which is not suitable in case of the quasi static measurement [54].

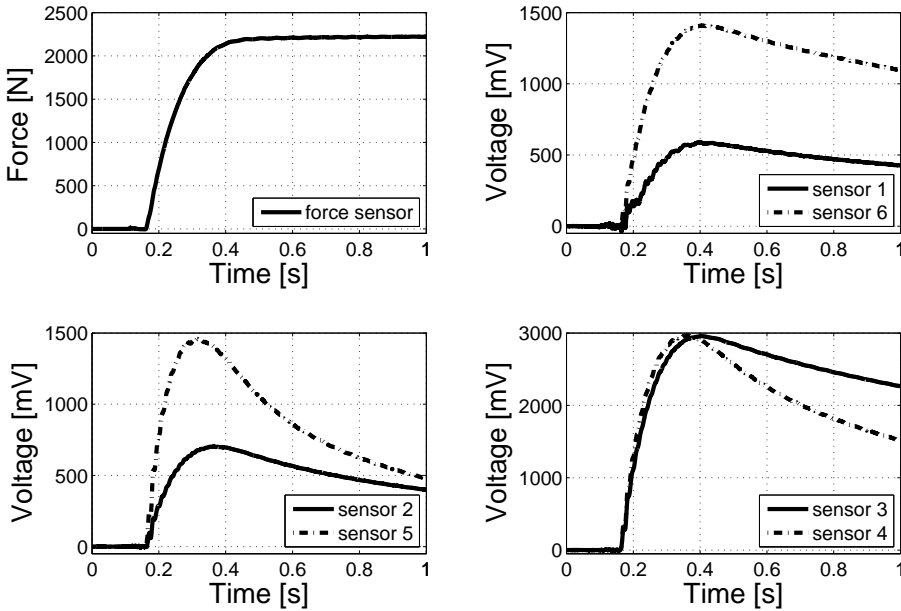


Figure D.3. An examples of the signal produced by the sensors.

In order to perform the calibration of the structure, the piston rod was mounted in various position. The fourteen locations were applied in the range  $(-60\text{ cm}, -50\text{ cm}, \dots, +70\text{ cm})$ . The numbers represents the excitation positions in relation to the center of the pipe.

The examples of the transfer function related to the excitation position measured by all of the sensors are illustrated in Fig. D.4. The vertical axis represents the ratio between the amplitude of the signal from the piezoelectric strain sensor and the amplitude of excitation.

A linear dependence between the excitation amplitude and sensors response was observed since the other tested parameters, i.e., the excitation position and the load rise time were constant. The results are illustrated in Fig. D.5.

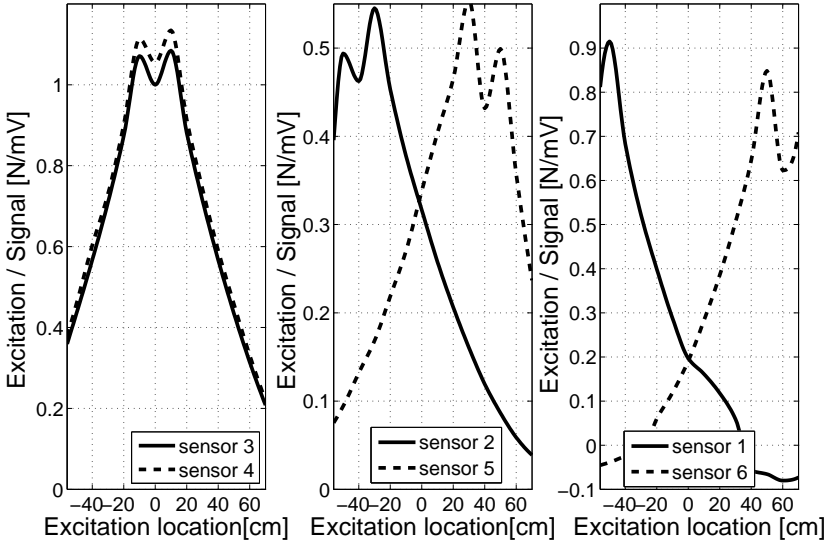


Figure D.4. Transfer function (amplitude of excitation/amplitude of signals) in terms of position of the excitation.

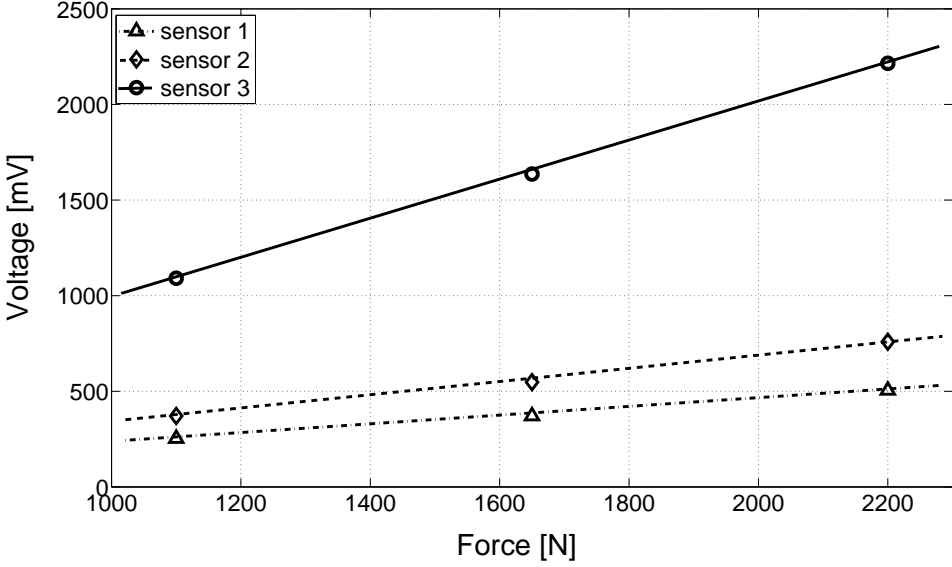


Figure D.5. Excitation force amplitude-measured sensors response relationship.

The sensitivity analysis between the amplitude of excitation (all three variants of the excitation amplitude) and the value of the signals generated by means of piezoelectric patches was carried out. For the analyzed excitations, a linear dependence was observed; some exemplary results are presented in Fig. D.6.

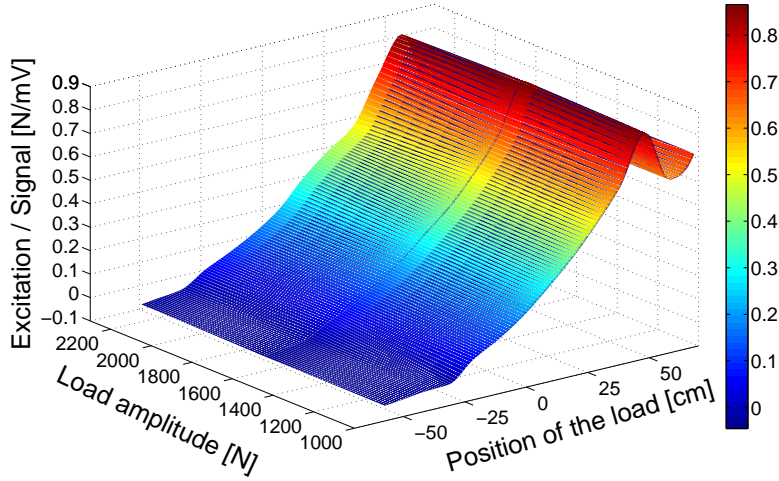


Figure D.6. Normalized response (amplitude of excitation/sensor 6 signal amplitude) in terms of the excitation position and the load value.

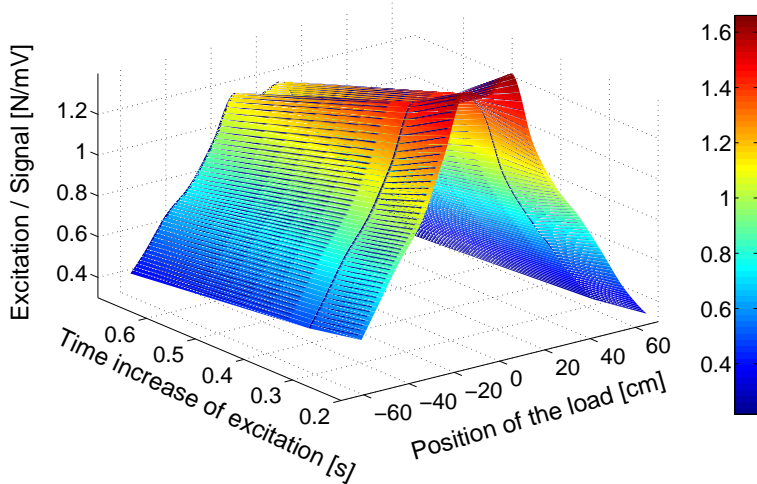


Figure D.7. Normalized response (amplitude of excitation/sensor 4 signal amplitude) in terms of excitation position and the rise-time of the load.

The sensitivity analysis of the time-rise of the excitation was performed for all three tested cases (216 ms, 328 ms, 673 ms) for the same amplitude of the excitation. The increase of the measured responses was observed as the rise-time increased. It was caused rather by the behavior of the measurement equipment (mentioned charge flow, see Fig. D.3) than the mechanical behavior of the system. The measurements results obtained by means of the sensor 4 are presented in Fig. D.7.

## Modal analysis of FE models

Modal analyses of the considered WIM devices (i.e., beam-shape and plate-shape) were conducted. The natural frequencies and the mode shapes of these structures were analyzed in order to find out their dynamic properties. This was needed due to the fact that the structural response is the strongest in case of the excitation frequency close to the natural frequency. Thus, the analysis was useful for the prediction of vibration responses to a given excitation.

The modal analyses were performed by using the FE models of the structures. The obtained modes numbers, natural vibration frequencies and modes types are shown in Table E.1 for the beam-shape structure and in Table E.2 for the plate-shape structure. Only the lowest frequencies were taken into consideration because they are probably the most prominent modes at which the structure will vibrate. Visualizations of some of the modal shapes are presented in Fig. E.1 for the beam-shape device and in Fig. E.2 for the plate-shape device.

Table E.1. Free vibration of the beam-shape WIM structure.

| Mode No. | Natural frequency Hz | Mode type                     |
|----------|----------------------|-------------------------------|
| I        | 114.5                | first torsional-bending mode  |
| II       | 131.3                | first bending mode            |
| III      | 222.1                | second torsional-bending mode |
| IV       | 335.5                | third torsional-bending mode  |
| V        | 347.4                | second bending mode           |

Table E.2. Free vibration of the plate-shape WIM structure.

| Mode No. | Natural frequency [Hz] | Mode type           |
|----------|------------------------|---------------------|
| I        | 845.8                  | first bending mode  |
| II       | 847.1                  | second bending mode |
| III      | 855.9                  | third bending mode  |
| IV       | 869.6                  | fourth bending mode |
| V        | 889.2                  | fifth bending mode  |



Figure E.1. Modal shapes of the beam-shape structure: (a) mode I, (b) mode II, (c) mode V.

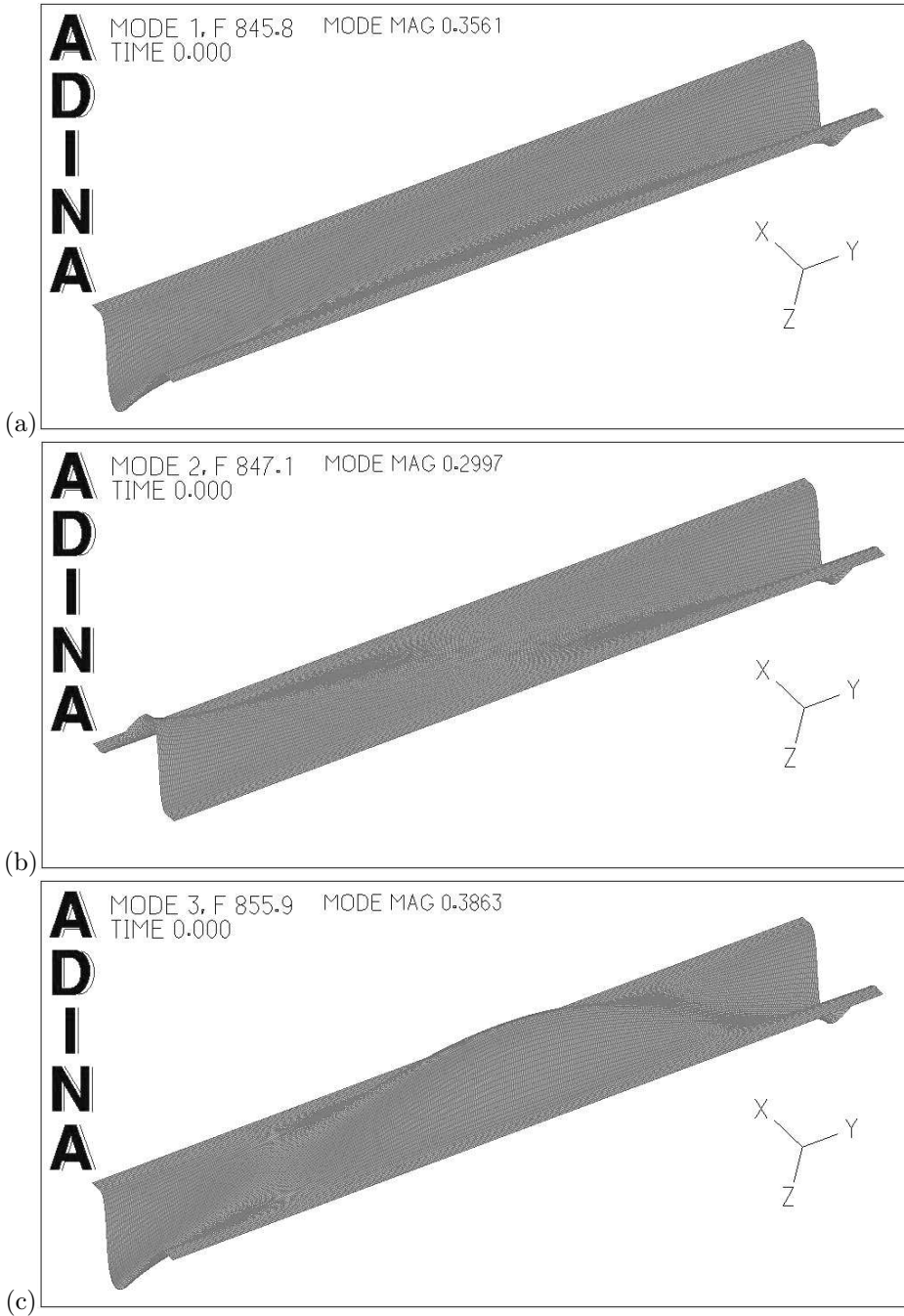


Figure E.2. Modal shapes of the plate-shape structure: (a) mode I, (b) mode II, (c) mode III.

The modal analysis enables to find out that the first natural frequency, in case of plate-shape device, is almost one order of magnitude higher than in case of beam-shape device. As a consequence, periods of the first free vibration modes are approximately 1.2 ms (plate-shape) and 8.7 ms (beam-shape). If the excitation has a similar periods, a strong structural response can be expected.

The structures are characterized by the width 8 cm (beam-shape) and 28 cm (plate-shape). Let us consider the tire footprint length of 25 cm. Hence, the velocities of the travelling excitation caused by the tires of a vehicle, the tire-device contact time correspond to the first mode periods are consequently equal: 135 km/h (beam-shape) and 1500 km/h (plate-shape). As a consequence, the beam-shape device is much more susceptible to strong structural response and unprofitable vibrations than in case of plate-shape device.

# Real-time impact mass identification methods

Chapter 4 of this thesis analyzed the case when identification process did not utilize the measurements from the sensor located on the impacting object. In this appendix different case is taken in to consideration.

## F.1 Mass identification based on force and acceleration

Let us consider the structure impacted by a falling mass  $M_1$ , (see Fig. F.1).

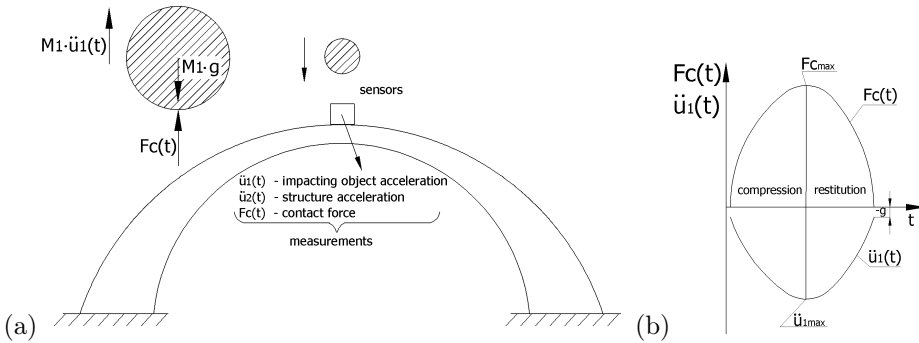


Figure F.1. Force-acceleration approach: (a) schema of structure and falling mass, (b) signals measured during contact of falling mass with structure.

Equation of motion for the free falling mass during the impact takes the following form:

$$F_C = M_1 g - M_1 \ddot{u}_1. \quad (\text{F.1})$$

Hence, the mass of the falling body can be determined as follows:

$$M_1 = \frac{F_C}{g - \ddot{u}_1}, \quad (\text{F.2})$$

where  $F_C$  is the contact force,  $\ddot{u}_1$  is the falling mass acceleration.

The proposed equation is fulfilled from the very beginning of the impact process. Therefore, the real-time mass identification is feasible, if measurements from two sensors (i.e., accelerometer and contact force sensor) are available.

## Verification

The verification was conducted by use of the drop testing stand. The objective was to minimize the impact identification time towards the real-time condition. Equation (F.2) and in addition the force and acceleration sensors measurements were used. Mass identification was tested in two cases, with the accelerometer attached to: (1) the falling body, and (2) the piston rod. Examples of accelerations measured in these two locations are shown in Fig. F.2, along with the measured force. Figure shows the very first impulse due to the first contact between the falling mass and the piston rod (beginning of the phase (A) of the impact see Fig. 4.5).

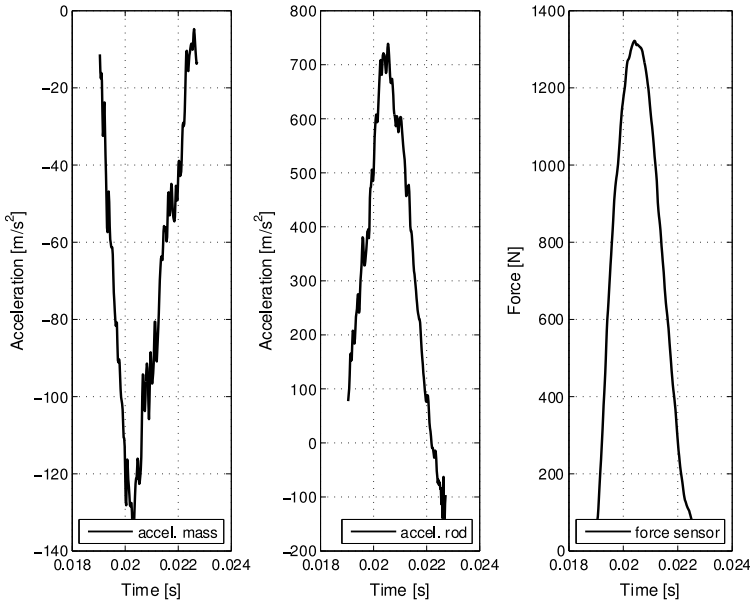


Figure F.2. Examples of measured signals in the first impulse (phase A of impact): (left) the falling mass acceleration, (middle) the piston rod acceleration, (right) the force.

The procedure was tested for different impacting masses. Chosen results of identification in the first phase of impact are presented in Fig. F.3. The identified falling mass  $M_1$ , see Fig. F.3(b), and piston rod mass, see Fig. F.3(a),

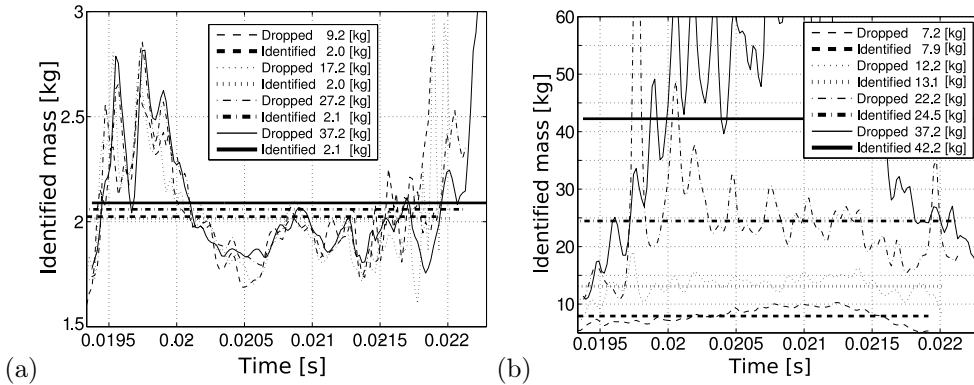


Figure F.3. Mass identification in the first phase of the impact (force and acceleration approach); acceleration measured on: (a) the piston rod of the pneumatic absorber, (b) the falling mass.

show a very unstable behaviour. This is mainly due to the intrinsic feature of accelerometers, which are very sensitive to external factors like e.g., unprofitable vibrations of the testing stand caused by the impact. The graph shows temporary values of the identified mass, the mean value in the considered time interval, and the accurate value of the falling mass. If accelerations of the piston rod are measured, Fig. F.3(a), the identified mass value is almost independent of the actual falling mass and its velocity. This behavior turned out to be typical for the first impact phase, which is characterized by several rebounds between the piston rod and the falling mass. In fact, when the accelerations are measured on the piston rod, only the mass of the piston rod can be estimated in the first impact phase. More practical results were obtained when the deceleration of the falling body was measured, see Fig. F.3(b). A reliable mass value ( $\pm 10\%$  accuracy) could be computed already after 5 ms from the very beginning of the impact.

The mass identification based on Eq. (F.2) has been also tested with the signals measured in the second phase (*B*) of the impact. Examples of measurements are shown in Fig. F.4, notice the different time scale than in Fig. F.3. A common joint movement of the piston rod and the falling mass occur, which is confirmed by similarity of the accelerations measured on the piston rod and on the falling mass. The results of the mass identification are presented in Fig. F.5. In the second impact phase, the mass identification is feasible and the location of the accelerometer does not have any crucial importance. The values obtained for both locations are relatively similar, however slightly more stable results were obtained for the accelerometer mounted on the falling mass. The accuracy was approx.  $\pm 5\%$ .

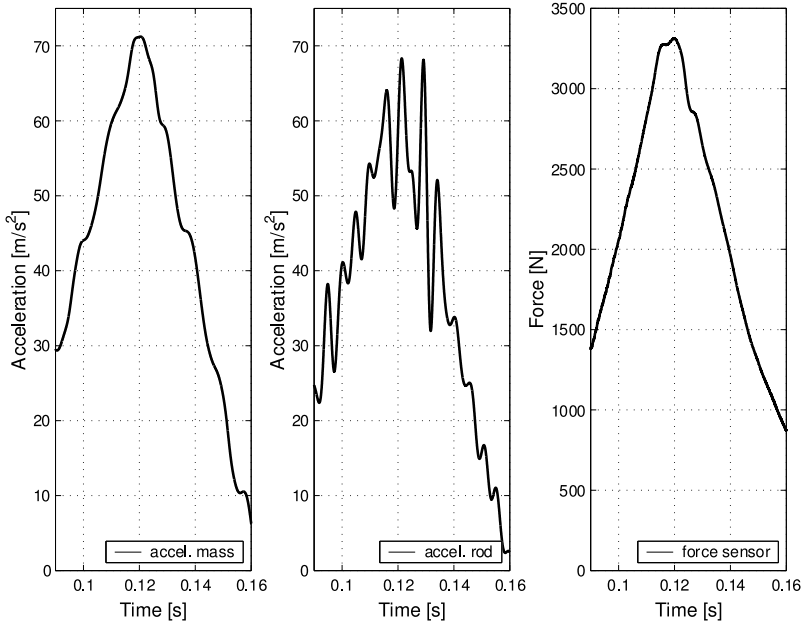


Figure F.4. Examples of measured signals in the second impact phase: (left) the falling mass acceleration, (middle) the piston rod acceleration, (right) the contact force.

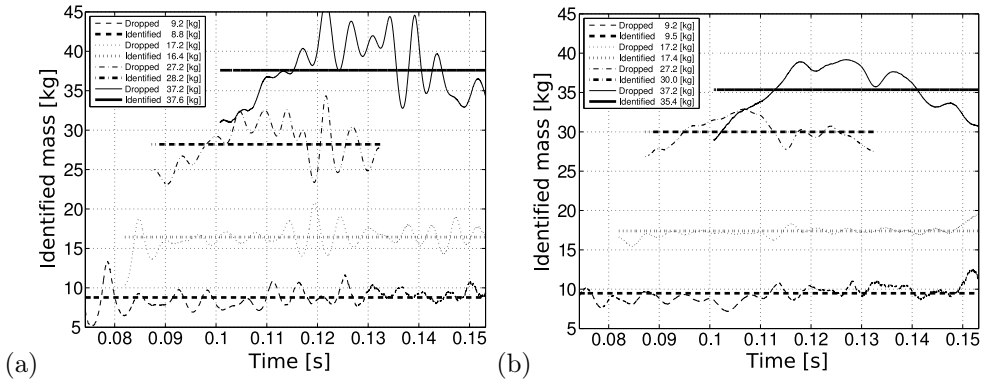


Figure F.5. Mass identification in the second phase of the impact (force and acceleration approach). Acceleration of: (a) the piston rod of the gas spring; (b) the falling mass.

## F.2 Mass identification based on impulse and momentum change

The results obtained by means of Eq. (F.2) were not very stable, the fluctuation of the mass value was observed. It was caused by the unprofitable measurement noise especially visible in case of the acceleration measurements. To

minimize this effect the procedure was slightly modified. The mass identification procedure presented in this section was proposed on the basis of the well known expression of impulse  $P_C$ . Let  $t^{00}$  and  $t^{02}$  denote the pre-impact and post-impact time instants. If the impacting body maintains a constant mass  $M_1$ , then

$$P_C = \int_{t^{00}}^{t^{02}} F_C(t) dt = M_1 (V_1^{00} - V_1^{02}). \quad (\text{F.3})$$

The velocity change of the impacted body  $\Delta V_1$  might be obtained on the basis of the integration of impacting body acceleration. To this end, the following relation can be used

$$\Delta V_1 = V_1^{02} - V_1^{00} = \int_{t^{00}}^{t^{02}} \ddot{u}_1(t) dt. \quad (\text{F.4})$$

Thus, the value of the impacting mass  $M_1$  can be determined by use of

$$M_1 = \frac{\int_{t^{00}}^{t^{02}} F_C(t) dt}{\int_{t^{00}}^{t^{02}} \ddot{u}_1(t) dt}. \quad (\text{F.5})$$

The parameters used in Eqs. (F.3), (F.4), (F.5) were illustrated in Fig. F.6. The graph presents the measurements of the impact force and acceleration of the falling mass. The result corresponds to the first phase of the impact process. The free fall was considered. Hence, the velocity change  $\Delta V_1$  determined by Eq. (F.4) must be corrected by the acceleration of gravity.

## Verification

The objective of the presented method was to minimize the mass identification uncertainty with fulfilled real-time condition. The method based on the Eq. (F.5) was tested for the wide variety of the impact parameters defined by mass and velocity. The obtained results are illustrated in the Fig. F.7(a). The identification precision for used boundary condition in most of the cases was better than  $\pm 10\%$ . The average impact mass identification precision for each constant value of mass with respect to the velocities variants is shown in Fig. F.7(b). In general, more correct result were obtained for the higher mass values.

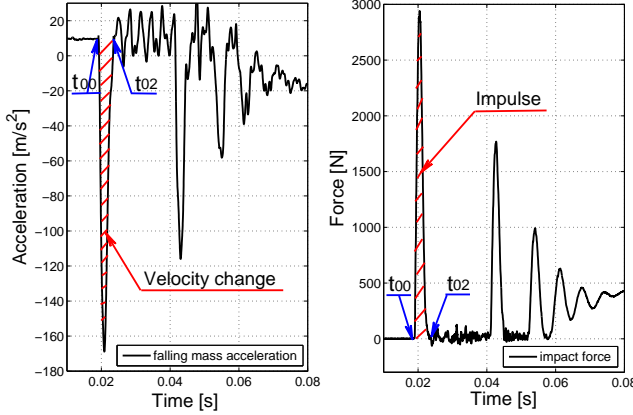


Figure F.6. Examples of measured signals: (left) the falling mass acceleration, (right) the force.

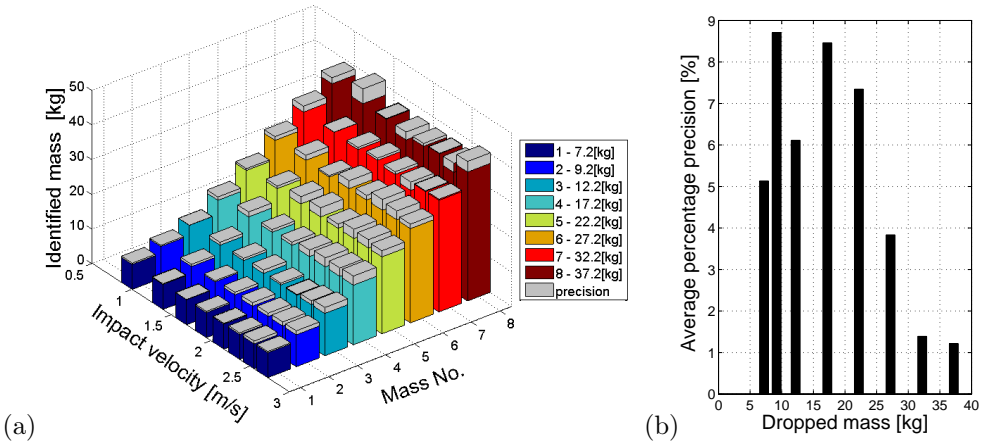


Figure F.7. Mass identification on the basis of Eq. (F.5): (a) the results presentation, (b) the average percentage precision.

It is worth to mention that for proposed procedure it is not necessary to perform the calculation for the time interval ( $t^{00}$  to  $t^{02}$ ) because Eq. (F.5) is also fulfilled for different intervals. Satisfied results were obtained for interval ( $t^{00}$  to  $t^{01}$ ) where  $t^{01}$  is the time instant when the maximum contact force is observed.

The method enables to real-time impacted object mass identification with acceptable precision. Nevertheless, the most serious limitation of it, is necessity to conduct the measurement when at least one of the sensors is fixed to the impacted object to be identified.

## The restitution coefficient discussion

In the classical impact theory, one of the basic parameters proposed originally by Newton is the restitution coefficient  $k$ . It can be formulated on the basis of the proportion of the relative velocities of the two colliding rigid bodies ( $M_1, M_2$ ), namely:

$$k = \frac{V_1^{02} - V_2^{02}}{V_1^{00} - V_2^{00}},$$

where  $V_1^{00}$  and  $V_1^{02}$  represent pre- and post-impact velocities for object 1,  $V_2^{00}$  and  $V_2^{02}$  represent pre- and post-impact velocities for object 2.

It can be noticed that in case of in-line collisions the actual values of velocities should be used in equation. But if the impact is oblique, then the velocity vector perpendicular to the plane of impact should be applied. The first case was analysed in the research.

In general the coefficient of restitution has values in the range  $0 < k < 1$ . Border case of elastic impact is identified with  $k = 1$ , plastic impact  $k = 0$ . Practically the intermediate cases are observed. According to the original assumptions, the coefficient of restitution was considered as a material constant independent of the impact properties. Later it was proved that this presumption was incorrect [169]. One of the quantity affecting the value of the restitution coefficient is the relative velocity of the colliding bodies in impact instant.

The type of the impact observed in case of analyzed system (see Figs. 4.3 and 4.4 in Chapter 4) was characterized by the coefficient of restitution. Calculations were performed for the wide variety of impact scenarios performed on the drop testing stand for the impact cases when the rebounds were observed. Atmospheric initial pressure case was analysed. The first rebounds in impact process was used for analysis. Experimental values of a restitution coefficients are presented in Fig. G.1 as a function of used boundary condition.

For the whole variety of the tested impacts scenarios, a restitution coefficients values stayed within the range 0.70–0.95 and showed poor sensitivity to the value of the impacting mass. The effect of the velocity was more signifi-

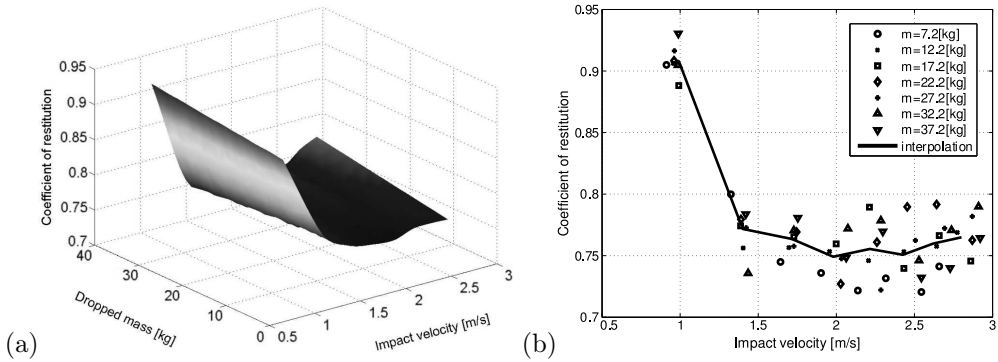


Figure G.1. Restitution coefficient in terms of the impact parameters: (a) mass and velocity effect; (b) velocity effect.

cant. The impact velocities higher than 1.5 m/s correspond to lower values of the restitution coefficient. Literature data [153, 160, 170] confirm the negative correlation between the restitution coefficient and impact velocities. Generally, it might be conclude that, the type of impact observed at the very beginning of the process, is rather elastic than plastic one.

# Sensitivity analysis of “Peak-to-peak” approach

This appendix is devoted to sensitivity analysis of the “Peak-to-peak” approach presented in Section 4.6. The analysis were conducted on the basis of the numerical results obtained using the model presented in Section 4.4 and the elastic model of contact force. The objective is to find the sensitivity of the method of unprofitable disturbances. This will lead to find the parameters of the absorption system suitable from identification precision point of view.

The methodology is based on the following equation

$$M_1(t^{01}, t^{11}) = \frac{\int_{t^{01}}^{t^{11}} F_C(t) dt}{\int_{t^{01}}^{t^{11}} (\ddot{u}_2(t) - g) dt}. \quad (\text{H.1})$$

It was found out that in order to obtain the reliable results, the characteristic time instants  $t^{01}$  and  $t^{11}$  (see Fig. 4.14(a)) must be determined with high precision. Hence, these time intervals were chosen for analysis and the following equation was used

Let us now introduce the following symbols:

$$\Delta V = V^{01} - V^{11} = \int_{t^{01}}^{t^{11}} (\ddot{u}_2(t) - g) dt,$$

$$(V^{01})' = a^{01}, \quad (V^{11})' = a^{11}, \quad P = \int_{t^{01}}^{t^{11}} F_C(t) dt.$$

In order to perform the sensitivity analysis, the condition numbers  $K_{01}$  and  $K_{11}$  were introduced. They were defined by the following formulas:

$$K_{01} = \frac{1}{M_1} \left| \frac{\partial M_1}{\partial t^{01}} \right| = \frac{1}{M_1} \left| \frac{-F_{C01} - P(V_{01})'}{\Delta V^2} \right| = \frac{1}{\Delta V} \left| -a^{01} - \frac{F_{C01}}{M_1} \right|, \quad (\text{H.2})$$

and

$$K_{11} = \frac{1}{M_1} \left| \frac{\partial M_1}{\partial t^{11}} \right| = \frac{1}{M_1} \left| \frac{F_{C11} + P(V^{11})'}{\Delta V^2} \right| = \frac{1}{\Delta V} \left| a^{11} + \frac{F_{C11}}{M_1} \right|. \quad (\text{H.3})$$

Finally, the sensitivity of the method is define by means of the condition number  $K_N$  determined as follows

$$K_N = \sqrt{K_{01}^2 + K_{11}^2}. \quad (\text{H.4})$$

## Analysis

Analysis objective was to find out the influence of the absorption system parameters on the mass identification precision. Three parameters have been considered:

- $M_2$  – the mass of the absorber piston rod,
- $P_0$  – the initial pressure inside the absorber cylinder,
- $k$  – stiffness of the contact element (i.e., rubber bumper see Fig. 4.3).

Thus, for the chosen impact scenario defined by initial condition (i.e., impacted mass  $M_1 = 30$  kg and  $V_1 = 2.5$  m/s) the parameters of the absorption system has been modified. Respectively  $M_2 = 0.5 \div 5$  kg, the pressure  $P_0 = 0 \div 1000$  kPa (0 correspond to the atmospheric one), and stiffness  $k = 1 \div 11 \times 10^5$  N/m. The sensitivity has been defined by the condition number  $K_N$  determined by Eq. (H.4). The obtained results are shown in Fig. H.1.

On their basis it was found that the mentioned factors are important if the identification precision is taken in to account. In general, it might be concluded that for precise impact mass estimation the following condition should be fulfilled:

- the mass of the absorber piston rod should be significant,
- the initial pressure inside the absorber cylinder should be high,
- the stiffness of the contact element should be low.

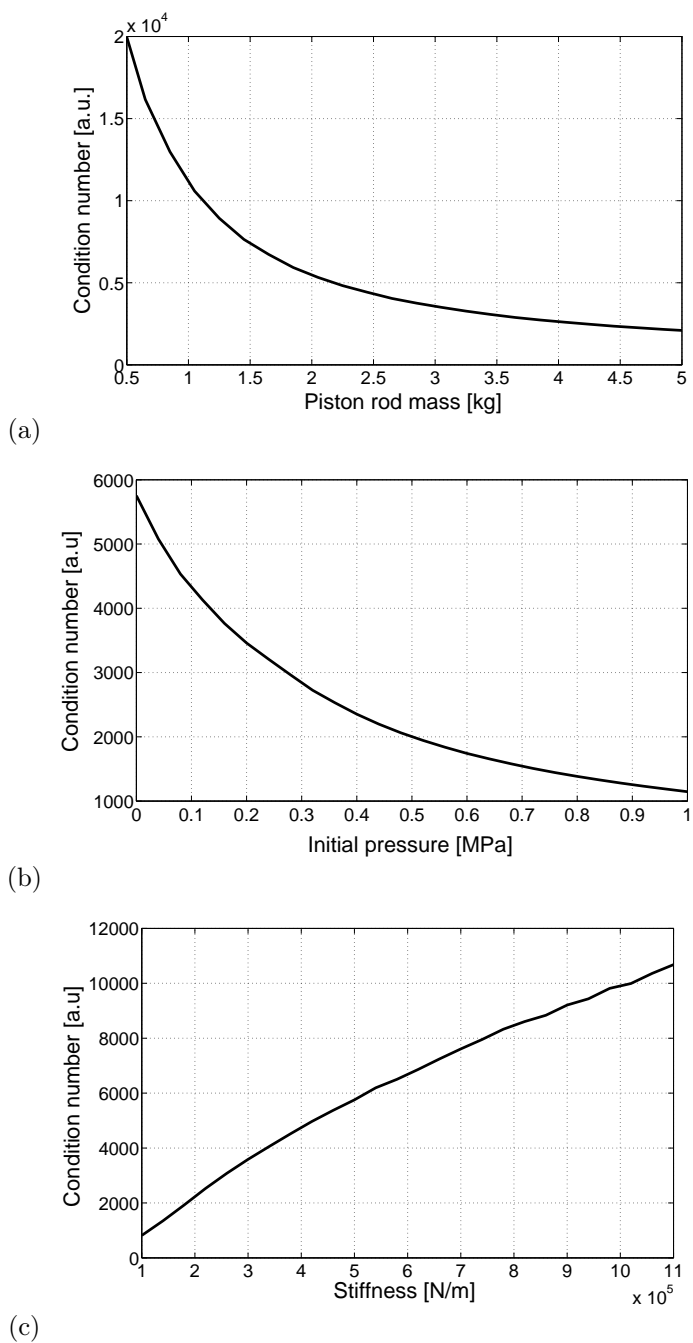


Figure H.1. Sensitivity analysis of absorption system: (a) the mass effect, (b) the initial pressure effect, (c) the stiffness effect.



# Podsumowanie

Celem rozprawy jest opracowanie aplikacyjnych technik pomiarowych pozwalających na identyfikację obciążeń dynamicznych w czasie rzeczywistym, a w szczególności:

- opracowanie nowej klasy tanich sensorów inteligentnych, wykorzystujących piezo-czujniki deformacyjne, zdolne do identyfikacji w czasie rzeczywistym obciążeń pojazdów drogowych i szynowych (przetworniki typu WIM z ang. weigh-in-motion),
- opracowanie nowej klasy sensorów inteligentnych, umożliwiających identyfikację w czasie rzeczywistym parametrów obciążeń uderzeniowych (masy i prędkości obiektu uderzającego).

Na początku rozprawy zdefiniowano problem identyfikacji obciążeń dynamicznych oraz określono motywacje dla wykonywanych badań. We wstępie zawarto rozważania i przegląd literatury dotyczące technik identyfikacji obciążeń. Dalej zdefiniowano systemy czasu rzeczywistego. Ze względu na to, że w badaniach eksperymentalnych szeroko były wykorzystywane techniki pomiarowe oparte na czujnikach piezoelektrycznych, został wykonany ich przegląd literatury i porównanie z innymi metodami np. tensometrią oporową.

Rozdział drugi rozprawy poświęcony jest dynamicznym wagom drogowym (ang. WIM weigh-in-motion) które stanowią przykład aplikacji wykorzystującej identyfikację obciążeń dynamicznych. Przedstawiono przegląd stanu techniki z dziedziny ważenia pojazdów w ruchu. Zaprezentowano wyniki badań ukierunkowanych na rozwój oraz testowanie nowego typu dynamicznej wagi drogowej. Zostały zaproponowane dwie wersje urządzenia (belkowa oraz płytowa). Ich działanie polega na pomiarze lokalnych odkształceń powstałych na powierzchni deformowanego obiektu. Do pomiarów wykorzystano piezoelektryczne czujniki odkształceń. Badania obejmowały testy w rzeczywistych warunkach polowych oraz symulacje numeryczne. Przeanalizowane zostały czynniki istotne ze względu na dokładność identyfikacji obciążeń przy zastosowaniu proponowanych urządzeń. Udowodniono, że amplituda mierzonego sygnału nie jest dobrą reprezentacją

obciążenia w sytuacji, gdy strefa kontaktu koła z nawierzchnią jest porównywalna do szerokości przetwornika nacisku. Sformułowano algorytmy identyfikacji dedykowane dla badanych urządzeń oraz zbudowano ich prototypowe wersje. Wykazano, że znacznie lepsza dokładność płytowego detektora nacisku stwarza większe możliwości praktycznego wykorzystania tego rozwiązania.

Trzeci rozdział pracy poświęcony jest implementacji systemu ważenia w ruchu dla transportu kolejowego. Urządzenie to może stanowić element większego systemu monitorowania stanu kratownicowych mostów kolejowych. Na początku rozdziału przedstawiono przegląd stanu techniki metod ważenia dynamicznego pojazdów kolejowych. Główną część rozdziału ukierunkowano na praktyczną implementację metody detekcji, która opiera się na pomiarze odkształceń szyny kolejowej wywołanych przejazdem pociągu. Badania wykonywane w warunkach polowych pozwoliły na weryfikację modelu numerycznego układu szynopodkład-podłoże. Testy eksperymentalne i symulacje numeryczne umożliwiły sformułowanie algorytmów identyfikacji oraz analizę parametrów, mających wpływ na dokładność wyznaczania obciążeń. Algorytm kalibracji doraźnej (wykorzystujący znaną masę lokomotywy) daje możliwość uniezależnienia wyników pomiaru od wpływu niektórych czynników zewnętrznych.

Wyniki badań przedstawione w rozdziałach drugim i trzecim wykazały, że piezoelektryczne czujniki odkształceń mogą mieć zastosowanie do identyfikacji obciążeń dynamicznych. Tego typu czujniki stanowią alternatywę dla bardziej popularnych technik pomiarowych np. tensometrii oporowej. Kluczowym aspektem jest właściwy dobór elementów układu kondycjonowania sygnału (szczególnie wzmacniacza) oraz kalibracja toru pomiarowego. Znacznie lepsze wyniki pomiarowe uzyskano stosując wzmacniacze ładunkowe zamiast napięciowych. W badaniach stosowane były dwa typy piezoelektrycznych czujników odkształceń (ceramiczne ang. piezo-ceramic oraz włókniste ang. piezo-fiber), dla których uzyskano podobne wyniki pomiarowe.

Rozważania przedstawione w rozdziale czwartym mają charakter badań podstawowych. Analizowany był proces uderzenia spadającego obiektu w absorber pneumatyczny. Rozważno identyfikację masy i prędkości uderzającego obiektu. Zaproponowano dwa algorytmy detekcji parametrów obciążenia. Metody zostały zweryfikowane numerycznie i eksperymentalnie. Obydwie techniki działają w czasie rzeczywistym i umożliwiają detekcję parametrów uderzenia w ciągu kilku początkowych milisekund procesu. Żadna z prezentowanych metod nie wymaga umieszczenia czujników na uderzającym obiekcie. Sprawdzono, że dokładność wyznaczenia masy uderzającego obiektu jest uzależniona od parametrów absorbera. Wykazano, że niezależnie od użytej metody identyfikacja prędkości jest możliwa z większą precyzją niż identyfikacja masy.

# Bibliography

1. P. Kołakowski, A. Orłowska, K. Sekuła, A. Świercz, and D. Sala. Two-year monitoring campaign of a railway truss bridge. In *EVACES'09*, 2009.
2. K. Sekuła and P. Kołakowski. Piezo-based weigh-in-motion system for the railway transport. *Structural Control and Health Monitoring*, doi: 10.1002/stc.416, 2010.
3. P. Kołakowski, D. Sala, K. Sekuła, Adaptronica Sp. z o.o. and Contec Sp.j. A method of monitoring the truss structure of a bridge and a system for monitoring the truss structure of a bridge, patent pending application, 2009.
4. G. Mikułowski. *Adaptive impact absorbers based on magnetorheological fluids*. PhD thesis, Institute of Fundamental Technological Research, 2008.
5. J. Holnicki-Szulc, editor. *Smart technologies for safety engineering*. Wiley, 2008.
6. T. Uhl. The inverse identification problem and its technical application. *Archive Applied Mechanics*, 77:325–337, 2007.
7. J. Shaw, J. Sirkis, E. Friebele, R. Jones, and A. Kersey. Model of transverse plate impact dynamics for design of impact detection methodologies. *AIAA J*, 33:327–1334, 1995.
8. N. Hu, H. Fukunaga, S. Matsumoto, B. Yan, and X. Peng. An efficient approach for identifying impact force using embedded piezoelectric sensors. *International Journal of Impact Engineering*, 34:1258–1271, 2007.
9. M. Martin and J. Doyle. Impact force identification from wave propagation responses. *International Journal of Impact Engineering*, 18:65–77, 1996.
10. A. Polak and J. Mroczka. Regularized identification of complex objects described by nonlinear models [in Polish: Regularyzacja identyfikacji obiektów złożonych opisanymi modelami nieliniowymi]. *Pomiary Automatyka Kontrola*, 9:190–194, 2007.
11. S. Kim and S. Lee. Experimental identification for inverse problem of a mechanical system with a non-minimum phase based on singular value decomposition. *Journal of Mechanical Science and Technology*, 22:1504–1509, 2008.
12. T. Uhl and K. Mendrok. Application of the inverse identification problem for determination of aggravating forces of mechanical constructions [in Polish: Zastosowanie odwrotnego zadania identyfikacji do wyznaczania sił obciążających

- konstrukcje mechaniczne]. *Wydawnictwo Instytutu Technologii Eksploracji* – PIB, 2005.
13. H. Choi, A. Thite, and D. Thompson. A threshold for the use of tikhonov regularization in inverse force determination. *Applied Acoustics*, 67:700–719, 2006.
  14. E. Jacquelin, A. Bennani, and P. Hamelin. Force reconstruction: analysis and regularization of a deconvolution problem. *Journal of Sound and Vibration*, 265:81–107, 2003.
  15. A. Björck. *Numerical Methods in Scientific Computing*. SIAM: Society for Industrial and Applied Mathematics, in press.
  16. N. Davendralingam and J. Doyle. Nonlinear identification problems under large deflections. *Experimental Mechanics*, 48:1741–2765, 2008.
  17. Q. Zhang, Ł. Jankowski, and Z. Duan. Identification of coexistent load and damage. *Structural and Multidisciplinary Optimization*, pages 1615–1488 (online), in press.
  18. C. Papadimitriou. Pareto optimal sensor locations for structural identification. *Computer Methods in Applied Mechanics and Engineering*, 194:16551673, 2005.
  19. Z. Li, J. Tang, and Q. Li. Optimal sensor locations for structural vibration measurements. *Applied Acoustics*, 65:807–818, 2004.
  20. Ł. Jankowski. Off-line identification of dynamic loads. *Structural and Multidisciplinary Optimization*, 37:609–623, 2009.
  21. C. Papadimitriou, Y. Haralampidis, and K. Sobczyk. Optimal experimental design in stochastic structural dynamics. *Probabilistic Engineering Mechanics*, 20:67–78, 2005.
  22. B. Błachowski. Dynamic load identification under constraints on number of sensors [in Polish: Identyfikacja obciążeń dynamicznych przy ograniczonej liczbie czujników]. *Modelowanie inżynierskie*, 33:19–26, 2007.
  23. G. Suwała and Ł. Jankowski. Model-free identification of added mass. In *Congress on Structural and Multidisciplinary Optimization*, 2009.
  24. M. Klinkov and C. Fritzen. An updated comparison of the force reconstruction methods. *Key Engineering Materials*, 347:461–466, 2007.
  25. J. Briggs. *Force identification using extracted modal parameters, with applications to glide height testing of computer hard disks*. PhD thesis, Massachusetts Institute of Technology, 1991.
  26. L. Mujica, J. Vehi, J. Rodellar, and P. Kołakowski. A hybrid approach of knowledge-based reasoning for structural assessment. *Smart Mater. Struct.*, 14:1554–1562, 2005.
  27. L. Mujica, J. Vehi, W. Staszewski, and K. Worden. Impact damage detection in aircraft composites using knowledge-based reasoning. *Structural Health Monitoring*, 7:215–230, 2008.

28. J. Doyle. Experimentally determining the contact force during the transverse impact of an orthotropic plate. *Journal of Sound and Vibration*, 118:441–448, 1987.
29. M. Martin and J. Doyle. Impact force location in frame structures. *International Journal of Impact Engineering*, 18:79–97, 1996.
30. J. LeClerc, K. Worden, W. Staszewski, and J. Haywood. Impact detection in an aircraft composite panel, a neural-network approach. *Journal of Sound and Vibration*, 299:672–682, 2007.
31. G. Yan and L. Zhou. Impact load identification of composite structure using genetic algorithms. *Journal of Sound and Vibration*, 319:869–884, 2009.
32. X. Cao, Y. Sugiyama, and Y. Mitsui. Application of artificial neural networks to load identification. *Computers and Structures*, 69:63–78, 1998.
33. E. Wu, C. Tsai, and L. Tseng. A deconvolution method for force reconstruction in rods under axial impact. *Journal of Acoustical Society of America*, 104:1418–1426, 1998.
34. J. Zhu and Z. Lu. A time domain method for identifying dynamic loads on continuous systems. *Journal of Sound and Vibration*, 148:137–146, 1991.
35. M. Tracy and F. Chang. Identifying impacts in composite plates with piezoelectric strain sensors, part I: Theory. *Journal of Intelligent Material Systems and Structures*, 9:920–928, 1998.
36. S. Law, J. Bu, X. Zhu, and S. Chan. Moving load identification on a simply supported orthotropic plate. *International Journal of Mechanical Sciences*, 49:1262–1275, 2007.
37. S. Law and Y. Fang. Moving force identification: optimal state estimation approach. *Journal of Sound and Vibration*, 239:233–254, 2001.
38. S. Vanlanduit, P. Guillaume, B. Cauberghe, E. Parloo, G. De Sitter, and P. Verboven. On-line identification of operational loads using exogenous inputs. *Journal of Sound and Vibration*, 285:267–279, 2005.
39. M. Klinkov and C. Fritzen. On line force reconstruction using robust observers. In *Third European Workshop on Structural Health Monitoring*, 2006.
40. M. Klinkov and C. Fritzen. On line estimation of external loads from dynamic measurements. In *Proceedings of the International Conference on Noise and Vibration Engineering (ISMA), Leuven, Belgium*, 2006.
41. P. Laplante. *Real-time systems design and analysis*. John Wiley & Sons, 2004.
42. I. Lee and J. Leong and S. Son, editors. *Handbook of real-time and embedded systems*. Taylor & Francis Group, 2008.
43. Q. Li and C. Yao. *Real-time concepts for embedded systems*. CMP Books, 2003.
44. P. Muhuri and K. Shukla. Real-time task scheduling with fuzzy uncertainty in processing times and deadlines. *Applied Soft Computing*, 8:1–13, 2008.

45. P. Muhuri and K. Shukla. Real-time scheduling of periodic tasks with processing times and deadlines as parametric fuzzy numbers. *Applied Soft Computing*, 9:936–946, 2009.
46. E. Olderog and H. Dierks. *Real-Time Systems: Formal Specification and Automatic Verification*. Cambridge University Press, 2008.
47. G. Gautschi. *Piezoelectric Sensorics*. Spriger-Verlag Berlin Heidelberg, 2002.
48. A. Rosochowski. Technical feasibility of a three-axis force transducer for measuring pressure and friction on the model die surface – prototype development. *Journal of Materials Processing Technology*, 115:192–204, 2001.
49. R. Measures. *Structural monitoring with fiber optic technology*. Academic Press, 2001.
50. R. Barret and J. Struts. Design and testing of 1/12th scale adaptive rotor. *Smart Mater. Struct.*, 6:491–497, 1997.
51. K. Uchino. Piezoelectric actuators 2006: Expansion from it robotics to ecological energy applications. *Journal of Electroceramics*, 20:301–311, 2007.
52. V. Giurgiutiu. *Structural health monitoring with piezoelectric wafer active sensors*. Elsevier, 2008.
53. H. Irschik, M. Krommer, and Y. Vetyukov. On the use of piezoelectric sensors in structural mechanics: Some novel strategies. *Sensors*, 10:5626–5641, 2010.
54. O. Mack. Investigations of piezoelectric force measuring devices for use in legal weighing metrology. *Measurement*, 40:778–785, 2007.
55. H. Georgiou and R. Mrad. Dynamic electromechanical drift model for pzt. *Mechanics*, 18:81–89, 2008.
56. A. Swiercz. *Identification of defects in the rod structures on the basis of Virtual Distorsion Method in frequency domain* [in Polish: *Identyfikacja defektów w konstrukcjach pretowych na podstawie Metody Dystorsji Wirtualnych w domenie częstości*]. PhD thesis, Institute of Fundamental Technological Research, 2007.
57. G. Mikułowski and J. Holnicki-Szulc. Adaptive landing gear concept-feedback control validation. *Smart Materials and Structures*, 16:2146–2158, 2007.
58. R. Wiszowaty, K. Sekuła, J. Holnicki-Szulc, Adaptronica Sp. z o.o., and Institute of Fundamental Technological Research. Method for mass and kinetic energy identification of an object impacting onto barrier and device for mass and kinetic energy identification of an object impacting onto barrier [in Polish: Sposób identyfikacji prędkości zderzenia, masy oraz energii kinetycznej obiektu uderzającego w przeszkodę i urządzenie do identyfikacji prędkości zderzenia, masy oraz energii kinetycznej obiektu uderzającego w przeszkodę], Patent, 2010.
59. K. Sekuła, R. Konowrocki, and T. Dębowski. Investigation of the new weight in motion system [in Polish: Badanie nowego typu systemu ważenia pojazdów w ruchu]. *Drogi i Mosty*, 3:69–88, 2009.

60. K. Sekuła and J. Holnicki-Szulc. Validation of the new sensors system for monitoring of traffic load. In *Fourth European conference on Structural Control, St. Petersburg, September 8-12, 2008*.
61. K. Sekuła, J. Holnicki-Szulc, and L. Knap. New sensors system for monitoring of traffic load. In *S.H.M. pp.541-547. ISBN No.1-932078-41*, 2004.
62. K. Sekuła, B. Dyniewicz, and T. Dębowski. Dynamic measurements of the railway transportation using piezoelectric sensors [in Polish: Pomiar wielkości dynamicznych w transporcie kolejowym z wykorzystaniem czujników piezoelektrycznych]. *Drogi i Mosty*, 1:31–44, 2010.
63. K. Sekuła and J. Holnicki-Szulc. Comparison of real time impact load identification procedures. In *III Eccomas Thematic Conference on smart structures and materials, Gdansk, Poland, July 9-11, 2007*.
64. K. Sekuła, C. Graczykowski, and J. Holnicki-Szulc. On-line impact load identification. *Structural Control and Health Monitoring*, Article ID:STC-10-0129, Under review.
65. P. Martin, Y. Feng, and X. Wang. Detector technology evaluation. Technical report, Department of Civil and Environmental Engineering University of Utah Traffic Lab, 2003.
66. C. Koniditsiotis and B. Peters. *Weigh-In-Motion Technology*. National Library of Australia, 2000.
67. J. Heidemann, F. Silva, X. Wang, G. Giuliano, and M. Hu. Sensors for unplanned roadway events-simulation and evaluation. Technical Report Metrans Project 04-08, METTRANS, May 2005.
68. R. Calderara. Long-term stable quartz wim sensors. In *National Traffic Data Acquisition Conference Albuquerque, New Mexico*, pages 613–626. Kistler Instrumente AG Winterthur CH-8408 Winterthur, Switzerland, 5–9 May 1996.
69. L. Seegmiller. *Utah commercial motor vehicle weight-in-motion data analysis and calibration methodology*. PhD thesis, Brigham Young University, Department of Civil and Environmental Engineering, December 2006.
70. R. Calderara, D. Barz, and E. Doupal. Advanced system solutions for new wim applications. Technical report, Kistler Instrumente AG and Transport Research Center, 2005.
71. J. Oleński. Concise statistical yearbook of Poland 2008. [in Polish: Mały rocznik statystyczny Polski 2008]. Zakład wydawnictw statystycznych, 2008.
72. J. Gajda, R. Sroka, M. Stencel, A. Wajda, and T. Żegleń. Weighing in motion systems [in Polish: Systemy ważenia pojazdów samochodowych w ruchu]. *Drognictwo*, 3/2001:78–81, 2001.
73. A. Regan, M. Park, S. Nandiraju, and C.H. Yang. Strategies for successful implementation of virtual weigh and compliance systems in california. Technical Report UCB-ITS-PRR-2006-19, University of California, Irvine, October 2006.

74. L. Cheng, H. Zhang, and Q. Li. Design of a capacitive flexible weighing sensor for vehicle wim system. *Sensors*, 7(8):1530–1544, 2007.
75. B. McCall. States successful practices weigh-in-motion handbook. Technical report, Center for Transportation Research and Education, Iowa State University, December 1997.
76. M. Hallenbeck and H. Weinblatt. Equipment for collecting traffic load data. Technical Report NCHRP 509, Transportation Research Board, 2004.
77. VTT. Weigh-in-motion of axle and vehicle for europe (wave)- calibration of the wim systems. Technical Report Work Package 3.2, Technical Research Centre of Finland, December 2000.
78. S. Yuan, F. Ansari, X. Liu, and Y. Zhao. Optic fiber-based dynamic pressure sensor for wim system. *Sensors and actuators*, 120:53–58, 2005.
79. P. Cosentino, B. Grossman, C. Taylor, W. Eckroth, R. Tongta, and T. Zhao. Fiber optic traffic sensor. In *National Traffic Data Acquisition Conference Albuquerque, New Mexico*, 5–9 May 1996.
80. E. O'Brien and A. Znidarie. Weigh-in-motion of axle and vehicle for europe (wave) – bridge wim systems (b-wim). Technical Report Work Package 1.2, University of Dublin, June 2001.
81. W. Schulz, J. Seim, E. Udd, M. Morrell, H. Marty Laylor, G. McGill, and R. Edgar. Traffic monitoring/control and road condition monitoring using fiber optic based systems. In *Smart Systems for Bridges, Structures, and Highways Conference, Newport Beach CA*, 1999.
82. J. Honefanger, J. Strawhorn, R. Athey, J. Carson, G. Conner, D. Jones, T. Kearney, J. Nicholas, P. Thurber, and R. Woolley. Commercial motor vehicle size and weight enforcement in europe. Technical Report FHWA-PL-07-002, Federal Highway Administration U.S. Department of Transportation, July 2007.
83. P. Burnos. Auto-calibration and temperature correction of wim systems [in Polish: Autokalibracja systemów wim, a korekta temperaturowa wyników ważenia]. In *Metrologia narzędzie poznania i droga rozwoju*, 2007.
84. L. Prochowski. *Mechanics of movement, Vehicles* [in Polish: *Mechanika ruchu. Pojazdy samochodowe*. WKŁ, 2005.
85. U. Sonmez, N. Sverdlova, R. Tallon, D. Klinikowski, and D. Streit. Static calibration methodology for weigh-in-motion systems. *International Journal of Heavy Vehicle Systems*, 7, No.2/3:191 – 204, 2000.
86. R. Quinley. Installation of weigh-in-motion systems. In *National Traffic Data Acquisition Conference Albuquerque*, May 5–9, 1996.
87. J. Gajda, R. Sroka, M. Stencel, and T. Żegleń. Statistical calibration of the weighing systems for the vehicles in motion [in Polish: Kalibracja systemów ważenia pojazdów w ruchu]. *Drogownictwo*, 1:90–94, 2002.

88. U. Sönmez, D. Streit, R. Tallon, and D. Klinikowski. Weigh-in-motion studies using strip-type sensors: the preliminary results. *International Journal of Heavy Vehicle Systems*, 15:1–26, 2008.
89. J. Gajda and R. Sroka. Multisensor data fusion in weigh-in-motion systems [in Polish: WieloczuJNIkowa fuzja danych w systemach ważenia pojazdów w ruchu]. *Pomiary Automatyka Kontrola*, 9:550–553, 2007.
90. F. Wang and R. Machemehl. Predicting truck tire pressure effects upon pavement performance. Technical Report SWUTC/06/167864-1, Center for Transportation Research, University of Texas, April 2006.
91. W. Cunagin and A. Grubbs. Automated acquisition of truck tire pressure data. *Transportation Research Record information*, 1123:112–121, 1987.
92. W. Siłka. *Theory of car moving* [in Polish: *Teoria ruchu samochodu*]. Wydawnictwo Naukowo-Techniczne, 2002.
93. H. Lee and D. Saravanos. The effect of temperature dependent material nonlinearities on the response of piezoelectric composite plates. Technical Report NASA TM–97-206216, National Aeronautics and Space Administration, Lewis Research Center Cleveland, November 1997.
94. J. Gajda, R. Sroka, M. Stencel, A. Wajda, and T. Żegleń. Traffic parameters measurement – precision assessment [in Polish: Pomiary parametrów ruchu drogowego – ocena dokładności]. *Drogownictwo*, 10:323–331, 2003.
95. *Theory and Modeling Guide Volume I: ADINA*.
96. A. Premount. Active vibration control. In *Structural Control and Health Monitoring Advanced Course – SMART’01*, 2001.
97. T. Kwon and B. Aryal. Development of a pc-based eight-channel wim system. Final Report MN/RC 2007-45, Northland Advanced Transportation Systems Laboratories University of Minnesota Duluth, October 2007.
98. C. Helg and L. Pfohl. Signal processing requirements for wim lineas type 9195. Technical report, Kistler Instrumente AG, Winterthur, Switzerland, 2000.
99. A. Matsumoto, Y. Sato, H. Ohno, M. Tomeoka, K. Matsumoto, J. Kurihara, T. Ogino, M. Tanimoto, Y. Kishimoto, Y. Sato, and T. Nakai. A new measuring method of wheel-rail contact forces and related considerations. *Wear*, 265:1518–1525, 2008.
100. H. Kanehara and T. Fujioka. Measuring rail/wheel contact points of running railway vehicles. *Wear*, 253:275–283, 2002.
101. F. Moses. Weigh-in-motion system using instrumented bridges transportation. *Engineering Journal*, 105:233–249, 1979.
102. R. Karoumi, A. Liljencranz, G. James, E. Bruwhiler, A. Herwig, and F. Carlsson. Sustainable bridges – assessment for future traffic demands and longer lives. Technical report, KTH and EPFL and DB and COWI and LTH, 2007.

103. P. Chatterjee, E. O'Brien, Y. Li, and A. Gonzalez. Wavelet domain analysis for identification of vehicle axles from bridge measurements. *Computers and Structures*, 84:1792–1801, 2006.
104. R. Karoumi, J. Wiberg, and A. Liljencrantz. Monitoring traffic loads and dynamic effects using an instrumented railway bridge. *Engineering Structures*, 27:1813–1819, 2005.
105. A. Liljencrantz, R. Karoumi, and P. Olofsson. Implementing bridge weigh-in-motion for railway traffic. *Computers and Structures*, 85:80–88, 2007.
106. M. Niedzwiecki and A. Wasilewski. New algorithms for the dynamic weighing of freight trains. *Control Engineering Practice*, 5:603–618, 1997.
107. D. Senyanskiy. Problem of increasing the accuracy of railway carriages weighing in motion. In *XVII IMEKO World Congress Metrology in the 3rd Millennium June 22-27*, 2003.
108. *Systemy wazenia DGW-B SHENK* (<http://www.schenckprocess.pl/wagi/wagi-kolejowe/>).
109. G. James. *Analysis of Traffic Load Effects on Railway Bridges*. PhD thesis, Structural Engineering Division Royal Institute of Technology, Stockholm, Sweden, 2003.
110. A. Johansson and J. Nielsen. Out-of-round railway wheels-wheel-rail contact forces and track response derived from field tests and numerical simulations. *Journal of Rail and Rapid Transit*, 217:135–146, 2003.
111. A. Laudati, G. Lanza, A. Cusano, A. Cutolo, M. Giordano, G. Breglio, and A. Antonelli. Railway monitoring and train tracking by fiber bragg grating sensors: a case study in Italy. In *Proc. of the 4th European Workshop on Structural Health Monitoring, Kraków, Poland, 2-4 July 2008, ISBN 978-1-932078-94-7*, 2008.
112. Gotcha company. Wheel flat detection and axle load measurement system. Technical report, TagMaster, 2005.
113. Kistler company. Railcar weighing on mainline tracks. Technical report, Kistler, 2008.
114. A. Bracciali and P. Folgarait. New sensor for lateral and vertical wheel-rail forces measurements. In *Conference on Railway Engineering*, London, 6–7 July, 2004.
115. H. Inoue, J. Harrigan, and S. Reid. Review of inverse analysis for indirect measurement of impact force. *Appl. Mech. Rev.*, 54:503–524, 2001.
116. J. Nielsen and J. Oscarsson. Simulation of dynamic train-track interaction with state-dependent track properties. *Journal of Sound and Vibration*, 275:515–532, 2004.
117. M. Bahrekazemi. *Train-induced ground vibration and its prediction*. PhD thesis, Royal Institute of Technology, Dept. of Civil and Architectural Engineering, 2004.
118. A. De Man. *Dynatrack: a survey of dynamic railway track properties and their quality*. PhD thesis, Delft University of Technology, 2002.

119. N. Chaar. *Wheelset structural flexibility and track flexibility in vehicle-track dynamic interaction*. PhD thesis, Royal Institute of Technology, Aeronautical and Vehicle Engineering, 2007.
120. K. Knothe and S. Grassie. Modelling of railway track and vehicle/track interaction at high frequencies. *Vehicle System Dynamics*, 22:209–262, 1993.
121. D. Steffens. *Identification and development of a model of railway track dynamic behaviour*. PhD thesis, Queensland University of Technology, Faculty of Built Environment and Engineering, 2005.
122. R. Bogacz and Z. Kowalska. Computer simulation of the interaction between a wheel and a corrugated rail. *European journal of mechanics. A. Solids*, 20:673–684, 2001.
123. A. Fenander. A fractional derivative railpad model included in a railway track model. *Journal of Sound and Vibration*, 212:778–892, 1998.
124. S. Iwnicki, editor. *A Handbook of Railway Vehicle Dynamics*. CRC Press, 2006.
125. W. Cai, Z. Wen, X. Jin, and W. Zhai. Dynamic stress analysis of rail joint with height difference defect using finite element method. *Engineering Failure Analysis*, 14:1488–1499, 2007.
126. W. Zhai and Z. Cai. Dynamic interaction between a lumped mass vehicle and a discretely supported continuous rail track. *Computers and Structures*, 63:987–997, 1997.
127. S. Kaewunruen. *Experimental and numerical studies for evaluating dynamic behaviour of prestressed concrete sleepers subject to the severe impact loading*. PhD thesis, University of Wollongong, 2007.
128. A. Soderberg and S. Bjorklund. Validation of a simplified numerical contact model. *Tribology International*, 40:926–933, 2008.
129. C. Bajer and P. Tokaj. Dynamics of the track with steel wedge-shaped sleepers [in Polish: Dynamika toru z podładami stalowymi klinowymi]. *Drugi i mosty*, 2:5–35, 2006.
130. S. Timoshenko. *Vibration problems in Engineering*. D. Van Nostrand Co., 1955.
131. R. Hinderbrand. Vertical vibration attention in railway track: a wave approach. *Journal of Sound and Vibration*, 247:857–874, 2001.
132. *Catalog of freight wagons* [in Polish: *Katalog wagonów towarowych*]. 2005.
133. X. Zhang. *Conceptual Study of Adaptive Energy Absorbers*. PhD thesis, The Hong Kong University of Science and Technology, 2009.
134. J. Holnicki-Szulc and L. Knap. Adaptive crashworthiness concept. *International Journal of Impact Engineering*, 30:639–663, 2004.
135. L. Knap. *Active control of collision energy in adaptive structures* [in Polish: *Aktywne sterowanie energii zderzeń w urządzeniach adaptacyjnych*]. PhD thesis, Institute of Fundamental Technological Research, 2000.

136. H. Janocha, editor. *Adaptronics and Smart Structures*. Springer-Verlag Berlin Heidelberg, 2007.
137. C. Graczykowski and J. Holnicki-Szulc. Protecting offshore wind turbines against ship impacts by means of adaptive inflatable structures. *Shock and Vibration*, 16:335–353, 2009.
138. M. Ostrowski, P. Griskevicius, and J. Holnicki-Szulc. Pyro-adaptive impact energy absorber. In *Odporność udarowa konstrukcji, December 5–8, Rynia near Warsaw, Poland*, 2006.
139. M. Wikło and J. Holnicki-Szulc. Optimal design of adaptive structures: Part i. remodeling for impact reception. *Structural and Multidisciplinary Optimization*, 37:305–318, 2009.
140. M. Wikło and J. Holnicki-Szulc. Optimal design of adaptive structures: Part ii. adaptation to impact loads. *Structural and Multidisciplinary Optimization*, 37:351–366, 2009.
141. M. Ostrowski, P. Griskevicius, and J. Holnicki-Szulc. Feasibility study of an adaptive energy absorbing system for passenger vehicles. In *CMM-2005 – Computer Methods in Mechanics*, June 21–24, 2005, Częstochowa, Poland.
142. W. Witteman. *Improved Vehicle Crashworthiness Design by Control of the Energy Absorption for Different Collision Situations*. PhD thesis, Eindhoven University of Technology, 1999.
143. S. Deshmukh and G. McKinley. Adaptive energy-absorbing materials using field-responsive fluid-impregnated cellular solids. *Smart Materials and Structures*, 16:106–113, 2007.
144. J. Holnicki-Szulc, P. Pawłowski, and M. Wikło. High-performance impact absorbing materials – the concept, design tools and applications. *Smart Mater. Struct.*, 12:461–467, 2003.
145. Ł. Jankowski and G. Mikułowski. Adaptive landing gear: optimum control strategy and improvement potential. In *International Conference on Noise and Vibration Engineering, 8–20 September, Leuven, Belgium*, 2006.
146. C. Graczykowski and J. Holnicki-Szulc. Protecting offshore wind turbines against ship impacts by means of adaptive inflatable structures. *Shock and Vibration*, 16:335–353, 2009.
147. C. Graczykowski and J. Holnicki-Szulc. Adaptive flow control based airbags for waterborne and aeronautical application. In *Proc. of the 4th European Conference on Structural Control, September 8–12, St. Petersburg, Russia*, 2008.
148. J. Holnicki-Szulc, C. Graczykowski, G. Mikułowski, A. Mróz, and P. Pawłowski. Smart technologies for adaptive impact absorption. *Solid State Phenomena*, 154:187–194, 2009.
149. G. Mikułowski and J. Holnicki-Szulc. Fast controller and control algorithms for MR-based adaptive impact absorbers – force based control. *Machine Dynamics Problems*, 30:113–122, 2006.

150. X. Wang. *Impact locations in structures using energy flow estimators with piezoelectric sensors*. PhD thesis, University of Sciences and Technology (INSA) Lyon-Department of Electrical Engineering, 2009.
151. H. Sekine and S. Atobe. Identification of locations and force histories of multiple point impacts on composite isogrid-stiffened panels. *Composite Structures*, 89:1–7, 2009.
152. J. Holnicki-Szulc, G. Mikułowski, J. Motylewski, P. Pawłowski, and Z. Wolejsza. Adaptive system for energy dissipation in landing gears [in Polish: Adaptacyjny system dyssypacji energii w podwoziu lotniczym]. In *XXXIV Ogólnopolskie Sympozjum Diagnostyka Maszyn, Węgierska Górka*, 2007.
153. W. Stronge. *Impact Mechanics*. Cambridge University Press, 2000.
154. N. Liepmann and A. Roshko. *Elements of Gasdynamics*. John Wiley & Sons, New York, 1957.
155. A. Shapiro. *The Dynamics and Thermodynamics of Compressible Fluid Flow*. Pergamon Press, New York, 1953.
156. G. Van Wylen and R. Sonntag. *Fundamentals of Classical Thermodynamics*. John Wiley & Sons, 1978.
157. T. Edwards. Effects of aliasing on numerical integration. *Mechanical Systems and Signal Processing*, 21:165–176, 2007.
158. M. Sjöberg and L. Kari. Testing of nonlinear interaction effects of sinusoidal and noise excitation on rubber isolator stiffness. *Polymer Testing*, 22:343–351, 2003.
159. J. Diani, B. Fayolle, and P. Gilormini. A review on the mullins effect. *European Polymer Journal*, 45:601–612, 2009.
160. R. Gryboś. *Impact theory in discrete mechanical systems* [in Polish: *Teoria Uderzenia w Dyskretnych układach mechanicznych*]. Państwowe Wydawnictwo Naukowe, 1969.
161. L. Gracia, E. Pena, J. Royo, J. Pelegay, and B. Calvo. A comparison between pseudo-elastic and damage models for modeling the mullins effect in industrial rubber components. *Mechanics Research Communications*, 36:769–776, 2009.
162. T. Szolc, P. Tazowski, R. Stocki, and J. Knabel. Damage identification in vibrating rotor-shaft systems by efficient sampling approach. *Mech. Syst. Signal Process*, 47:533–557, 2009.
163. W. Staszewski. Intelligent signal processing for damage detection in composite materials. *Composites Science and Technology*, 62:941–950, 2002.
164. C. Graczykowski, G. Mikułowski, K. Sekuła, A. Mróz, Adaptronica Sp. z o.o., and Contec Sp.j. Methodology of impact energy and pneumatic absorber [in Polish: Sposób dyssypacji energii uderzenia i absorber pneumatyczny]. Patent, 2009.
165. A. Preumont and V. Piefort. Finite element modeling of smart piezoelectric shell structures. In *5th National Congress on Theoretical and Applied Mechanics-Louvain-la-Neuve*, May 2000.

166. T. G. Zieliński. *Application of Virtual Distortion Method for modeling and identification of structural defect*. [in Polish: *Metoda Impulsowych Dystorsji Wirtualnych z zastosowaniem do modelowania i identyfikacji defektów w konstrukcjach*. PhD thesis, IPPT-PAN, 2003.
167. R. Le Letty, F. Claeysen, F. Barillot, and N. Lhermet. Amplified piezoelectric actuators for aerospace applications. In *AMAS Workshop on Smart Materials and Structures SMART-03*, pages 51–62, September 2003.
168. T. Ikeda. *Fundamentals of Piezoelectricity*. Oxford University Press, 1990.
169. J. Daily, R. Strickland, and J. Daily. Crush analysis with under-rides and the coefficient of restitution. In *24th Annual Special Problems in Traffic Crash Reconstruction*, 2006.
170. R. Brach. *Mechanical impact dynamics: rigid body collisions*. John Wiley & Sons, 1991.